UNIVERSITA' DEGLI STUDI DI TRIESTE
IRCCS SANTA LUCIA – ROMA

XXVI CICLO DI DOTTORATO DI RICERCA IN
NEUROSCIENZE E SCIENZE COGNITIVE – INDIRIZZO NEUROBIOLOGIA

In vivo characterization of cerebral networks with functional and structural magnetic resonance techniques

SETTORE SCIENTIFICO DISCIPLINARE BIO/09 FISIOLOGIA

DOTTORANDO
Chiara Mastropasqua

COORDINATORE E SUPERVISORE TESI
Prof. Paolo Battaglini

CO-SUPERVISORI DI TESI
Dott. Marco Bozzali
Prof. Mara Cercignani

ANNO ACCADEMICO 2012 /2013

Loss is nothing else but change,
and change is Nature's delight.

CONTENTS

ABBREVIATIONS

AMT	Active Motor Threshold
AD	Alzheimer's Disease
AV	Anterior Ventral
ADC	Apparent Diffusion Coefficient
AUC	Area-Under-Curve
AAL	Automated Anatomical Labeling
Dax	Axial Diffusivity
BIT	Behavioural Inattention Test
BOLD	Blood-Oxygenation Level Dependent
BA	Brodmann Area
CM	Centromedian
CSF	Cerebrospinal Fluid
DMN	Default Mode Network
deoxyHB	Deoxygenated Haemoglobin
DTI	Diffusion Tensor Imaging
DWI	Diffusion Weighted Imaging
DLPFC	Dorso-Lateral Prefrontal Cortex
EPI	Echo Planar Imaging
EEG	Electroencephalography
FDR	False-Discovery Rate
FWER	Family-Wise Error Rate
FLAIR	Fluid Attenuated Inversion Recovery
FA	Fractional Anisotropy
FC	Functional Connectivity
fMRI	Functional Magnetic Resonance Imaging
GM	Grey Matter
HCP	Human Connectome Project
ICA	Independent Component Analysis
LGN	Lateral Geniculate Nucleus
LP	Lateral Posterior
LH	Left Hemisphere
MRI	Magnetic Resonance Imaging
MPRAGE	Magnetization-Prepared Rapid Gradient Echo
MEG	Magnetoencephalography

MGN	Medial Geniculate Nucleus
MD	Medial-Dorsal
MCI	Mild Cognitive Impairment
MDEFT	Modified Driven Equilibrium Fourier Transform
NBS	Network Based Statistic
OC	Occipital Cortex
PF	Parafascicular
PET	Positron Emission Tomography
PPC	Posterior Parietal Cortex
PFC	Prefrontal Cortex
PMC	Premotor Cortex
S1/S2	Primary And Secondary Somatosensory
M1	Primary Motor Cortex
Pu	Pulvinar
Drad	Radial Diffusivity
RF	Radiofrequency
ROC	Receiver Operating Characteristic
ROI	Region-Of-Interest
RS	Resting State
RSNs	Resting State Networks
RH	Right Hemisphere
SBA	Seed-Based Analysis
TC	Temporal Cortex
MD	Mean Diffusivity
TBS	Theta Burst Stimulation
TFCE	Threshold-Free Cluster Enhancement
TC	Time Courses
TBSS	Tract Based Spatial Statistic
Tdcs	Transcranial Direct Current Stimulation
tms	Transcranial Magnetic Stimulation
VA	Ventral Anterior
VPL	Ventral Posterolateral
VL	Ventro Lateral
VBM	Voxel Based Morphometry
WM	White Matter

INTRODUCTION

The human brain is a complex network. It consists of spatially distributed, but functionally linked regions that continuously share information with each other (van den Heuvel and Hulshoff Pol, 2010). It is generally accepted that to better understand the functioning of a network, one must know its elements and their interconnections (Sporns *et al.* 2005). Thus the characterization of brain connectivity is necessary to increase our understanding of how functional brain states emerge from their underlying structural substrate and how neurons and neural networks process information. Moreover, this approach can provide new mechanistic insights to understand the correspondence between structural disruption and the consequent changes in brain functioning (Sporns et al., 2005).

When applied to the brain, the term connectivity refers to several different and interrelated aspects of brain organization (Horwitz, 2003). It can be defined as a pattern of anatomical links ("anatomical connectivity"), of statistical dependencies ("functional connectivity") or of causal interactions ("effective connectivity") between distinct units within a nervous system. Depending on the context, the “units” correspond to individual neurons, neuronal populations, or anatomically segregated brain regions (Sporns et al., 2007). In fact, brain connectivity can be described at several levels of scale: the microscale, with individual neurons linked by individual synaptic connections; the mesoscale, with networks connecting neuronal populations,

and the macroscale level, characterized by fiber pathways connecting brain regions (Sporns et al., 2007).

In this work, I focused on the macroscale properties of brain networks in which very large numbers of neurons and neuronal populations forming distinct brain regions are interconnected by inter-regional pathways, forming large-scale patterns of anatomical and functional connectivity. The characterization of cerebral connections at the macroscale attempts to identify anatomically distinct portions of the brain characterized by different pattern of connectivity that, together, shape large brain systems.

To date, brain connections have been non invasively assessed in humans using techniques focused on three general network properties: anatomical, functional and effective connectivity (Fox et al., 2012).

The first of these, anatomical connectivity, refers to a network of physical or structural connections linking sets of neurons or neuronal elements, as well as their associated structural biophysical attributes encapsulated in parameters such as synaptic strength or effectiveness. The physical pattern of anatomical connections can be considered relatively stable at shorter time scales, while it is likely to change in morphology and plasticity at longer time scales (Sporns et al., 2007).

It has been established that knowledge of anatomy is important to define the connectivity space thereby providing plausible biological constraints for theories and inferences about neuronal interactions when analyzing functional data (Lee et al., 2003a). Anatomical connectivity has relied predominantly on

diffusion imaging techniques (Fox et al., 2012), such as Diffusion Tensor Imaging (DTI), which is able to characterize the main white matter tracts of the brain in vivo.

The second network property, functional connectivity, is defined as a correlation between remote neurophysiological events in temporal domain (Friston et al., 1993a; Horwitz, 2003). It fundamentally represents a statistical concept. In fact, it investigates whether two regions share mutual information, that is to say the degree to which they have similar behaviour or statistical interdependence. In other words, the characterization of brain activity in terms of functional connectivity is 'model free' (Lee et al., 2003a): functional connectivity is often calculated between all elements of a system, regardless of whether these elements are connected by direct structural links. In that sense, it does not make any explicit reference to specific directional effects or to an underlying structural model (Sporns et al., 2007). In the last few years, functional connectivity has been assessed using a wide variety of technique, including neurophysiological methodologies such as electro- and magnetoencephalography (EEG/MEG), positron emission tomography (PET) and functional magnetic resonance imaging (fMRI) (Fox et al., 2012).

A third network property that has served as the basis for non-invasive assessment of human brain connectivity is effective connectivity. It is defined as the influence that one neural system exerts over another either directly or indirectly (Friston et al., 1993b). It describes networks of directional effects of one neural element over another. For this reason effective connectivity may be

considered as the union of structural and functional connectivity. In principle, the study of the brain's response to a perturbation or stimulation or time series analysis represents the best approaches to infer causal effects (Sporns et al., 2007). In that sense, while functional connectivity emphasizes pairwise interaction, often in terms of correlations or covariance, the effective connectivity approach incorporates additional information, such as anatomical connections and/or neurophysiological parameters, considering the interaction between several components to quantify the effect one element has on the another (McIntosh, 1999). This additional information, however, comes at the price of the need to identify regions of interest *a-priori*, thus limiting the detection of interactions to a pre-selected network. Moreover, the analysis can be conducted only to identify the relationships between a limited number of brain areas, compromising the study of complex brain networks.

The availability of these non-invasive techniques has prompted neuroscientists to characterize the wiring diagram of the human brain (Sporns 2005). These efforts have led to a number of multi-centric projects aiming at depicting the "human connectome". The main one is the Human Connectome Project (HCP) (http://www.humanconnectomeproject.org/), (Van Essen et al., 2013), led by Washington University, University of Minnesota, and Oxford University (the WU-Minn HCP consortium). The aim of this and other similar projects is to comprehensively map the human brain circuitry in a target number of 1200 healthy adults using resting-state fMRI, diffusion imaging, task-related fMRI, magnetoencephalography and electroencephalography

(MEG/EEG). In addition, behavioral data will be related to brain circuits to characterize individual differences in cognition, perception, and personality.

The size and the attention received by these initiatives result from the realization that examining the brain as an integrative network of anatomically and functionally interacting brain regions can provide new insights about large-scale neuronal communication. It provides a platform to examine how cerebral connectivity and information integration relates to human behavior and how this organization may be altered in several diseases (Bullmore and Sporns, 2009).

Indeed, it is becoming increasingly recognized that many behavioral manifestations of neurological and psychiatric diseases are not solely the result of abnormality in one isolated region but represent alterations in brain networks and connectivity (Fox et al., 2012). Thus, the improved characterization of brain networks can have an enormous relevance in discovering the basis of common disorders of the brain, response to recovery from brain injury, individual differences, heritability, normal development and aging.

While all relying primarily on DTI and fMRI, a broad range of neuroimaging network analysis approaches to study brain connectivity have been proposed. In the last few years, in fact, novel techniques and analysis methods have enabled the examination of whole brain connectivity patterns, enabling the in-vivo examination of functional and anatomical connectivity on a whole-brain scale (van den Heuvel and Hulshoff Pol, 2010).

In this context, the aim of the present work is to examine different aspects of brain connectivity by using various approaches. Some of the experimental designs were carried out in order to examine the importance of traditional techniques in determining differences between healthy controls and patients affected by different pathologies (Chapter 1 and 2).

In addition, two other studies have been performed to assess the validity of combining neuroimaging and neurophysiological techniques to explore brain networks in groups of healthy controls (Chapter 3 and 4).

The work described in this thesis thus offers some contribution towards the comprehension of the organization of brain networks both in physiological and pathological conditions, and provides new evidence of the importance of neuroimaging techniques in the characterization of the human brain.

CHAPTER 1:

NEUROIMAGING AND NEUROPHISILOGICAL TECHNIQUES TO STUDY BRAIN CONNECTIVITY

1.1 PRINCIPLES OF MAGNETIC RESONANCE IMAGING

Magnetic resonance (MR) imaging is well established as both a diagnostic and research tool in many areas of medicine because of its ability to provide excellent contrast between soft tissue.

To better understand Magnetic Resonance Imaging, it is worth describing the basic physical concepts and the mechanisms at the basis of image acquisition.

Production of a magnetic field

In MRI, the static magnetic field (conventionally called B_0) is typically generated by superconducting magnets. The production of the B_0 field comes from a large electric current that flows through a loop of wires immersed in liquid helium at superconductive temperature. In these conditions, the wires have no electrical resistance and therefore can carry large amounts of electrical current with no losses.

Conventionally, in the MRI system frame of reference, the direction parallel to the main magnetic field is the longitudinal direction (also called the "z") and it corresponds to the head-to-foot orientation in the most common MRI systems. The plane perpendicular to this direction is called the transverse plane or the x-y plane.

Hydrogen Protons

Nuclear magnetism is at the basis of the MRI signal. Nuclear magnetism is a form of paramagnetism that characterizes all nuclei with an odd number of protons and/or neutrons. Hydrogen is the most frequently imaged nucleus thanks to both its great abundance in biological tissues (in the form of water molecules) and its particular magnetic properties. In simple terms, the proton in the hydrogen nucleus is positively charged and spins about its axis, thus acting like a tiny rotating magnet that could be represented by a vector. The sum of all the tiny magnetic fields of each proton (called spins) is called net magnetization or macroscopic magnetization.

Net magnetization

In the absence of an external magnetic field, vectors are randomly oriented so that their magnetic fields do not add up but rather cancel out. Thus, the sum of all the spins gives a null net magnetization. When placed in a strong magnetic field (B_0), however, approximately half of the spins will tend to align in the direction of the magnetic field (parallel - low energy state) and the remainder will align in the opposite direction (anti-parallel - high energy state).

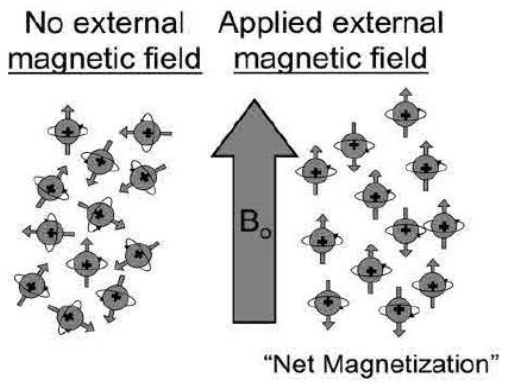

Fig. 1: Reproduced from (Pooley, 2005). Alignment of protons with b0 field

The magnetic fields from many protons will cancel out, but a slight excess of the protons will be aligned

with the main magnetic field, producing a "net magnetization" with a longitudinal component aligned with B_0 (Fig.1).

Precession

Precession corresponds to the gyration of the rotating axis of a spinning body about an intersecting axis. If the hydrogen protons that are spinning and acting like tiny magnets are placed in a magnetic field, the force from the magnetic field interacts with the spinning protons and results in the precession of the protons.

The proton precessional frequency is determined by the Larmor equation, in which the frequency of precession, f, is proportional to the main magnetic field strength

($f = \gamma B0$) through a constant γ known as the gyromagnetic ratio. The gyromagnetic ratio is specific to a given nucleus. For hydrogen, γ is 42.6 MHz T^{-1}.

Resonance

Resonance is the process that promotes the exchange of energy between two systems at a specific frequency. Magnetic resonance can be achieved through the energetic interaction between spins and electromagnetic radiofrequency (RF).

Radiofrequency Energy

In MRI, RF energy comes in the form of rapidly changing magnetic and electric fields. The magnetic component of the RF field is often referred to as B_1. Typically the RF is transmitted for a short period of time and for this reason it is called "RF pulse". If an RF pulse is generated by an RF transmit

coil at the precessional frequency of the protons (given by the Larmor equation) the resonance process will occur with a transfer of energy from the RF coil to the protons (excitation) with a consequent modification of spin equilibrium. According to the Larmor equation, the operating frequency of an MRI scanner depends on the static magnetic fields (γB_0): 1.5T scanners operate at 64 MHz, while 3T scanners operate at 128 MHz.

MRI signal: Action mechanisms

When protons in our body are placed in a strong magnetic field, the excess of spins parallel to the main field form a net magnetization pointing in a direction parallel to B_0 (longitudinal magnetization). At the quantum level, this results from the RF pulse providing enough energy to cause a single proton to jump to a higher energy state. At macroscopic level, this process is described as the spins beginning to precess around the RF magnetic field B_1, as well as around B_0. This results in the macroscopic net magnetization vector spiralling down (nutating) towards the XY plane. In a frame of reference rotating around z at the Larmor frequency, the net magnetization vector simply tips down during excitation, by an angle (flip angle) that depends on the strength and duration of the RF pulse. During excitation, the longitudinal component of magnetization decreases while a transverse component of magnetization is formed and gradually increases. At microscopic level, the decrease of longitudinal magnetization is due to an increase in the number of spins in anti-parallel state, while the generation of transverse magnetization is due to spins starting to precess in phase. Let us consider the case of 90° flip

angle for example: when the RF pulse is turned off, no longitudinal magnetization can be detected (equal proportion of parallel and anti-parallel spins) and the transverse magnetization assumes its maximum value (complete phase coherence).

Relaxation is the process that governs the return to equilibrium of the net magnetization combining two different mechanisms: the recovery of longitudinal magnetization (longitudinal relaxation) and the transverse magnetization decay (transverse relaxation). The rates at which these processes occur are governed primarily by three relaxation times - T1, T2, and T2*. Details of them are given in the next sections.

MR signal detection is obtained using receiver coils, thanks to the property of a magnetic field near and perpendicular to a loop of wire of producing an electric current in the loop. In this case, the magnetic field is the transverse magnetization. When the transverse magnetization is completely in phase, the measured MR signal is at a maximum. After the RF pulse is turned off, the transverse magnetization begins to dephase and the measured MR signal begins to decrease until the magnetization is completely dephased, at which time the measured MR signal is zero.

T1 relaxation and contrast

The longitudinal relaxation is also known as T1 relaxation. By definition, T1 is the time necessary for longitudinal magnetization to reach 63% of its maximal value and it depends on the molecular interaction at the level of different tissues (Fig.2). For this reason, the rate at which relaxation occurs is

different for protons associated with different tissues: this difference represents the fundamental source of contrast in T1-weighted images. In particular, White Matter (WM) has a very short T1 time (relaxes rapidly); cerebrospinal fluid (CSF) has a long T1 (relaxes slowly); Grey Matter (GM) has an intermediate T1. Thus, in the T1 weighted images WM, CSF and GM appear respectively with lighter, darker and intermediate intensity. It is important to note that the more the curves are separated at the time of acquisition, the higher is the T1

weighted contrast

.A)

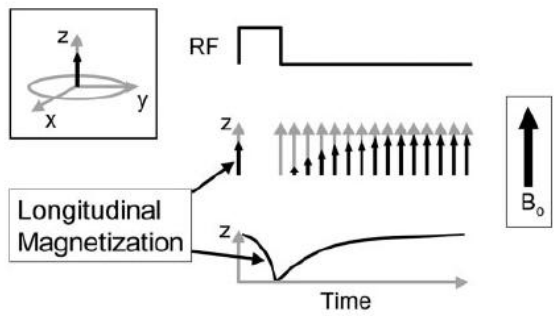

B)

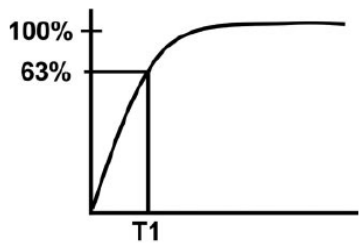

Fig. 2 Reproduced from Pooley et al.,2005 (Pooley, 2005) a) definition of t1.b) longitudinal t1 relaxation. Application of a 90° rf pulse causes longitudinal magnetization to become zero. Over time, the longitudinal magnetization will grow back in a direction parallel to the main magnetic field.

T2 Relaxation and Contrast

Transverse relaxation is also called T2 relaxation. During the RF pulse, the protons become "in phase" and the transverse magnetization increases. Immediately after the 90° RF pulse, the protons begin to dephase and the transverse magnetization starts to decay.

By definition, T2 is the time that it takes for the transverse magnetization to decay to 37% of its original value. T2 is a parameter correlated to the different amount of water and the different rate of dephasing for the protons associated with different tissues: WM has a short T2 (dephases rapidly); CSF has a long T2 (dephases slowly); GM has an intermediate T2 (dephases at a slightly slower pace than WM). Thus, in the T2 weighted images CSF, WM and GM appear respectively with lighter, darker and intermediate intensity. It is possible to take advantage of these differences and produce images based on this contrast mechanism, called T2-weighted.

The dephasing of the protons is due to several effects: spin-spin interactions, magnetic field inhomogeneities, magnetic susceptibility, chemical shift effects. Dephasing normally occurs due to all four effects (phenomenologically described by T2* decay or T2* relaxation). The spin echo is a "trick" that can be used to recover dephasing due to all effects except spin-spin interactions. After a 90° RF pulse, protons that were in phase begin to dephase in the transverse plane. After a certain amount of time, if a 180° RF pulse is applied, the spins are rotated over to the opposite axis, so that, after an interval equal to that between the 90^{o} and 180^{o} pulses, they are

rephased, creating what is called an "echo". If several 180° RF pulse are applied, the curve formed by connecting the peaks of the echoes represents decay by T2 effects (spin-spin interaction) (Fig.3).

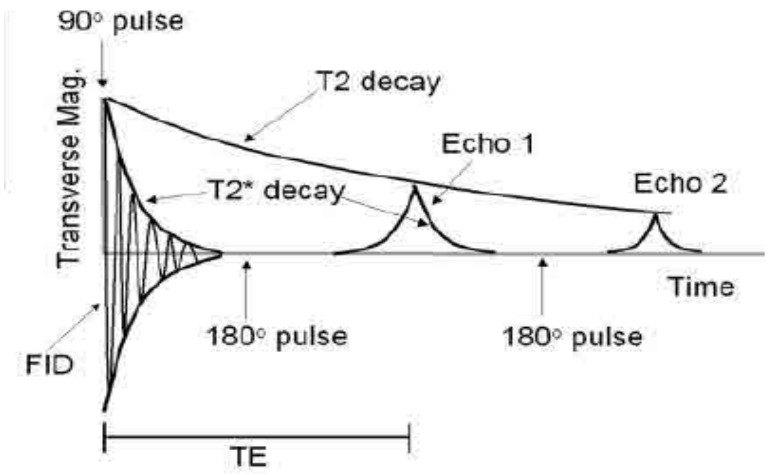

Fig. 3 Reproduced from Pooley et al.,2005 (Pooley, 2005) formation of spin echoes. Application of a 90° rf pulse results in an immediate signal (called a free induction decay [*fid*]), which rapidly dephases due to t2* effects. Application of a 180° rf pulse will allow formation of an echo at a time *te*. Multiple 180° pulses will form multiple echoes.

It's important to note that the T1 and T2 relaxation processes occur simultaneously. After a 90° RF pulse, dephasing of the transverse magnetization (T2 decay) occurs while the longitudinal magnetization grows back parallel to the main magnetic field. In brain tissue, usually T1 is longer than T2 (by approximately a factor of 10).

Image acquisition parameters: TE and TR

TE (Echo Time) is the time between the peak of the 90° RF pulse and the centre of acquisition time. TR (Repetition Time) is the time between 2 subsequent excitation pulses (i.e., the time it takes to run through the pulse

sequence one time). Both TE and TR can be used to control the contrast of the MRI images: varying their values, in fact it is possible to obtain T1, T2 or proton density weighted images. Beside the relaxation times, other biophysical processes can affect the MR signal and thus be used to vary the contrast on MR images. Some of these advanced techniques are particularly useful for characterizing brain connectivity and will be described in the next section.

1.2 DIFFUSION-WEIGHTED AND DIFFUSION TENSOR IMAGING PRINCIPLES

The most widely employed structural MRI technique to study anatomical connectivity is diffusion weighted imaging (DWI). It is sensitive to the micro-movements of water molecules inside voxels and it can be considered as the only tool currently available to evaluate the degree of water diffusion noninvasively, offering the possibility to probe the microstructural properties of biologic tissues. In order to explain the principles of DWI, some basic concepts are reviewed in the following sections.

Brownian motion

The term "Brownian motion" refers to constant random microscopic molecular motion due to thermal agitation. At a fixed temperature, the rate of diffusion can be described by the Einstein equation: $\langle r^2 \rangle = 6Dt$, where $\langle r^2 \rangle$ is the mean squared displacement of the molecules, t is the diffusion time, and D is the diffusion constant, a constant of proportionality for the particular

substance being measured (Mukherjee et al., 2008).Water molecules within tissue move according to this process.

Diffusion coefficient

The diffusion coefficient, typically expressed in units of square millimeters per second, relates the average displacement of a molecule over an area to the observation time, with higher values of this constant indicating more mobile water molecules.

Apparent diffusion coefficient (ADC)

Thanks to the high sensitivity of MRI to any kind of motion, it is possible to measure the water diffusion coefficient in-vivo using DWI. When the technique was first introduced, it was observed that this experimental measurement could not separate diffusion from other sources of water mobility, such as active transport, flow along pressure gradients, and changes in membrane permeability (Mukherjee et al., 2008), and the term "apparent" diffusion coefficient (ADC) was introduced. This also refers to the fact that the diffusion coefficient of water within tissue is always lower than the diffusion coefficient of free water at body temperature.

Isotropic diffusion

Diffusion is isotropic when molecular motion is equally fast in all directions. The property of isotropy depends on the medium where diffusion takes place. In biological tissue, diffusion is isotropic in CSF and all homogeneous tissues.

Anisotropic diffusion

In anisotropic diffusion, molecular motion is not equally fast for all directions. The hidnrance can be due to the presence of obstacles that limit molecular

movement in some directions more than in others. WM tracts are a typical example of anisotropic diffusion: tightly packed coherently oriented fiber bundles hinder water displacement perpendicular to the direction of the fibers.

Diffusion weighted imaging

In order to obtain a diffusion weighted image, it is necessary to add a pair of diffusion-sensitizing gradients, also known as motion-probing gradients, to a T2-weighted spin-echo sequence. The diffusion gradients are applied along the same directional axis both before and after the 180° refocusing pulse (Fig. 4).

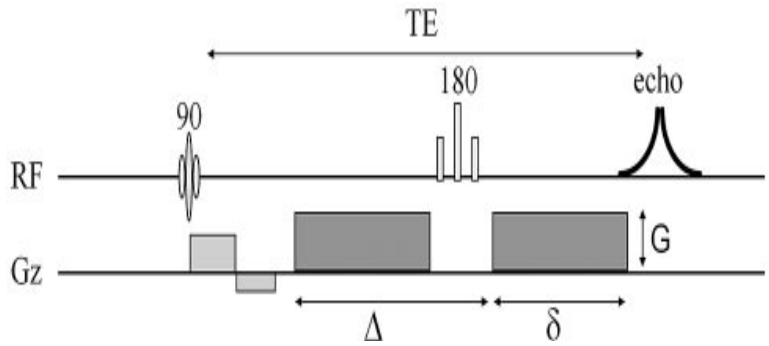

Fig. 4 Reproduce from Mukherjee et al.,2008 (Mukherjee et al., 2008). Pulse sequence diagram for a diffusion-weighted acquisition.2 diffusion sensitizing gradients added to a spin-echo sequence.

If spins were stationary, the amount of dephasing accumulated during the first gradient would be identical and opposite to that accumulated during the second one. However, since protons are transported by diffusion, there will be an incomplete rephasing of water proton spins, and a consequent attenuation of the spin echo.

This diffusion-weighted contrast can be fit to an exponential model:

$S_i = S_0 \exp(-b\ ADC_i)$

where S_i is the diffusion-weighted signal intensity observed at a given voxel with the diffusion-sensitizing gradients applied along direction *i*, S_0 is the signal intensity at the same voxel measured without diffusion-sensitizing gradients, and ADC_i is the ADC in the *i* direction (Mukherjee et al., 2008). The combination of three images obtained with three gradients with three different direction gives rise to an ADC map, commonly used in clinical practice to identify cerebral ischemia.

The diffusion-weighting factor, b, in the above equation depends on the amplitude of the diffusion gradient (G), the duration of each diffusion gradient (δ), and the interval between the onset of the diffusion gradient before the refocusing pulse and that following the refocusing pulse (Δ). Because of the presence of the motor-probing gradients, diffusion-weighted sequences are also very sensitive to bulk motion. For this reason, data are usually acquired using single-shot techniques, such echo-planar imaging (EPI).

Diffusion tensor imaging

When diffusion is isotropic, the choice of direction for the diffusion sensitizing gradient in not important because ADC_i is identical for any direction *i*. Instead, more than one diffusion-encoding direction is required to characterize regions of anisotropic diffusion. Acquiring DWI images with diffusion-sensitization in different directions allows the magnitude, the preferred orientation, and the degree of anisotropy to be determined at once.

To fully describe the degree and direction of anisotropy, diffusion is often modelled as a tensor.

Diffusion tensor imaging (DTI) requires the combination of a series of DWI acquisitions, with encoding in different directions to allow the determination of the diffusion tensor. The most intuitive way to conceptualize the information provided by the diffusion tensor is to view it geometrically. The tensor effectively fits the angular variation of the ADC values to the shape of a 3D ellipsoid.

The diffusion ellipsoid is a shape defined by 6 variables that describes the ADC of water molecules in each direction at a particular time (Mukherjee et al., 2008). The tensor is fully characterized by three orthogonal eigenvectors and their associated lengths, or eigenvalues ($\lambda 1$, $\lambda 2$, $\lambda 3$). The shape of the ellipsoid contains information about the directional dependency of the diffusion signal (Fig. 5).

Because of the symmetry of the tensor (the elements of the tensor above the diagonal are always equal to those below the diagonal), only six elements are independent. For this reason, the calculation of the tensor requires at least six different directions of diffusion-encoding.

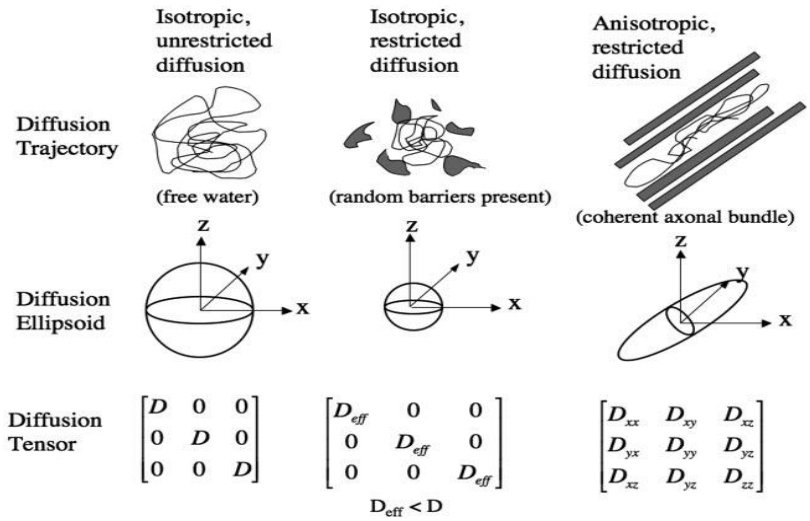

Fig. 5 Reproduce from mukherjee et al. (Mukherjee et al., 2008). The diffusion ellipsoids and tensors for isotropic unrestricted diffusion, isotropic restricted diffusion, and anisotropic restricted diffusion are shown.

Fractional anisotropy

Within the tensor model, directional dependency is quantified by the parameter fractional anisotropy (FA) (Pierpaoli and Basser, 1996), which is calculated from the eigenvalues of the tensor and ranges from zero (fully isotropic) to one (fully anisotropic); typical values for WM of the corpus callosum are 0.6–08.

1.2.1 DIFFUSION-WEIGHTED IMAGING PROCESSING

Diffusion anisotropy describes how variable the diffusion is along different directions and is most commonly quantified via a fractional anisotropy (FA) (Pierpaoli et al., 1996). FA is a useful quantity to compare across subjects as it is computable voxelwise, and is a scalar value that is independent of the local fibre orientation (and therefore a relatively objective and straightforward

measure to compare across subjects). Other useful parameters are represented by the three eigenvalues, which express the magnitude of diffusion along the principal axes of diffusion, and their average, the mean diffusivity (MD). Moreover, Song et al. (Song et al., 2002) introduced the idea that the principal eigenvalue reflects "axial diffusivity" (Dax) and the average of the second and third eigenvalues the "radial diffusivity" (Drad). Animal studies suggest that these 2 indices can be used to characterize axonal and myelin damage, respectively. Thanks to this increased specificity, they have become very popular for the assessment of white matter alterations (Wheeler-Kingshott and Cercignani, 2009) .

The steps involved in obtaining these parametric maps starting from a a series of diffusion-weighted EPI data are summarised below.

The first step is represented by the correction for eddy-current induced distortions. When a magnetic field is time-varying (such as a ramping up/down diffusion-encoding gradient), electric currents (eddy currents) will be generated in nearby conductors, generating local magnetic field gradients that will either add to or subtract from the gradients that are used for spatial encoding. Eddy currents result in geometric distortions which can be represented by a shift, a shear and a stretch of the image, which vary with the diffusion gradients (Haselgrove and Moore, 1996). Thus, in order to compensate for both, involuntary motion and eddy current distortions, all the diffusion-weighted volumes are often co-registered onto the first b0 volume. Co-registration is an operation that attempts to match the shape of differing

images based on the maximisation (or minimisation) of a function that reflects the similarity between the two images.

Once the raw data that have been corrected for eddy-current induced distortions and subject motion, the next stage is to estimate the tensor in each voxel. Estimation of the diffusion tensor within each voxel requires the acquisition of images with diffusion-encoding gradients applied along non-collinear and non-coplanar directions (Jones and Cercignani, 2010). The diffusion-weighted signal intensity, DWI_m, obtained with the diffusion-encoding gradients applied along the m^{th} vector direction, is given by

$$DWI_m = I_0 \exp(-\mathbf{B}_m \mathbf{D})$$

where I_0 is the signal intensity in the absence of the diffusion gradients, $\mathbf{B}_m$ is the B matrix describing the direction and the amplitude of the diffusion gradients for the m^{th} measurement, and **D** is the diffusion tensor, i.e., the quantity we want to estimate.

This equation can be fitted to the data using linear least squares, a method that minimizes the sum of squared distances between the observed responses in the dataset, and the responses predicted by the linear equation. There are three widely used approaches used for estimating the tensor in the literature. The first is nonlinear least squares (NLLS), second is weighted linear least squares (WLLS) and the most popular is ordinary least squares (OLS) (Jones and Cercignani, 2010).

Once the tensor is estimated, the usual practice is to derive the three eigenvalues (and associated eigenvectors) and use these to derive scalar indices, including the trace or mean diffusivity, and the anisotropy.

For the purpose of the studies presented in this thesis, DWI data were processed according to a number of differing approaches, including tract-based spatial statistics, connectivity-based segmentation, and tractography. An overview of each of them is given below.

1.2.2 TRACT BASED SPATIAL STATISTICS

In the context of a group comparison study, there are many ways of obtaining relevant intensities from the maps of these parameters in a format suitable for a statistical comparison.

One of the most popular approaches is voxel-wise comparison. This method relies on the accurate alignment of images from different subjects onto a common template, to achieve a correspondence between a particular voxel position in each image and the same anatomical structure across subjects. Voxel-wise statistics is then carried out across the whole brain, removing the need for making an a priori spatial selection.

This method has some limitations: a successful alignment of topological characteristics can be achieved without an exact alignment of WM tracts; the need for "smoothing" (a blurring of the image, achieved by spatial filtering with (usually) a 3D Gaussian kernel) to increase the signal-to-noise ratio, increases also the degree of partial volume and compromises the exact localization of between-group changes.

Tract Based Spatial Statistic (TBSS) was introduced in 2006 by Smith and collaborators (Smith et al., 2006): it provides an alternative method to voxel-wise statistics addressing some of its limitations. In order to ensure that registration of every subject's data to a common space has been totally successful and to solve the problems of arbitrary choice of smoothing extent, a carefully tuned nonlinear registration, followed by projection onto an alignment-invariant tract representation (FA skeleton) was introduced. This projection is achieved by searching perpendicular to the local skeleton structure for the maximum value in the subject's FA image. This maximum value is assumed to represent the nearest relevant tract centre. The introduction of this additional step makes the spatial smoothing not necessary in the images processing. Running TBSS first involves running a few simple steps, which are implemented in a series of scripts freely available with the FMRIB software library (FSL, www.fmrib.ox.ac.uk/fsl/):

- apply nonlinear registration of all FA images into standard space
- create the mean FA image and skeletonise it
- project all subjects' FA data onto the mean FA skeleton
- feed the 4D projected FA data into general linear model framework to perform voxel-wise statistics.

TBSS steps are reported below.

1-Non linear registration

The alignment of all FA images to a common target is obtain using nonlinear registration, necessary to avoid either extreme: it is important to align subjects' data together to make local comparison possible, but with some restriction applied to the applied warp so that the overall structure topology is preserved. The target image used in the registration can either be pre-defined or can be automatically chosen to be the most typical subject in the study.

2 - Creation of mean FA and skeleton

After target selection, all subjects' FA images are aligned to this, and then the entire aligned dataset is affine-transformed into $1x1x1mm^3$ MNI152 space; all subsequent processing is carried out using this space and resolution. The transformed FA are averaged to create a mean FA image that is then fed into the tract skeleton generation, which aims to represent all tracts which are "common" to all subjects.

The skeleton represents each such tract as a single line (or surface) running down the centre of the tract. To search for the centre of each tract, at each voxel the FA value is compared with the two closest neighbours on each side, in the direction of the tract perpendicular. If the FA value is greater than the neighbouring values, then the voxel is marked as lying on the skeleton. If all the processing so far has worked well the skeleton should look like the examples shown in Fig. 6

3 – FA Projection onto the skeleton

The last TBSS script carries out the final steps necessary before voxelwise cross-subject stats. Each subject's aligned FA image is projected onto the

mean FA skeleton (Fig 2.3). The aim is to account for residual misalignments between subjects after the initial nonlinear registrations. At each point in the skeleton, this script searches a given subject's FA image in the (already-computed) perpendicular tract direction to find the maximum FA value, and assigns this value to the skeleton voxel. This effectively achieves alignment between the skeleton and this subject's FA image without needing perfect nonlinear pre-registration. Any systematic difference in exact tract location between groups of subjects will thus not bias the comparison of FA values between the groups (Smith et al.,2006).

4 - voxelwise statistics on the skeletonised FA data

Voxel-wise statistics is carried out across all voxels in the skeleton to identify areas of FA differences between two groups or to correlate FA values to specific parameters. If WM structure alignment is successful, the data should be normally distributed and there is no need for smoothing. In order to further remove the need for smoothing, very often the analysis is carried out using permutation tests. To achieve this object the FSL tool "randomize" can be used. It is a simple permutation program enabling modelling and inference using standard GLM design set. Two options for this type of correction are available:

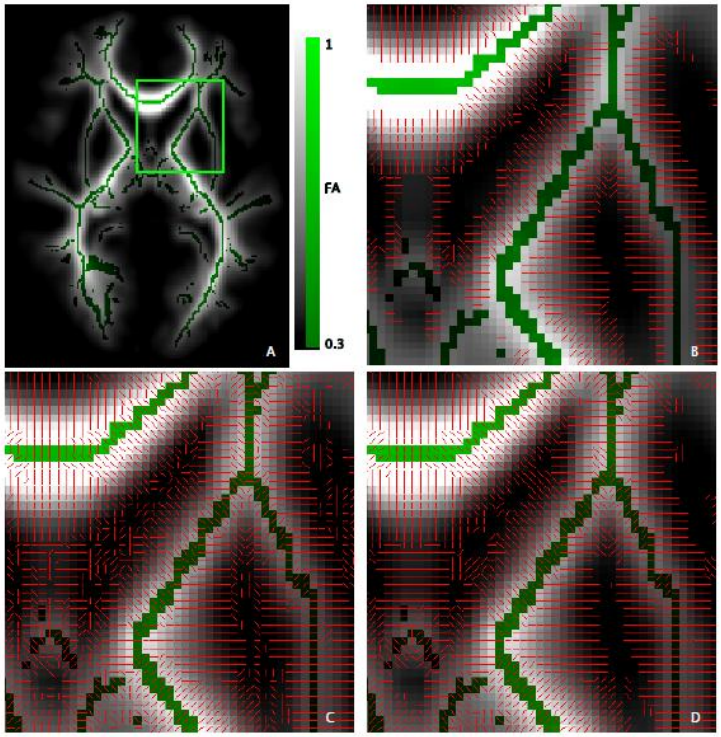

Fig. 6 Reproduced from Tract-Based Spatial Statistics: Voxelwise Analysis of Multi-Subject Diffusion Data (Smith et al,2006). Different skeletonisation stages. A: original mean FA image with final skeleton and the ROI used for the remaining subimages. B: skeletonisation stage 1, using local FA centre-of-gravity to find tract perpendiculars. C: skeletonisation after stage 2, using FA image second-derivative to find remaining perpendiculars. D: result of smoothing the perpendicular direction vector image

- Voxel-level correction, obtained by using the null distribution of the maximum (across the image) voxel-wise test statistic.
- TFCE (Threshold-Free Cluster Enhancement) is a new method finding "clusters" in your data without having to define cluster in a binary way (Smith and Nichols, 2009). Cluster-like structures are enhanced but the image remains fundamentally voxel-wise. This option was used in the present study.

In the present work TBSS has been used to assess differences in diffusion indices (such as FA, MD, Dax, Drad) to indirectly asses regional alterations of white matter fibers in the left (non-lesioned) hemisphere of patients with neglect. Moreover, the same approach has been performed to evaluate the presence of correlations between FA and clinical or neuropsychological variables in the same cohort. The aim of study was to indirectly assess the presence of disconnection between hemispheres in patients with right brain damage, and its contribution in determining the presence and severity of neglect (Chapter 2).

1.2.3 TRACTOGRAPHY

DTI essentially provides three types of information about the property of water diffusion: the magnitude of diffusion, the extent of diffusion anisotropy and its orientation. By assuming that the largest principal axis of the diffusion tensor aligns with the predominant fiber orientation in an MRI voxel, a 3D vector field representing the fiber orientation at each voxel can be obtained. The 3D reconstruction of tract trajectories, or tractography, is a natural extension of such vector field (Mori and van Zijl, 2002). Diffusion tractography is a general term indicating various methods of reconstructing WM pathways in vivo, based on the assumption that the principal direction of diffusion in WM is parallel to the main fibre direction in every voxel.

In most cases, tractography is initiated from a number of voxels, which constitute the “seed-points”, and the main WM tract traversing these voxels is followed until some stopping criteria (e.g. an anisotropy or curvature

threshold) are reached. Tractography can also be initiated from all voxels in the brain (brute-force approach) (Huang et al., 2004) and then only the tracts passing through some *a priori* specified regions are retained.

The most common application of tractography in clinical research is the extraction of a specific pathway and the calculation of diffusion parameters along it (Jones et al., 2006; Price et al., 2008; Yogarajah et al., 2008). In other words, these methods use tractography to identify voxels from which to take FA (or other parameters like MD) values for cross-subject comparison. Other types of application include the quantification of tract shape (Batchelor et al., 2006), cortical parcellation based in diffusion strength of connection (Behrens et al., 2003), and the develoment of new models of brain anatomy (Jones et al., 2006; Parker et al., 2003).

Two kinds of tractography can be performed. Deterministic tractgraphy follows directional estimates derived from a tensor model to reconstruct estimates of the path of fibre bundles. The basic assumption at the basis of deterministic algorithms is that the principal eigenvector is parallel to the main direction of fibres in every voxel, and therefore this type of algorithm produces a single trajectory (usually described as a *streamline*). The main shortcomings of such an approach are the inability to account for fibre branching, and to assess the level of confidence that can be assigned to a reconstructed trajectory (Jones and Pierpaoli, 2005).

The probabilistic approach (Behrens et al., 2003; Parker et al., 2003) aims to address these issues by considering multiple pathways emanating from a

single seed-point, and assigning a probability of connection to the seed-point to every voxel in the brain. At the tractography stage, rather than drawing a single line through direction estimates, sampling techniques are used to draw thousands of streamlines through this probability field to build up a connectivity distribution, where the density of streamline samples reflects the probability of interconnection with the seed voxel. There are many benefits from operating within a probabilistic framework (Johansen-Berg and Rushworth, 2009). First, tracking can continue in the presence of uncertainty and thus paths can be traced to their gray-matter targets. Second, these techniques provide a quantitative measure of the probability of a pathway being traced between two points; such measures can be used to perform quantitative comparisons between groups of subjects, although we should be cautious about how to interpret such values in biological terms. Finally, probabilistic models can be extended to fit multiple fiber populations (Behrens et al., 2007; Parker and Alexander, 2005; Tuch et al., 2003), a critical feature if paths are to be traced through regions of fiber complexity.

As mentioned above, one of the applications of DTI tractography is that it has enabled the parcellation of the cortex into functionally specialized subregions via their unique complement of connections *in vivo*. Connectivity based parcellation segregates a grey matter region on the basis of information about remote connectivity derived from tractography, effectively enabling a segmentation of the region based on its connectivity pattern (Behrens et al., 2003).

Several different tractographic parcellation approaches have been developed but all share the same core processing stages. Connectivity profiles are first established for each subunit within the cortical region to be parcellated. These connectivity profiles are subsequently compared via various measures of similarity, and clustered into regions such that within-cluster subunits share highly similar patterns of connections, whilst between-cluster connectivity profiles are markedly distinct (Cloutman and Lambon Ralph, 2012).

The determination of a connectivity profile for each subunit within the region under examination is possible by starting tractography from each seed within the brain area being parcellated and the target brain regions connected to each seed.

Two different approaches have been mainly used so far. They vary in relation to whether the profiles encompass information regarding connectivity from the seed to the whole brain (Anwander et al., 2007; Johansen-Berg et al., 2004; Mars et al., 2011; Tomassini et al., 2007) or a subset of key predetermined neuroanatomical regions (Beckmann et al., 2009; Behrens et al., 2003; Broser et al., 2011; Johansen-Berg et al., 2005; Leh et al., 2007).

One of the main advantages of this latter method is represented by the ability to infer functional roles to the delineated subregions and assess explicit structure-function hypotheses. However the discrimination of functional subdivisions that may exist within the regions identified is less fine. In contrast, using whole-brain connectivity patterns it is possible to discern all

anatomical/functional subdivisions within a cortical region and no *a priori* hypotheses is required before performing the connectivity based parcellation.

Several studies have been performed so far to parcellate different brain regions including the medial frontal cortex, inferior frontal cortex, precentral gyrus, postcentral gyrus, inferior parietal cortex, temporo-parietal junction, insula, and cingulated cortex, as well as a number of subcortical structures including the thalamus, sub thalamic nucleus, basal ganglia, amygdale and the substantia nigra. These studies pointed out the importance of tractography in the detection of distinct connectivity profiles to characterization the parcellation brain structures (Cloutman 2012). In the present thesis, the parcellation of the thalamus on the basis of its cortical connections has been carried out in order to evaluate the correspondence between anatomical and functional connectivity in a group of healthy participants (Chapter 4).

1.3 FUNCTIONAL IMAGING PRINCIPLES

Functional MRI (fMRI) measures local changes in magnetic susceptibility caused by variations in the capillary concentration of deoxyhemoglobin due to blood flow and blood volume increases in response to neuronal activation.

Most of the energy used for neuronal activity is expended as a result of the postsynaptic neuronal depolarisation and, to a lesser extent, the action potentials generated (Attwell and Laughlin, 2001). The energy cost therefore arises from information transfer and its integration postsynaptically. Substrate delivery for energy metabolism is increased with increased local blood flow.

The origin of the associated BOLD (blood-oxygenation level dependent) fMRI signal change lies in the different magnetic properties of haemoglobin carrying oxygen (oxyHb) and deoxygenated haemoglobin (deoxyHb). DeoxyHb is slightly paramagnetic relative to brain tissue, whereas oxyHb is diamagnetic (Pauling, 1977). Vessels containing oxygenated arterial blood thus cause little or no distortion to the magnetic field in the surrounding tissue, while capillaries and veins containing blood that is partially deoxygenated distort the magnetic field in their vicinity (Ogawa et al., 1990). The microscopic field inhomogeneities associated with the presence of deoxyHb lead to destructive interference from signal within the tissue voxel, a process that tends to shorten the T2* relaxation time. Thus, as oxygen extraction falls with enhanced local blood flow in a region of greater neuronal activity, the T2* becomes longer and the MRI signal intensity increases relative to the baseline state. The precise amount by which the MRI signal intensity increases depends on several factors. There is a contribution from water molecules in blood (the intravascular compartment) and from water molecules in the tissue space around the vessels (the extravascular compartment). The observed signal (BOLD) is a volume weighted average of signal changes both from intravascular water in local capillaries and veins and water in the immediate extravascular compartment.

BOLD signal change increases linearly with the static field strength of the MRI scanner for blood vessels that are of greater radius than approximately 8

mm and quadratically when considering blood vessels that are smaller than this value (Ogawa et al., 1993).

Typical fMRI research focuses on the change in BOLD signal caused by the neural response to an externally controlled stimulus task. The fMRI signal during ‘‘on’’ periods is contrasted with recordings during a baseline or control condition, resulting in the relative signal change because of the specific process being studied.

Recently, increased attention has been directed at investigating the features of the baseline state of the brain (Resting State fMRI). Even at rest, in fact, the spontaneous (intrinsic, not task evoked) BOLD signal is characterized by slow fluctuations (<0.1 Hz). It was noted more than a decade ago that spontaneous BOLD signal fluctuations are temporally correlated (or coherent) between brain regions of similar functionality (Biswal et al., 1995; Fox and Raichle, 2007).

RS-fMRI does not require any active cooperation from studied subjects, and allows to measure functional brain connectivity as expressed by synchronization of neural activity across different brain regions (Biswal et al., 1995; Friston et al., 1993b; Lowe et al., 2000). Some studies (Biswal et al., 1995; Damoiseaux et al., 2006; Lowe et al., 2000) investigating spontaneous neural activity within resting brains, identified synchronous fluctuations within anatomically separated regions by comparing the time courses (TC) of BOLD signal for each voxel in the brain.

There is an ongoing discussion as to whether these fluctuations in the BOLD signal predominantly reflect changes of the underlying brain physiology independent of neuronal function, or instead reflect the neuronal baseline activity of the brain when goal-directed neuronal action and external input are absent. The view that coherencies in resting fluctuations represent functional resting-state networks linked to underlying neuronal modulations is consistent with the appearance of these coherencies within cortical gray matter areas of known functional relevance (Damoiseaux et al., 2006).

Moreover, support for a possible neuronal basis of resting-state fMRI signals comes from the observation that most of the resting-state patters tend to occur between brain regions that overlap in both function and neuroanatomy (Biswal et al., 1995; Damoiseaux et al., 2006; De Luca et al., 2006; Lowe et al., 2000; van den Heuvel et al., 2008). Further support for this hypothesis comes from studies reporting that the observed spontaneous BOLD signals are mainly dominated by lower frequencies (< 0.1 Hz) with only a minimal contribution of higher frequent cardiac and respiratory oscillations (N 0.3 Hz) (Cordes et al., 2001).

Taken together, more and more studies are in support of a neuronal basis of the resting-state fMRI signal (van den Heuvel and Hulshoff Pol, 2010).

The most common task fMRI analysis techniques are model-based, using the onset and offset of an external stimulus to specify the model. In resting-state fMRI, by definition, no external stimulus is presented; therefore new analytic approaches had to be applied.

1.3.1 RESTING STATE DATA PREPROCESSING

Data preprocessing is a necessary step, in fMRI analysis, to correct for the variability in the experimental data that is not related to neuronal activity. A good pre-processing is essential because the measured BOLD signal is very small compared to the total intensity of the MR signal. Moreover, the task related signal change is very small compared to the total spatial and temporal variability across scans.

The preprocessing steps most commonly undertaken include: slice timing correction, head motion correction, co-registration with a high-resolution image, normalization and smoothing. Slice timing correction accounts for the fact that slices, which compose the total volume of the brain, are acquired at different times over TR. Most analysis techniques presume that every voxel is sampled exactly at the same time. Slice timing correction is particularly important when the TRs are long and the expected hemodynamic response may vary significantly between slices. The correction of head motion is needed because, despite the imposed physical restrictions to movement of the subject, involuntary motion and physiological motion are bound to occur and must be corrected for. This task is performed to ensure that each voxel represents a unique part of the brain (estimating the translations and rotations of motion). Additional physiological noise correction can also be performed. Co-registration is used to align the functional images with anatomical images that have better resolution, enabling the identification of the activations in the subject's individual brain. Normalization is the process of mapping the

obtained image into a standard anatomical space (usually in Montreal Neurorological Instute [MNI] coordinates) in order to allow a generalization of the results to a larger population. Doing this improves the comparison between other studies and subjects. Finally, the last step is the smoothing of the data, i.e., spatial filtering using achieved using 3D Gaussian kernels. Smoothing is used to improve both the signal noise ratio (SNR) (Lazar et al., 2008).

While these steps are sufficient for task fMRI, when dealing with RS-fMRI, data are often further filtered in the time domain to suppress high-frequency variations. This is typically achieved using low-pass filters with cut-off frequencies in the range of 0.08-0.12 Hz.

After preprocessing, data are further analyzed. Data processing strategies used for fMRI studies can be characterized into two major schemes: model-dependent and model-free methods. Multiple analysis techniques are used to look at the datasets. The most commonly employed ones are the seed based analysis (SBA) and the independent component analysis (ICA).

1.3.2 INDEPENDENT COMPONENT ANALYSIS

Model-free methods are designed to look for general patterns of (unique) connectivity across brain regions. Independent Component Analysis (ICA) represents one of the most widely used methods for model-free analysis. It is a statistical technique that does not involve any a priori assumption and allows the exploration of multiple whole-brain networks. ICA uses a mathematical algorithm to decompose a set of signals into independent components also

known as source signals. In particular, on the basis of the measured signals, ICA can reveal the hidden sources which have generated them, under the assumptions that sources are statistically independent. Independency can be imposed either in the time domain (temporal ICA) or in the spatial domain (Spatial ICA). For the purpose of RS-fMRI analysis, usually spatial ICA is used, and will be described here.

Introduced for the first time by McKeown et al. (McKeown et al., 1998), when applied to RS-fMRI, ICA is able to extract from the BOLD time series a number of independent components which are spatial maps associated with the time courses of the signal sources. Each component can be interpreted as a network of similar BOLD activity. These decompositions can simultaneously extract a variety of different coherent resting state networks (RSNs) and separate such effect from other signal modulations such as those induced by head motion or physiological confounds, such as cardiac pulsation or respiratory cycle (Damoiseaux et al., 2006).

The studies using ICA have shown a high level of consistency in the reported components suggesting that ICA is a powerful technique that can be applied to the study of multiple connectivity patterns (Calhoun et al., 2001; Esposito et al., 2008; van den Heuvel and Hulshoff Pol, 2010).

Specific (RSNs) have been identified investigating spontaneous neural activity in resting brains. The most widely studied RSNs include the so-called "*default mode network*" (DMN), connecting the precuneus and the posterior cingulate cortex to more frontal regions like the medial frontal cortices and

the inferior parietal regions (Damoiseaux et al., 2006; Fox and Raichle, 2007; Greicius et al., 2003). Another well-known network include the *core*, or *salience*, network, linking bilateral insular regions and anterior cingulate cortex (Dosenbach et al., 2007), which is important for monitoring the salience of external inputs and internal brain events. The *sensory-motor component* involves precentral gyrus, postcentral gyrus and supplementary motor area. It has been demonstrated that the sensory-motor network is associated with functionally relevant neural activity, that is, the spontaneous fluctuations observed in this network are likely to reflect the neural activity which subserves active motor tasks (Damoiseaux et al., 2006; Rosazza and Minati, 2011). Throughout literature up to three distinct *visual components* have been reported, one corresponding to mesial visual areas, the other associated with lateral visual areas, the last one associated with activity in the striate cortex and in polar visual areas. The different number of visual components observed across studies may be related to the effects that the choice of decomposition parameters and the intensity of physiological and other artefactual signal components have on ICA decomposition. The *Executive control component* is identifiable in medial frontal gyrus, superior frontal gyrus and anterior cingulate cortex. These regions are generally involved in tasks relying on executive functions, such as control processes and working memory. Two *lateralized fronto-parietal components* are commonly found through literature, one predominantly in the right hemisphere and the other in the left hemisphere usually with a specular pattern. They involve the

inferior frontal gyrus, the medial frontal gyrus, the precuneus, the inferior parietal. Although they have been demonstrated to be associated with memory, language, attention and visual processes, the role of this networks remain unclear. The *auditory component* involves superior temporal gyrus, Heschl's gyrus, insula and postcentral gyrus. This component show a good overlap with obtained using a text-listening task. The *temporo-parietal component* is characterized by the engagement of regions typically associated to language processing including inferior frontal gyrus, medial temporal gyrus, superior temporal gyrus, angular gyrus. Overall, these results support the view that patterns of resting-state functional connectivity reflect an intrinsic functional organization underlying cognitive processes (Damoiseaux et al., 2006; Rosazza and Minati, 2011).

One of the main advantages of using ICA is its ability to generate a 'complete' picture of the functional hierarchy of integrative and dissociative relationships making up the spontaneous and evoked activity of the human brain (Smith et al., 2009). RSNs identified by ICA can be less prone to artefactual effects from noise (including fluctuations in the mean global signal) than those of other techniques due to the ability of the method to account for the existence of such structured noise effects within additional (non- RSN) ICA components.

Nevertheless, this approach also has limitations. First, it can be difficult to determine whether a component represents physiological noise or a cortical network. Second, the decomposition results can vary depending on the choice

of number of components, and the exact separation pattern may be not repeatable from one subject to another (Rosazza et al., 2012). Next, the stochastic nature of ICA induces a degree of run-to-run variability, so results obtained from such an analysis can differ between analysis runs on even the same data. While approaches exist to optimally select the number of independent components for a given dataset according to statistical criteria, it must be recognised that there can be no single, 'best' dimensionality or model order for the underlying neurophysiology of multiple distributed systems. Further, one ICA decomposition of a given dataset may hide the fact that any given brain region may, over time, share varying connectivity patterns with multiple networks. This variability, or ambiguity, of regional co-activations between network nodes can be referred to as the 'non-stationarity' of a given area in terms of its connectivity with one or more RSNs (Cole et al., 2010).

An example of ICA analysis is reported in chapter 3, in which this approach has been compared with graph-based analysis in patients with amnestic Mild Cognitive Impairment patients (aMCI) at high risk of developing Alzheimer Disease.

1.3.3 SEED-BASED ANALYSIS

In the first resting-state fMRI study (Biswal et al., 1995), the time course of a seed region-of-interest (ROI) in the left motor cortex was correlated with the time course of all other brain voxels. The resulting map demonstrated functional connectivity between the left and right motor cortex even in the

absence of a task. Since its initial demonstration, this model-dependant approach has been widely applied.

This method called seed-based analysis (SBA), requires the a priori selection of a voxel, cluster or atlas region from which to extract time series data. Next, time series of the selected region can be correlated with the time series of the other voxels, in order to calculate whole-brain, voxel-wise functional connectivity maps of covariance with the seed region. The SBA technique has proven useful in revealing the connectivity properties of many seed areas, and has been applied in the literature by many groups (Fox et al., 2005; Greicius et al., 2003; Margulies et al., 2007).

The primary advantage of SBA over other methods is that the interpretation of the results is straightforward: it provides a direct answer to a direct question – it shows the network of regions most strongly functionally connected with the seed voxel. Recent assessment of the test-retest reliability of these methods has indicated that RSN connectivity relationships can be identified by SBA with moderate to high reliability (Shehzad et al., 2009). On the other hand, one potential weakness of SBA methods concerns the influence of structured spatial confounds, such as other RSNs (than the one under consideration) or structured noise, e.g., residual head motion effects or scanner-induced artefacts. Some of these effects may be partially removed by incorporating specific preprocessing such as temporal filtering , although the risk of residual confounding factors remains (Murphy et al., 2009). Moreover, there are as many possible ‘networks’ to be derived as there are possible seeds:

biologically, the choice of seed may bias connectivity findings towards specific, smaller or overlapping sub-systems, rather than larger, distinct networks (Buckner et al., 2008). Finally, an intrinsic limitation of this approach is that the seed ROI must be selected by the investigator, possibly inducing a selection bias.

In this thesis I performed SBA to estimate thalamo-cortical functional connection in a group of healthy subjects. The study was conducted using the thalamus as a model to assess the correspondence between functional and anatomical connections (Chapter 4). Moreover, the same approach was used to evaluate functional correlations to a region (the dorso-lateral prefrontal cortex) that was stimulated using transcranial magnetic stimulation (TMS). For details see chapter 5.

1.3.3 NETWORK ANALYSIS

Recently, new advances in RS analysis techniques have shown the possibility of examining the overall structure of the brain network still with high level of spatial detail, using graph analytical methods, thus providing new valuable insights in how the human brain operates.

Graph theory provides a theoretical framework in which the topology of complex networks can be examined, and can reveal important information about both the local and global organization of functional brain networks (Bullmore and Sporns, 2009; Sporns et al., 2005). The graph model of the brain is an abstract structure used to represent pairwise relations between interregional ensembles of neuronal elements, referred to as *nodes*. These

pairwise relations, or *links*, can be either of functional origin and represent coherent physiological activity between neuronal ensembles, or they can be of a structural origin and represent anatomical connections formed by white-matter fiber tracts (Zalesky et al., 2010).

For RS data, within such a graph theoretical framework, the nodes of the brain network can be represented as cortical regions, which can be a small number of large-scale brain regions based on a predefined cortical template (like the Brodmaan Areas template) or MRI voxels. The level of functional connectivity between two regions is computed as the level of correlations between the time-series of two brain regions. Computing the level of functional connectivity between all possible node-pairs and determining the existence of a functional connection by using a predefined cut-off threshold or by using a weighted approach, results in a graph representation of functional brain network and allows for the examination of its organization using graph theory. The correlation between each node is reported in a square matrix with binary elements called connectivity or adjacency matrices. The number of rows and columns in this matrix is the total number of nodes in the network, and the elements are defined as connectivity measure of choice of each pair of nodes.

The connectivity matrix defines a graph, representing the network, for which several topographical parameters of interest can be extracted in order to characterize the network properties and eventually compare them between groups. The graph can be directed (if the direction of each connection is

defined) or undirected. When based on DTI or RS-fMRI, graphs are undirected.

In the present thesis four of them were analyzed: node degrees, network completeness, clustering coefficient and global network efficiency (see Chapter 3).

The *node degree* describes the number of connections of a node to the rest of the network. This is the most fundamental network measure and most other measures are ultimately linked to the node degree. *Completeness* of a network is property of undirected graphs in which every pair of distinct vertices is connected by a unique edge. A complete graph has no sub-graph and all its nodes are interconnected. The *clustering coefficient* is calculated as the proportion of connections that exist between the nearest neighbours of a node over the maximum number of possible connections. *Path length* is the minimum number of edges that must be traversed to go from one node to another. *Efficiency* is inversely related to path length and describes topological distances between elements of disconnected graphs.

Based on graph theory, several tools have been implemented to study brain networks. One of them is represented by the Network Based Statistic Toolbox (NBS) (Zalesky et al., 2010). It is a validated nonparametric statistical method for performing statistical analysis on large networks. The user provides a series of connectivity matrices from different cohorts, or from the same subject during different experimental conditions. Connectivity matrices are inferred from RS data and they reflect the pairwise interactions for each node.

The method is used to control the family-wise error rate (FWER), in the weak sense, when performing mass univariate hypothesis testing on all graph edges. Rather than clustering in physical space, the NBS clusters in topological space, where the most basic equivalent of a cluster is a graph component. FWER-corrected p-values are calculated for each component using permutation testing.

In the present work, network analysis was performed to identify the effect of perturbation induced by transcranic magnetic stimulation on a group of healthy volunteers (Chapter 5). Also, network analysis was performed to assess if it can be considered relevant to the study of Alzheimer disease and may improve the differentiation between patients and controls by detecting disease-related changes and progression of pathology (Chapter 3).

1.4 TRANSCRANIAL MAGNETIC STIMULATION

Transcranial magnetic stimulation (TMS) is a technique that uses a magnetic field to produce indirect electrical stimulation of the brain (Barker et al., 1985). Faraday's law of induction states that when an electrical current is passed through a wire, it generates a time-varying magnetic field. If a second wire is placed nearby, the magnetic field induces electrical current flow in that second wire. In TMS, the 'first wire' is the stimulating coil and the 'second wire' is a targeted region of the brain. The most common coil in use in TMS is a figure-of-eight shape in which electrical current flows in opposite directions around each of the windings, converging at the centre-point where

the currents summate. This allows one to target focal regions of cortical tissue. The coil is placed on the scalp, and the resulting magnetic field passes through the skull and induces an electrical field in the underlying cortex (O'Shea and Walsh, 2007). This electromagnetic induction can be used to experimentally manipulate brain activity, and is capable of inducing long-term (ranging from minutes to days) changes in cortical excitability.

TMS can be used following different protocols. TMS pulses can be applied at varying intensities, and in single pulses or in repetitive trains (rTMS) of low or high frequency. The choice of stimulation parameters determines whether the effects of stimulation are excitatory or inhibitory. For example, two single pulses separated by less than 5 milliseconds can produce intra-cortical inhibition, while two single pulses separated by a gap greater than 10 and less than 30 milliseconds can produce intracortical facilitation.

Repetitive TMS at a frequency of 1 Hz has the effect of depressing cortical excitability for a period of time after the train of pulses has finished, whereas repetitive stimulation at 10 Hz or more may increase excitability (O'Shea and Walsh, 2007).

In the case of single pulses of TMS, the effect is not thought to last long beyond the time of stimulation (Pascual-Leone and Walsh, 2001). In contrast, when trains of multiple pulses of TMS are applied to the brain with a short inter-stimulus interval (1Hz or greater), the net effects are longer-lasting changes in cortical excitability, that can be sustained well beyond the time of stimulation (Pascual-Leone et al., 1994).

As explained above, rTMS is able to change and modulate activity beyond the stimulation period. An appealing hypothesis is that the effects of rTMS on the brain are long-term depression (LTD)-like or long-term potentiation (LTP)-like, as the duration of the effects seems to implicate changes in synaptic plasticity (Hoogendam et al., 2011).

LTP is an increase in the synaptic strength that could last for days or even weeks and months, which could be induced in experimental conditions as a result of brief high-frequency stimulation. LTD, on the contrary, encompasses long-lasting weakening of a neuronal synapse. The exact mechanisms underlying these plastic changes vary, depending on the synapses and the circuits in which they operate (Hoogendam et al., 2011). The fact that it may be possible to induce LTP/LTD-like changes in the human brain has important implications for therapeutic applications. In fact, the hope is that rTMS-induced changes of synaptic connections will promote recovery of function in parts of the brain damaged by an acute or a chronic lesion (Ridding and Rothwell, 2007).

1.4.1 THETA BURST STIMULATION

One approach for producing lasting effects in the brain is the recently introduced theta burst stimulation (TBS) protocol (Di Lazzaro et al., 2008). It refers to a rTMS protocol where pulses are applied in bursts of three, delivered at a frequency of 50 Hz and an inter-burst interval of 200 ms (5 Hz). These parameters were originally developed based on studies in both the

rodent and human brain indicating that theta rhythms are associated with LTP (Hill, 1978; Klimesch et al., 1996; Larson et al., 1986).

TBS protocols appear to lead to sustained changes in cortical activity lasting well beyond the duration of the TMS application, providing a putative index of underlying LTP and LTD processes that can be recorded in vivo from the human brain. Additionally, these effects appear to be dependent on NMDA (N-methyl-D-aspartate) receptors suggesting that the after-effects might be mediated by LTP-like synaptic plasticity (Huang et al., 2007). It is important to note that different patterns of delivery of TBS have different, opposite effects on excitability (Hoogendam et al., 2011). There are two commonly used patterns of TBS, continuous (cTBS) and intermittent (iTBS). In cTBS, bursts of 3 pulses at 50 Hz are applied at a frequency of 5 Hz for either 20 seconds (100 bursts) or 40 seconds (200 bursts). In iTBS, 20 2s periods (10 bursts) of TBS are applied at a rate of 0.1 Hz. Note that in both protocols the total number of stimuli is equal (600 pulses). It has been suggested that TBS in humans produces a mixture of facilitatory (iTBS increases motor evoked potential (MEP) amplitude producing an LTP like phenomena) and inhibitory (cTBS reduces (MEP) amplitude LTDlike phenomena) effect (Di Lazzaro et al., 2008; Hoogendam et al., 2011; Oberman et al., 2011).

Here, cTBS was performed to induce inhibitory effect over the right prefrontal area of healthy subject to identify its effect on functional connections at rest (Chapter 5).

1.5 COMBINATION OF NEUROIMAGING TECHNIQUES AND TMS

In the last decade combined TMS-neuroimaging studies have greatly stimulated research to characterize brain connectivity. The combination of different methodologies is necessary to compensate for the limitations of each technique alone, providing insight into a variety of neuroscience questions.

A first approach towards the combination of these techniques is to determine whether the "connectivity" assessed with RS-fMRI, DTI and TMS reflects the same pattern.

The functional repertoire of any system is ultimately determined by its structural composition. Equally important in the brain, the underlying structure is continually reshaped by function in relation to experience (Zhang et al., 2010). For that reason, as one might expect, connectivity assessed using either RS-fMRI or TMS is related to and constrained by underlying anatomical connectivity.

DTI has been shown to relate well with TMS (Voineskos et al., ; Wahl et al., 2007) and with RS-fMRI (De Luca et al., 2006; Greicius et al., 2009; Honey et al., 2009; Koch et al., 2002; Lowe et al., 2008; van den Heuvel et al., 2008; van den Heuvel et al., 2009; Zhang et al., 2010).

Nevertheless, differences between each technique do exist, underlying that each of them measures different aspects of connectivity.

It is important to note that connectivity assessed with either RS-fMRI or TMS, in fact, involves polysynaptic connections, while DTI is able to directly

detect only monosynaptic connections (Fox et al., 2012). In light of these differences, caution is warranted when inferring functional interactions strictly on the basis of DTI tractography, and vice versa. Each technique provides unique and complementary information that should be interpreted in their corresponding context (Zhang et al., 2010).

For what concerns the correlation between connectivity assessed with RS-fMRI and TMS, a study conducted by Koch and collaborators revealed a remarkable correlation between hemodynamic signals recorded by RS-fMRI and physiological interactions tested by TMS (Koch et al. 2012) when looking at parieto-frontal circuits.

Overall, by comparing results across different studies some useful insights can be gained (Fox et al., 2012). Both techniques have revealed results potentially consistent with excitatory versus inhibitory connections, however interpretations of these results is likely to be complicated. An important issue is the context dependence of measures connectivity. In fact, while accumulating evidence support the idea that TMS depends on task context (Koch et al., 2009; Koch and Rothwell, 2009; Ruff et al., 2009), the context dependence of connectivity assessed with RS-fMRI remains less clear, due to its poorer temporal resolution and inability to exert casual perturbations (Fox et al., 2012).

Finally, both methodologies have identified connectivity changes across a range of altered states including neurological and psychiatric disorders with both concordant and discordant results (Burt et al., 2002; Fox and Greicius,

2010; Greicius et al., 2007; Hallett, 2007; Zhang et al., 2010). Further studies should be performed in this direction to clarify the correspondence between these methodologies.

A second way to combine these methodologies is using neuroimaging techniques to guide TMS. In fact, several studies conducted so far have focused on the stimulation site alone and have not taken into account the distributed network properties of the targeted region (Fox et al., 2012). Despite its potential, surprisingly few studies have used distributed network connectivity to guide TMS target selection.

In an excellent example of how connectivity can guide TMS, DTI was used to identify subject-specific targets in the middle frontal gyrus that were connected to a particular portion of primary somatosensory cortex (Hannula et al., 2010). A few studies have used task-based fMRI measures (as opposed to RS-fMRI) to identify stimulation targets (Bien et al., 2009; de Graaf et al., 2009; Zanto et al., 2011). Finally, a handful of studies have begun using resting state RS-fMRI to guide TMS target selection to modulate DMN (Eldaief et al., 2011) to guide therapeutic TMS in patients with schizophrenia (Hoffman et al., 2007) and to address the above referenced clinical problem of determining where to target rTMS in the dorso-lateral prefrontal cortex (DLPFC) to improve antidepressant response (Fox et al., 2012). Targeting TMS based on individualized connectivity with distributed brain networks could have a great value, although there are a number of challenges to

overcome in order to validate the clinical utility of such a targeting approach (Fox et al., 2012).

Finally, a third modality to combine different techniques is to assess changing in structural and functional MRI by manipulating connectivity using TMS.

A unique advantage of TMS compared to RS-fMRI, and every other noninvasive approach for assessing connectivity, is that TMS can also be used to manipulate connectivity. The ability to experimentally activate or deactivate an area of the brain is a powerful method for exploring functional connectivity.

TMS can be applied while neuroimaging is being performed (referred to as on-line TMS-neuroimaging approach). In this case, neuroimaging provides a temporo-spatial assay of the immediate effects of TMS on neuronal activity. Concurrent TMS-neuroimaging can probe how the neuronal context at the time of stimulation determines the induced activity changes locally as well as in connected brain areas (Siebner et al., 2009). On-line neuroimaging experiments are technically demanding because TMS may adversely affect data acquisition during neuroimaging. This requires methodologic refinements to effectively avoid or control for TMS induced artifacts. Alternatively, TMS may be applied off-line before and/or after neuroimaging. This approach is mainly used determine the after-effect of TMS by the examination of functional connections comparison between and after stimulation. Off-line designs are technically easier to establish because rTMS and neuroimaging are separated in time and they can also be separated in space: TMS can be

performed outside the scanner room, making the stimulation easier to deliver and reducing the possibility that it adversely affect data acquisition during neuroimaging (Siebner et al., 2009).

The mechanisms that lead to functional connectivity changes induced by TMS, are still unclear: it is important to consider whether an observed change in connectivity actually reflects a change in connection strength between remote areas or whether it could be explained by local effects of the rTMS alone. While it can be argued that the local effects of TMS on cortical excitability are due to changes in connectivity within the stimulated region itself, it is becoming evident that TMS could induce changes in connectivity between brain regions (Fox et al., 2012). This have been studied using a wide variety of connectivity measurement techniques including task-based effective connectivity with PET (Lee et al., 2003b), task-based effective connectivity with fMRI (Grefkes et al., 2010; Pleger et al., 2006), and finally RS-fMRI (Eldaief et al., 2011; van der Werf et al., 2010; Vercammen et al., 2010b). In this contest it is important to note that when connectivity is being assessed during a task, it could be difficult to determine if the measured change in connectivity is actually due to a change in behavior. For that reason, assessing TMS induced connectivity changes with RS-fMRI may help avoid some of the above interpretive difficulties. To conclude, the combinations of neuroimaging techniques and TMS is becoming increasingly important to better characterize brain connectivity.

In this thesis four different studies have been performed in order to i) evaluate the validity of neuroimaging techniques in the detection of abnormal changes of brain connectivity in different groups of patients (Chapter 2 and 3); ii) investigate the functional and anatomical connectivity in healthy volunteers in order to identify the correspondence between structural (DTI) and functional (RS-fMRI) neuroimaging techniques in the assessment of brain connections; iii) estimate the effect of perturbation induced by TMS on functional connections in a group of healthy subjects in order to provide new evidence of the important role of the combination of neuroimaging and neurophysiological techniques in the characterization of brain connectivity.

CHAPTER 2

MICROSTRUCTURAL DAMAGE OF THE POSTERIOR CORPUS CALLOSUM CONTRIBUTES TO THE CLINICAL SEVERITY OF NEGLECT.

This chapter describes study aiming at assessing the anatomical connectivity changes occurring in the non-lesioned hemisphere of patients with neglect, with respect to a group of healthy subjects. This work was carried out in collaboration with other researchers.

INTRODUCTION

Neglect is clinically defined as the impaired ability to process or to react to sensory stimuli when presented in the hemispace contralateral to a brain lesion, in the absence of any remarkable sensory loss (Bisiach et al., 1986; Heilman et al., 2000; Vallar et al., 2003). This condition is frequently observed in the case of an acute/sub-acute damage affecting the right hemisphere (RH), while, in contrast, neglect symptoms are rarely observed after damage localized to the left hemisphere (LH) (Karnath et al., 2002). According to previous literature, neglect has an incidence of about 45% in acute strokes of the RH, and persistent deficits are observed in one third of cases (Cassidy et al., 1998). Despite its clinical relevance, the pathophysiology of neglect is still poorly understood. In the context of an intense debate within the scientific community, two major hypotheses have

been formulated so far. One is based on the assumption that the RH controls attention orienting in both left and right hemispace, while the LH controls the direction of attention in the right hemispace only (i.e., "hemispheric specialization" hypothesis) (Heilman and Van Den Abell, 1980; Mesulam, 1981). This hypothesis is supported by the far greater prevalence of neglect following RH than LH damage, as well as by imaging studies demonstrating a greater extent of activations in the RH than in the LH during tasks involving shifts of visuo-spatial attention (Corbetta et al., 1993; Gitelman et al., 1999; Nobre et al., 1997). Alternatively, Kinsbourne's theory has proposed a mechanism of hemispheric rivalry (Kinsbourne, 1977). This second hypothesis assumes that an asymmetric dynamic balance exists between parieto-frontal circuits in the two hemispheres, with the RH prevailing over the LH (i.e., hemispheric competition hypothesis) (Kinsbourne, 1977). Each hemisphere is thought to be responsible for orienting attention toward the contralateral hemi-space and to control the contralateral hemisphere trough mechanisms of reciprocal inhibition, with a right hemispheric prevalence in inhibiting the LH (Koch et al., 2012a). This theory is supported by clinical evidence that patients with extinction (the failure to acknowledge left-sided tactile hand stimuli upon double-simultaneous stimulation – (Hier et al., 1983) often manifest directional biases, favoring stimuli that are relatively ipsi-lesional over those which are relatively contra-lesional within and between visual fields. In support to the hemispheric competition hypothesis, it has been recently demonstrated that the right, but

not the left human posterior parietal cortex (PPC) exerts a strong inhibitory activity over the contralateral homologous area by a short-latency connection, using a combined method of trifocal TMS and diffusion MRI (Koch et al., 2011). Notably, it has been demonstrated that this interaction is mediated by direct transcallosal projections located in the posterior portion of the corpus callosum through callosal fibers crossing the regions IV and V (Koch et al., 2011). These data suggest that this anatomo-functional network might represent a possible neurophysiological basis for interhemispheric functional asymmetry. In order to be confirmed, however, this interpretation requires a direct demonstration that, in patients with a right parietal lesion and neglect, the posterior part of the corpus callosum and its projections to the LH are microscopically damaged (anatomical disconnection) in the absence of macroscopic abnormalities. Further, this anatomical disconnection should be associated with the presence and severity of neglect. Pathological abnormalities that modify tissue integrity, including microscopic degeneration of white matter fibers, can result in an altered diffusion coefficients. As described in Chapter 1, Tract-Based Spatial Statistics (TBSS) (Smith and Nichols, 2009) allows testing for group comparisons of regional diffusion indices, such as FA, MD, Dax, Drad, to indirectly asses regional alterations of white matter fibers as well as for correlations between these quantities and clinical or neuropsychological variables. The aim of the current study was to assess the presence of disconnection between hemispheres in patients with

right brain damage, and its contribution in determining the presence and severity of neglect.

METHODS

SUBJECTS

Eleven consecutive patients [F/M=4/7; mean (SD) age: 59.7 (10.0) years] with clinical and radiological evidence of macroscopic damage to the right hemisphere, were recruited from the Specialist Rehabilitation Clinic of Santa Lucia Foundation (Rome, Italy). All patients had to be right-handed (as assessed by the Edinburg Handedness Inventory (Busch et al., 2010) and to have suffered from an acute ischemic stroke over an interval of 1-6 months before enrolment. Exclusion criteria were: a previous history of cognitive decline, the absence of sensory deficits, and current impairment in cognitive domains other than visuo-spatial attention (see below). Major systemic, psychiatric and other neurological illnesses were carefully investigated and excluded in all patients. Critical for this study, the presence and severity of left-side neglect was carefully quantified in each patient, as detailed below. Finally, all patients underwent MRI scanning at 3T, detailed below, and conventional MRI scans (i.e., dual echo and fluid attenuated inversion recovery [FLAIR]) were reviewed by an expert neuroradiologist. Patients were excluded in the presence of any macroscopic abnormality in addition to the right-hemispheric lesion. A group of 11 right-handed, age-and sex-matched healthy volunteers [F/M=4/7; mean (SD) age: 59.3 (9.3) years] were also recruited for the study and served as controls. Major systemic, psychiatric

and neurological illnesses were carefully investigated and excluded in all of them. On the basis of conventional MRI, subjects were excluded in the presence of any macroscopic abnormality. The current study was conformed to the ethical principles of the Helsinki Declaration, and received approval by the Ethics Committee of Santa Lucia Foundation. Written informed consent was obtained from all participants before study initiation.

ASSESSMENT OF VISUOSPATIAL NEGLECT

The Behavioural Inattention Test (BIT) (Wilson et al., 1987) was used to determine the presence and severity of hemispatial neglect. This is a comprehensive battery of tests for the evaluation of visuo-spatial deficits, which includes both conventional (BIT-C) and behavioural scales (BIT-B). The conventional tests include: 1) line crossing, 2) letter cancellation, 3) star cancellation, 4) figure and shape copying, 5) line bisection, and 6) representational drawing. The behavioural tests assess specific aspects of daily life activities, and include: 1) picture scanning, 2) telephone dialling, 3) menu reading, 4) newspaper article reading, 5) telling and setting the time, 6) coin sorting, 7) address and sentence copying, 8) map navigation and card sorting. The cut-off scores of normality for the conventional and behavioural tests are 129 (0-146, maximum score 146) and 67 (0-81, maximum score 81), respectively. Patients are classified as suffering from neglect when their score is below the cut-off score in either or both the BIT-C and BIT-B.

MRI ACQUISITION

Brain imaging was obtained in a single session using a head-only 3.0T MR scanner (Siemens Magnetom Allegra, Siemens Medical Solutions, Erlangen, Germany). The acquisition protocol included the following sequences: 1) dual-echo turbo spin echo [TSE] (TR=6190 ms, TE=12/109 ms); 2) FLAIR (TR=8170 ms, TE=96 ms); 3) 3D Modified Driven Equilibrium Fourier Transform (MDEFT) scan (TR=1338 ms, TE=2,4 ms, Matrix=256x224x176, in–plane FOV=250x250 mm^2, slice thickness=1 mm); 4) Diffusion weighted twice-refocused SE EPI (TR=7000 ms, TE=85 ms, maximum b factor=1000 smm^{-2}, isotropic resolution 2.3mm^3). This sequence collects 7 images with no diffusion weighting (b_0) and 61 images with diffusion gradients applied in 61 non-collinear directions.

MRI IMAGE ANALYSIS AND STATISTICS

Lesion assessment

For each patient, lesions were outlined on the MDEFT scans, using a semi-automated local thresholding contouring software (Jim 4.0, Xinapse System, Leicester, UK, http://www.xinapse.com/). A binary lesion mask was obtained for every subject by setting all voxels within the lesion to 1 and the background to zero. The MDEFT scans were then normalised to standard space using tools from the FMRIB software library (FSL, www.fmrib.ox.ac.uk/fsl/). First, the brain extraction tool (bet) was used to strip off the skull from every subject's MDEFT scan. Next, FLIRT (Jenkinson and Smith, 2001) was used to compute the affine transformation that matches this skull-stripped image to the MNI brain atlas provided with FSL. Then,

FNIRT (http://www.fmrib.ox.ac.uk/analysis/techrep/) was used to compute the deformation field that warps the original MDEFT to the atlas, setting as starting estimate the affine transformation computed by FLIRT. Finally, the non-linear transformation was applied to the lesion binary mask. The masks from all patients were added and translated into a percentage unit to obtain a visual representation of the anatomical location of the lesions in the patient cohort (Fig. 1). Lesion volumes were calculated from each patient's scan and correlated with the corresponding scores obtained at BIT, using the Spearman's Rank correlation test.

DTI and TBSS image processing

Diffusion data were processed using tools from FSL. After eddy current correction the diffusion tensor was estimated in a voxel-wise fashion (Basser et al., 1994), and FA maps were derived for every subject. Maps of FA, MD, Dax and Drad were obtained. FA maps were then fed into TBSS (Smith et al., 2006) to obtain a projection of all subjects' FA data onto a mean FA tract skeleton. As reported in Chapter 1, usually the skeleton is obtained by aligning every subject's FA image into a common space using non-linear registration, and then averaging the normalised images to create a mean FA map, which is finally thinned so that the FA skeleton represents the center of all tracts common to the group. Each subject's FA data is then projected onto the skeleton and voxel-wise statistics is carried out within the skeleton. The projection is achieved by searching perpendicular to the local skeleton structure for the maximum value in the subject's FA image. This maximum

value is assumed to represent the nearest relevant tract centre. To avoid that the presence of lesion of the right hemisphere could affect the correct reconstruction of the skeleton, the TBSS pipeline was modified as follows. First, all FA images were affine registered to the FA template provided with FSL, masking out the lesion, which was outlined on b=0 images. Once in standard space, the same portion of the right hemisphere (MNI coordinate x>18 mm) was removed from the images of all subjects. Note that in order to avoid edge effects along the midsagittal section of the corpus callosum, part of the right hemisphere (0<MNI coordinate x<18), unaffected by the lesions, was included in the analysis. The left hemisphere FA maps obtained through this procedure were transformed back into native space, and TBSS was performed as normal, but using a half-brain (including sagittal slices with x<18) template. The same transformation and projection were applied to MD, Dax and Drad maps. The healthy controls underwent an identical procedure in order to minimise any bias.

Statistical analysis

All TBSS voxel-wise statistics was carried out on the skeletonized images using the FSL tool "randomise", which is based on permutation tests (500 iterations). A between-group comparison was first performed to identify regional FA, MD, Dax, and Drad differences, between patients and healthy controls. According to the specific processing, the analysis included all voxels in the left hemisphere and in the medial part of the corpus callosum. Then, in these same brain voxels, voxel-wise associations were investigated between

patients' regional diffusion indices and total neuropsychological scores reported at BIT-C and BIT-B. For both, between-group comparison and correlation analyses, statistical significance was computed using permutation tests. A correction for multiple comparisons was obtained using the threshold-free cluster enhancement (TFCE) method (Smith and Nichols, 2009). P-values were accepted as significant if inferior to 0.05 after TFCE correction.

RESULTS

ASSESSMENT OF NEGLECT

According to the criteria defined in the methods section, all patients were demonstrated to suffer from hemispatial neglect. As reported below, 3 patients were excluded from the analysis due to the poor quality of their MRI data (motion artifacts). From the remaining 8 patients, 1 reported scores above the cut-off normality in the BIT-B subtest only, 2 in the BIT-C subtest only, and 5 in both subtests. A detailed description of patients' performance at BIT is summarized in Table 1.

	Mean (SD) score		Mean (SD) score
BIT-C total score	**11.1 (26.5)**	**BIT-B total score**	**56.4 (20.9)**
BIT-C subtests		*BIT-B subtests*	
Line crossing	32.3 (5.9)	Picture scanning	3.1 (2.6)
Letter cancellation	32.0 (4.3)	Telephone dialling	7.1 (2.7)
Star cancellation	43.7 (15.3)	Menu reading	6.4 (3.8)
Figure and shape copying	2.1 (1.3)	Article reading	5.9 (4.3)
Line bisection	5.7 (3.1)	Telling and setting the time	7.4 (1.7)
Representational drawing	2.3 (0.5)	Coin sorting	6.3 (3.1)
--		Address and sentence copying	7.6 (2.4)
--		Nap navigation	7.1 (3.1)
--		Card sorting	5.4 (2.5)

Table 1. Clinical assessment of visuospatial neglect. BIT-C = conventional scale of the Behavioural Inattention Test; BIT-B = behavioural scale of the Behavioural Inattention Test. See text for further details.

MRI ACQUISITION

Three out of 11 patients were excluded from image analysis for the poor quality of their MR images due to motion artefacts. According to the exclusion criteria, none of the patients who entered the analysis had any detectable macroscopic abnormality in the left hemisphere. None of the healthy controls' MRI scan revealed any macroscopic abnormality.

MRI IMAGE ANALYSIS AND STATISTICS

Lesion assessment

Figure 1 summarises the lesion data, which are presented here for completeness. Neglect patients typically had substantial lesions centred on right perisylvian structures, similar to many previous studies of neglect. Correlation analysis between patients' lesion volumes and BIT scores did not return significant results (p=0.6).

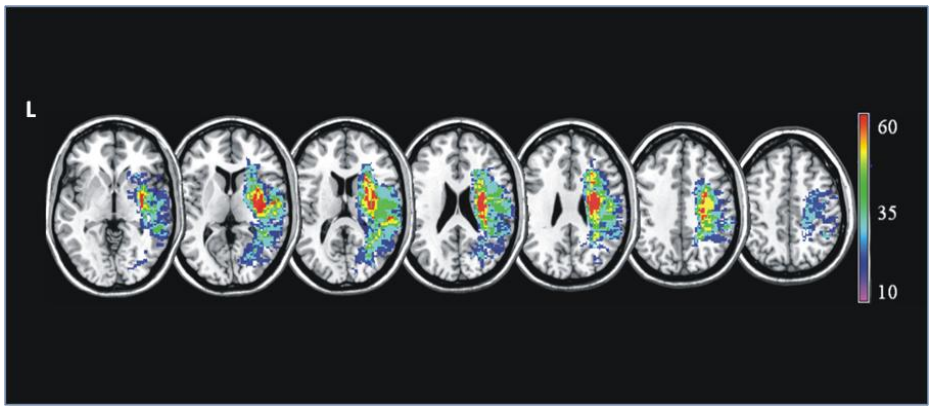

Fig. 1 Lesion distribution. The damage visible on mri images was outlined and warped to MNI sapce for each studied patient. The image was produced using MRIcro software. A T1-weighted template comprising 12 axial slices was used to demarcate lesions for every patient. The colour scale indicates the percentage of patients presenting damaged tissue in any given image voxel.

TBSS

The patient group compared to controls revealed a widespread reduction of regional FA in most of the left hemisphere tracts, with a predominant involvement of the corpus callosum and its projections towards the parietal WM (Fig. 2A). Widespread increases in Drad and in MD were also found in patients, located in the same tracts where FA was reduced and beyond (Fig.

2B and 2C, respectively).Areas of increased Dax were also found in patients, mainly located within the corona radiata (Fig. 3). No significant increases in FA, nor decreases in any of the other indices were observed.

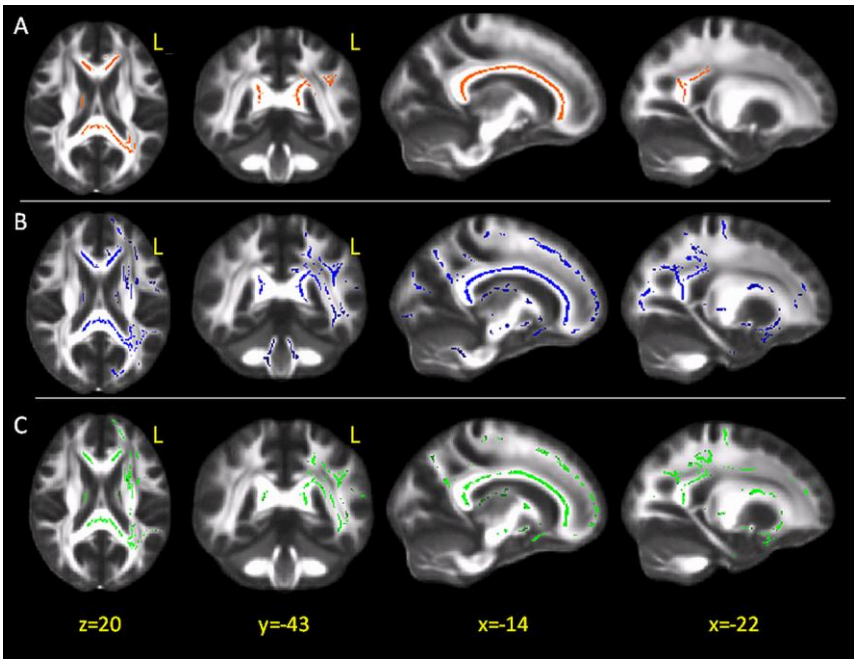

Fig. 2 TBSS results: patients vs. Controls. (a) Red indicates the areas where fractional anisotropy (FA) values of patients are significantly reduced with respect to those of healthy controls, overlaid onto the group-averaged FA image. FA values are significantly reduced in the corpus callosum and its projections on the parietal white matter. (b) Blue indicates the areas of increased radial diffusivity in patients. The same sections as in panel A are shown to ease the comparison with FA results. (c) Green indicates tracts where MD was increased in patients. Again, the same sections as in panels a and b are shown. L=left; x,y,z, indicate the MNI coordinates.

Voxel-wise correlation analysis revealed a direct association between the patients' BIT scores and regional FA in a cluster located in the posterior portion of the corpus callosum, as shown in the top panel of Figure 4. Randomise provides the p-values but not the corresponding correlation coefficients.

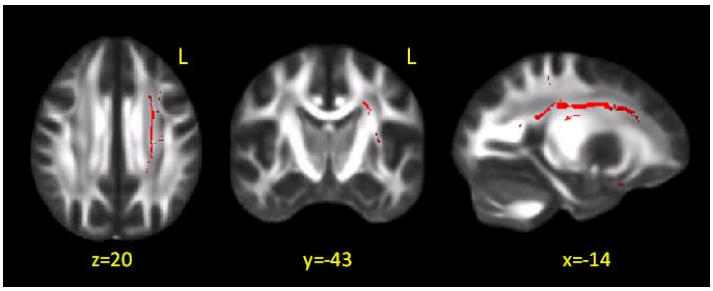

Fig. 3 TBSS results: axial diffusivity. Red indicates tracts where axial diffusivity (Dax) increases in patients compared to healthy subjects. Changes were mainly located within the corona radiata, an area of crossing fibres. The interpretation of these changes can be challenging (Wheeler-Kingshott and Cercignani, 2009) .

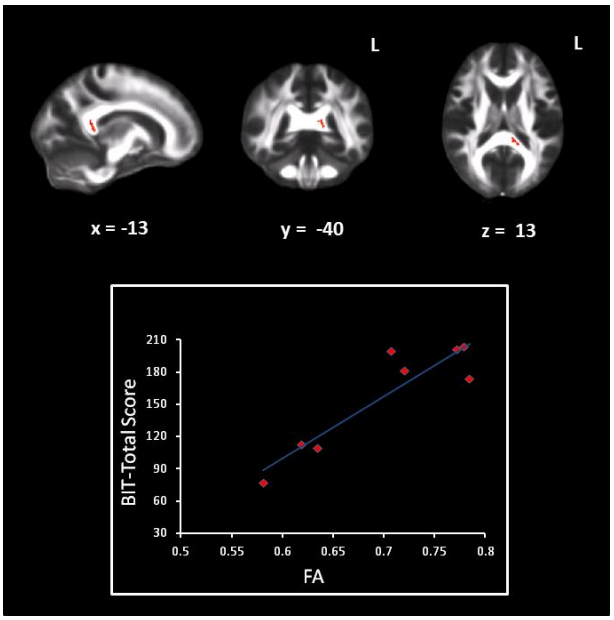

Fig. 4 Correlation between patients' FA and behavioural inattention test (BIT) total scores. The top panel shows in red the region of the posterior corpus callosum, whose fractional anisotropy (FA) value correlates with patients' performance at BIT. In the bottom panel, the FA values extracted from that region are plotted, patient by patient, against their correspondent performance obtained at bit. The post-hoc R value (pearson correlation coefficient) was 0.91.

In order to have an estimate of the latter, we extracted, subject by subject, the mean FA of the significant cluster and computed post-hoc the Pearson correlation coefficient between this mean value and the BIT score. The bottom panel of Figure 4 shows the corresponding scatter plot. The correlation

coefficient was 0.91. No associations were observed between the BIT scores and any of the other diffusion indices explored.

DISCUSSION

We recruited here a group of patients who suffered from an acute stroke of the RH and presented with symptoms of neglect. A detailed clinical assessment of neglect, based on the BIT, confirmed the presence of neglect in all recruited patients, with different degrees of severity. According to inclusion criteria, none of the patients had any macroscopic abnormality in the left hemisphere, as assessed on the T2 and FLAIR scans. Conversely, despite the absence of lesions, TBSS analysis was able to demonstrate subtle changes in the FA values along several WM tracts of the left hemisphere in patients. Wallerian degeneration is a well-described phenomenon, consisting of anterograde degeneration of axons and myelin sheaths after proximal axonal or cell body injury (Vargas and Barres, 2007). In our patients, this reduction of FA fits with the expected evolution of the stroke lesion, which affected a proportion of neurons projecting from the right to the left hemisphere through the corpus callosum. Further analyses of Drad showed that this parameter was increased within and beyond the tracts where FA was found to be reduced. Conversely, Dax was found to be increased only in the corona radiata, an area where the crossing of several white matter pathways (corpus callosum, cortico-spinal tract, superior longitudinal fasciculus) is known to occur. Although changes in Drad and Dax have been associated with myelin and axonal damage,

respectively (Song et al., 2003; Song et al., 2002), caution should be exercised when interpreting these indices in areas of crossing fibres (Wheeler-Kingshott and Cercignani, 2009). Given these observations, we can therefore conclude that our data support the hypothesis that the main damage occurring in the left hemisphere of these patients is dominated by demyelination in the context of Wallerian degeneration phenomena. While the occurrence of Wallerian degeneration in one hemisphere can be expected in cases of macroscopic damage in the other hemisphere, an intriguing result of this study is that FA changes in the ‘‘healthy’’ hemisphere also accounted for the severity of neglect symptoms observed in our patients. Moreover, no association could be found between patients’ severity of neglect symptoms and the volumetric assessment of the macroscopic lesions. When we performed the correlation analysis with the severity of neglect symptoms assessed by the BIT, TBSS analysis returned a well localized area of the posterior portion of the corpus callosum, which is known to transfer white matter fibers between the two homologues parietal cortices. The FA reduction is interpreted here as axonal demyelination/loss and, as a consequence, structural disconnection, correlated, without any a priori hypothesis on its anatomical location, with patients’ performance at the BIT. This finding is consistent with the hypothesis that neglect follows a disinhibition of parietal-frontal circuits of the left intact hemisphere (due to the release of right hemisphere control) in patients with neglect, as suggested by previous evidence based on TMS experiments (Koch et al., 2008).

We believe that the current finding provides novel anatomical evidence in support for a critical role of this inter-hemispheric networks in neglect. On the other hand, against the "hemispheric specialization" theory of neglect (Heilman and Van Den Abell, 1980; Mesulam, 1981), no association could be found between patients' clinical severity and the volumetric assessment of their macroscopic lesions. Moreover, it should be noted that the data reported in the current study are not only interesting for clarifying the pathophysiology of neglect. There is a growing body of evidence that non-invasive brain stimulation techniques such as repetitive TMS or transcranial direct current stimulation (tDCS) may be used for therapeutic purposes (Ridding and Rothwell, 2007). For instance, relatively to neglect treatment, it was recently reported that theta-burst stimulation is able to accelerate recovery from neglect symptoms in stroke patients over a time window of few weeks (Koch et al., 2012b). In this context, but also in other clinical conditions of focal brain damage, the identification of the most critical networks producing specific symptoms may represent the target for neurophysiological treatments. This is particularly relevant in neurorehabilitation, for which non-invasive brain stimulation might contribute to improve the final outcome of the protocols currently in use.

It has to be acknowledged that a main limitation of the current study, which has to be considered as explorative, is the small sample size. Future studies on larger populations of patients are needed to confirm and extend our preliminary findings. On the other hand, the results presented here were

obtained in a completely data-driven fashion, suggesting that the effect we observed in 8 patients only is likely to be rather strong.

In conclusion, this study provides new anatomical evidence supporting the notion that changes in right-left balance between the posterior parietal cortices rather than an isolated involvement of the right hemisphere can be critical for the occurrence of neglect symptoms, such as those explored by the BIT.

CHAPTER 3

WIDESPREAD ALTERATIONS IN FUNCTIONAL BRAIN NETWORK ARCHITECTURE IN AMNESTIC MILD COGNITIVE IMPAIRMENT.

This chapter presents a network analysis of RS-fMRI data aiming at the identification of networks parameters able to predict the development of Alzheimer's disease (AD) in patients with amnestic mild cognitive impairement (MCI). The performance of this technique was also compared with that of a more standard ICA to underline differences and similarities between different approaches. The study was carried out collaboration with other researchers. In particular Dr Ludovico Minati, form BSMS Brighton and Sussex Medical school, who developed the methodological approaches. I contributed to the study acquiring and processing of RS-fMRI data.

INTRODUCTION

MCI defines a transitional state along a continuous spectrum that goes from normal aging to fully developed dementia (Petersen, 2000). This clinical classification is critical to the identification of individuals at high risk for developing Alzheimer's disease (AD). From this perspective, MCI represents an interesting target for the investigation of AD patho-physiology, and also for the identification of patients at early clinical stages of AD, who might enter clinical trials at a time when their cognitive functions are still relatively preserved.

MCI patients typically complain of cognitive deficits that do not interfere, or interfere only mildly, with their everyday-life activities. Early cognitive dysfunctions in MCI patients can be multifaceted (Petersen, 2004), in most cases including memory deficits and leading to the classification of a-MCI (amnestic MCI) (Petersen, 2004). a-MCI is widely considered as the condition most commonly associated with a high risk of conversion to AD (10–15%; see (Petersen, 2000) , and is therefore regarded by most authors as a prodromal state of AD (Gauthier et al., 2006). However, a-MCI includes a heterogeneous population of subjects. While 10–15% of a-MCI patients convert to AD, a small proportion of a-MCI patients can remain stable with an isolated cognitive impairment (Perri et al., 2007), or even develop other forms of dementia (Perri et al., 2007; Petersen, 2000).

The neuro-pathological bases underlying MCI and the conversion from MCI to AD have been investigated extensively (Price and Morris, 1999), and neuroimaging studies have consistently described in vivo a progressive atrophy starting in the medial temporal lobes, and gradually extending into the temporo-parietal cortex, the cingulum and the frontal cortex (Bozzali et al., 2006).

The evolution of neurodegenerative processes appears to parallel the progression of the cognitive decline, with an initial involvement of functions and brain structures associated with memory, which then extends to affect other higher level functions and related brain structures.

The progressive nature of the clinical modifications and the link between the onset of multiple cognitive dysfunctions and the conversion to AD suggest that a preclinical investigation of cognitive domains may permit a better identification of individuals at high risk of developing dementia. It has been demonstrated that fMRI is ideally suited to reveal any such selective change prior to overt neuropsychological or structural brain abnormality (Bookheimer et al., 2000). As such there is increasing interest in the use of this technique to detect alterations of brain function in prodromal AD. Studies of functional connectivity in MCI patients, investigated using ICA or SBA of RS-fMRI, have demonstrated disconnection across DMN, primarily in precuneus and posterior cingulate cortex. However, the low amplitude and limited topographical extent of these changes restricts the potential usage of these approaches in studies aimed at determining biomarkers of early AD (Gili et al., 2011; Rosazza and Minati, 2011).

There is converging evidence that graph-based network analyses are highly relevant to the study of AD and may improve the differentiation between patients and controls with respect to ICA and SBA. Recent reports have suggested that measurement of network architecture parameters can substantially improve detection of disease-related changes, and progression of pathology may itself be determined by brain network architecture (Buckner et al., 2009; de Haan et al., 2012; Petrella and Doraiswamy, 2013; Tijms et al., 2013). For this reason, in this study network analysis was performed in order to identify network parameters that can predict for the development of AD.

Moreover, an explicit comparison between ICA and graph-based has been conducted by undertaking a cross-sectional comparison of graph-based analysis and ICA of RS-fMRI in patients with amnestic MCI (aMCI) (Jack et al., 2011) at high risk of developing AD.

METHODS

STUDY POPULATION

We recruited Forty-nine patients with a diagnosis of aMCI: 25 female, aged 70.2±8.7 years, mean MMSE score 26.4±1.8, Clinical Dementia Rating 0.5, Rey auditory verbal learning test corrected scores 31±6 immediate, 4.6±2.4 delayed, 26 single-domain and 23 multiple-domain. At one year follow-up 13/34 aMCI patients had converted to AD. The control group comprised 32 cognitively normal participants, 14 female, age 65.9±8.0 years, mean MMSE score 30±0. Approval from the ethics committee was obtained. All participants gave written informed consent and the study was conducted in accord with the ethical principles of the Helsinki Declaration.

DATA ACQUISITION

All imaging was obtained using a head-only 3.0T MR scanner (Siemens Magnetom Allegra, Siemens Medical Solutions, Erlangen, Germany). The acquisition protocol included the following sequences: 1) a magnetization-prepared rapid gradient echo (MPRAGE) sequence (TR = 2500ms; TE = 2.74 ms; TI = 900 ms; Flip angle = 8°; matrix = 256×208×176; slab thickness = 1mm; FOV = 256×208×176mm^3). 2) a series of T2* weighted echo planar imaging (EPI) scans, sensitized to blood oxygenation level dependent contrast

(BOLD) (TR:2080 ms, TE:30 ms, 32 axial slices parallel to AC-PC line, matrix:64×64, pixel size:3×3 mm^2, slice thickness:2.5 mm, flip angle:70°) for RS-fMRI. BOLD EPIs were collected during rest for a 7 min and 20 s period, resulting in a total of 220 volumes. Dual-echo turbo spin echo, fast-FLAIR scans and structural scans were assessed by a neuroradiologist to exclude additional pathology.

CONNECTIVITY ANALYSIS

RS-fMRI data preprocessing was performed using SPM8 (Wellcome Trust Centre for NeuroImaging, London, UK), followed by graph analysis as previously described (Minati et al., 2013). As described in Chapter1, slice-timing correction, realignment/unwarping and normalization were performed, then segmented grey matter maps were averaged across all participants. The brain with smallest squared difference from average was chosen and iteratively parcellated at high resolution, yielding 742 regions with volume 1.55±0.33 ml. These were overlaid to each participant's anatomy assigning each grey matter voxel to the nearest region, intrinsically removing potential atrophy-related confounds. The realignment parameters were temporally filtered with the same settings as the BOLD data prior to regression. Inter-regional connectivity was determined through pair-wise linear regressions; resulting Pearson coefficients were thresholded for r>0.15, 0.2...0.75 and node degrees calculated. Network completeness, clustering coefficient and global network efficiency were also computed (Rubinov and Sporns, 2010). Additional equi-completeness analyses were performed, thresholding Pearson

coefficients with individually-determined values yielding fixed completeness across all participants; such analyses were conducted for 13 completeness levels, corresponding to the average completeness across all patients and controls observed at each r-level threshold in the fixed r-value analyses (Fig. 1a). For comparison, we also performed group-level spatial ICA, using the Group ICA Toolbox v. 2.0e (University of New Mexico, USA) assuming 12 components as given by the minimum description length criterion and using the same temporal filtering settings. Voxel-based morphometry was performed using the VBM8 toolkit of SPM8 (Gili et al., 2011). It is a neuroimaging technique that allows a voxel-wise comparison of the local concentration of gray matter between two groups of subjects.

STATISTICAL ANALYSIS

After co-varying for age and root-mean-square volume-to-volume head displacement, global network parameters were compared between aMCI patients and controls using two-tailed t-tests, with false-discovery rate (FDR) correction over the 13 correlation thresholds. Individual node degree maps were smoothed, averaging between each region and its neighbors with a factor of 0.75; subsequently, the number of regions for which node degree was significantly reduced in patients was calculated for all thresholds using two-tailed t-tests, with FDR correction over the 742 regions. The threshold yielding the largest difference, r>0.60 (see results), was selected for generation of the presented maps, shown at $p_{FDR}<0.05$. To facilitate comparison with previous studies using the more coarsely parcellated

Automated Anatomical Labeling (AAL) atlas, node degrees were also averaged over the 90 AAL regions and compared using analyses of variance.

Statistical analysis of ICA and VBM maps was performed using SPM8, co-varying for age and root-mean-square volume-to-volume head displacement. For each ICA component, an inclusive mask was determined by thresholding the main effect over all participants at $p_{FWE}<0.05$; subsequently, patients and controls were compared applying a voxel-level threshold of $p<0.005$, followed by a corrected cluster level inference threshold of $p_{FWE}<0.05$. The DMN component was identified by visual inspection of the main effect maps with reference to established topographical maps, upon agreement of 3 observers. To exclude potential confounding effects related to smoothing scale, ICA was repeated after smoothing the functional images with a Gaussian kernel having FWHM 20 mm, which corresponded to the FWHM of the distribution of voxel counts for a ROI with its neighbors, 20.3±5.3 mm. VBM results are presented for $p<0.05$; this extremely permissive voxel-level threshold was deliberately chosen to determine whether VBM would reveal any atrophy in areas of significant disconnection. As for ICA, the presence of significant difference was inferred at the cluster level, applying a corrected cluster threshold of $p_{FWE}<0.05$. Receiver operating characteristic (ROC) curves for discrimination between aMCI patients and controls were calculated for regional and global parameters. Regional connectivity, intended as average node degree and ICA z-score, was measured over the precuneus and posterior cingulate region, which forms the core of the DMN (Rosazza and Minati,

2011); to avoid circularity, this region was identified on the AAL atlas, without any reference to the topographic maps of connectivity differences between patients and controls. Global DMN connectivity was measured by averaging the ICA z-score over the precuneus/posterior cingulate cortex, lateral parietal and medial prefrontal regions. For comparison, the Pearson correlation coefficient averaged over all combinations of the 742 regions used for network analysis was considered. The area under the resulting ROC curves, representing classification accuracy, was compared as described elsewhere (Hanley and McNeil, 1982).

RESULTS

For all thresholds r>0.35, aMCI patients were consistently characterized by decreased network completeness (k in Fig. 1a; for r>0.60: 0.0135±0.023 vs. 0.0081±0.0051, $t(77)=3.0$, $p_{FDR}=0.01$), decreased clustering coefficient (C_P in Fig. 1a; for r>0.60: 0.292±0.092 vs. 0.233±0.087, $t(77)=2.9$, $p_{FDR}=0.02$) and reduced global network efficiency (E_{GLOB} in Fig.1a; for r>0.60: 0.0681±0.0293 vs. 0.0486±0.0222, $t(76)=3.3$, $p_{FDR}=0.02$).

The number of regions for which node degree was lower in patients than controls gradually increased for r>0.25 and peaked at r=0.60. At this threshold, reduced node degree in aMCI was widespread and most pronounced in cuneus and pre-cuneus (extending to posterior cingulate cortex), supramarginal and angular gyri, inferior and superior parietal lobules, pre- and post-central gyri (Fig. 2).

Reduced connectivity was also detected in insula and inferior frontal operculum, predominantly on the right, and in posterior inferior temporal gyrus, thalamus and putamen. Average node degree was reduced in 29/45 bilateral AAL regions (Fig. 1b), with the most significant differences in the precuneus, inferior and superior parietal lobules, supramarginal gyrus, post- and pre-central gyri, Rolandic operculum, superior occipital lobe, extending to the insula, cuneus, middle and inferior occipital, lingual and fusiform gyri; there were no lateralization effects.

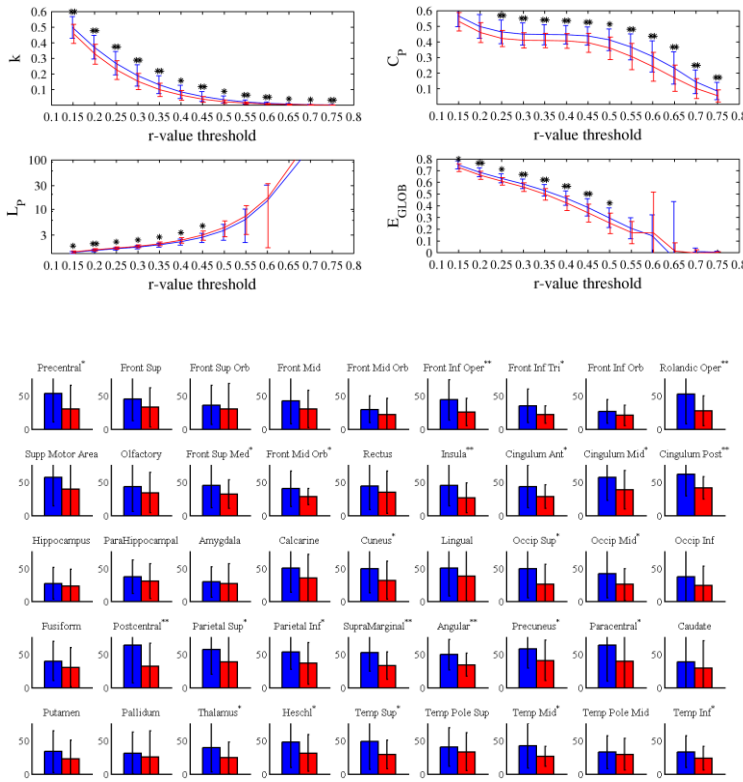

Fig. 1 Differences in global network parameters as a function of correlation threshold. Blue: controls, red: amnestic mci patients. K: network Completeness,cp: average clustering coefficient,eglob: global efficiency, %regions: proportion of regions for which significant disconnection Was observed. B) bar plots of node degrees calculated for |r|>0.6 for regions of the aal atlas. Error bars denote±1 standard deviation. *pfdr < 0.05, **pfdr < 0.01, ***pfdr < 0.001.

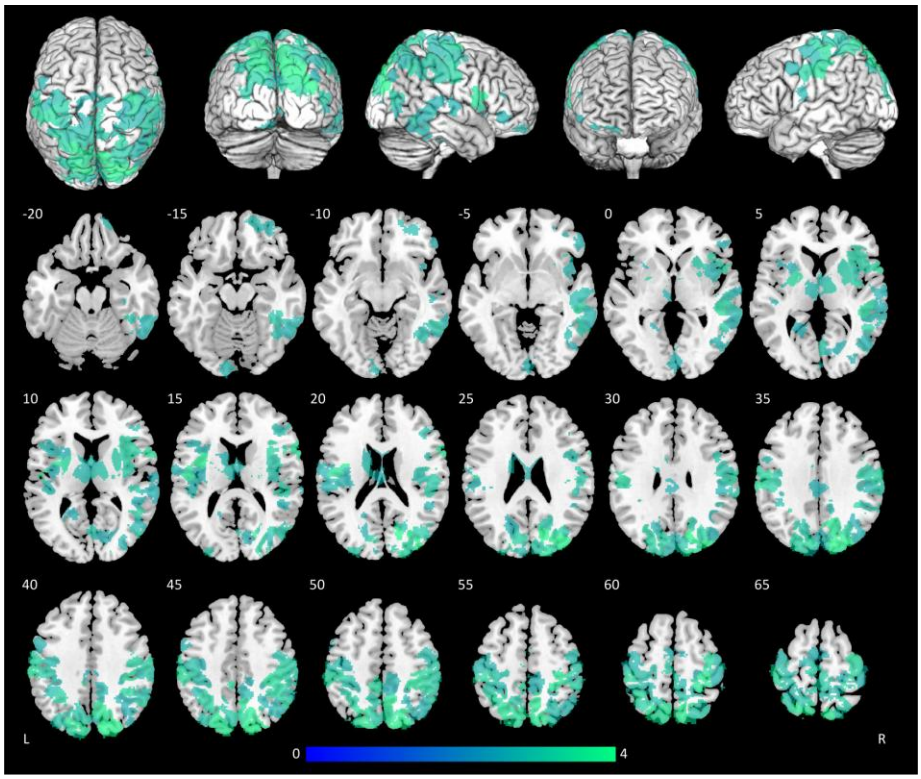

Fig. 2 Topographical distribution of node degree reduction in amnestic mci patients compared to controls.

The corresponding equi-completeness analysis (for k=0.01) revealed weaker effects, with decreased degree in the superior parietal lobule, superior occipital lobe and post-central gyrus and increased degree in the inferior, middle and medial frontal lobe, anterior cingulate and temporal pole; there were no lateralization effects and no differences in average clustering coefficient and global network efficiency.

ICA revealed decreased DMN connectivity in the medial parietal region, as well as in precuneus and posterior cingulate cortex, particularly on the right (Fig. 3, x=8, y=-44, z=26 mm, k_E=447 voxels, cluster-level p_{FWE}=0.01); increasing smoothing to 20 mm FWHM confirmed this effect (x=10, y=-44, z=26 mm, k_E=424 voxels, cluster-level p_{FWE}=0.02) without other areas of significant difference. The only additional effect observed in non-DMN components was a cluster of decreased connectivity in the cuneus (x=16, y=-88, z=-14 mm, k_E=439 voxels, cluster-level p_{FWE}=0.01) for the visual component. VBM analyses showed cerebral grey matter atrophy primarily confined to medial temporal structures, and precuneus to a lesser extent; these effects were weak, and did not survive correction for multiple comparisons (Fig. 3).

The best discrimination accuracy was provided by node degree measured in the posterior cingulate and precuneus region, with an area-under-curve (AUC) of 0.72. The AUC for average ICA z-score in this region, 0.49, was significantly lower (z=2.7, p=0.007; Fig. 4a) and did not change with 20 mm smoothing (p=0.5). By comparison to average ICA z-score calculated over the whole DMN (AUC 0.46), the average correlation coefficient (AUC 0.67), network completeness (AUC 0.66), average clustering (0.67) and global efficiency (AUC 0.68) calculated for r>0.6 all provided between discrimination accuracy ($p \leq 0.02$ for all comparisons; Fig. 4b).

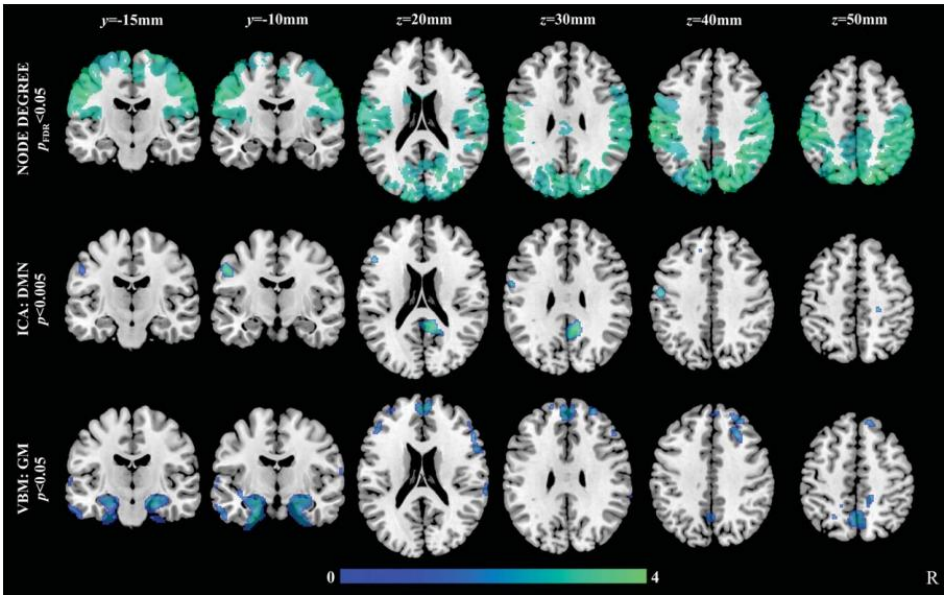

Fig. 3 comparison of node degree changes, reduced connectivity in the default-mode network as determined by ica, and reduced grey matter volume as revealed by VBM.

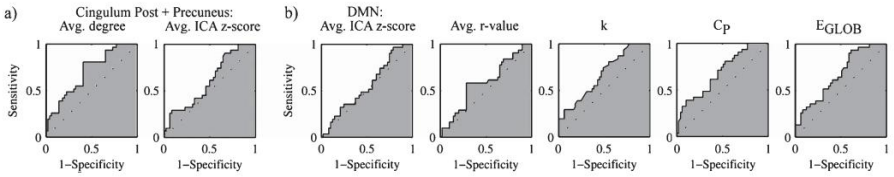

Fig. 4 ROC curves for discrimination of aMCI patients and controls. A) node degree and ica z-score averaged over the precuneus and posterior Cingulate cortex. B) In order: average ica z-score averaged over precuneus/posterior cingulate cortex, lateral parietal and medial frontal regions, Pearson correlation coefficient averaged over all combinations of 742 regions, network completeness (k), mean clustering (cp) and global Efficiency (eglob) at |r|>0.6

DISCUSSION

Graph-based analyses have shown that in aMCI there is marked disconnection of the precuneus, parietal and temporal areas, regions representing densely interconnected cortical hubs within which early deposition of extracellular amyloid is observed (Buckner et al., 2009; Liu et al., 2013; Wang et al., 2013). However these analyses also demonstrate disruption of network connectivity in brain regions where AD pathology is not manifest until late disease stages, such as sensorimotor cortex and insula, thalamus and basal ganglia. These changes may represent the downstream consequences of disconnection of the hub regions which are also involved in the DMN. The importance of modeling network architecture was underlined by the observation that computation of global network parameters, which are agnostic to topographical localization of changes, demonstrated disruption of small-world architecture. The extent and magnitude of these changes contrasts with the results obtained using ICA, which revealed weaker and much more restricted connectivity changes in the precuneus-posterior cingulate region, consistent with several previous studies using ICA and SBA in aMCI (Gili et al., 2011; Petrella and Doraiswamy, 2013; Rosazza and Minati, 2011; Tijms et al., 2013).

The widespread changes in functional network architecture contrasted markedly with the relatively restricted topographical distribution of atrophy. Even at an extremely permissive uncorrected threshold, volume loss as determined by VBM was primarily limited to medial temporal lobe regions with relative sparing of parietal regions. This decoupling of changes in

network connectivity and brain volume supports the notion that altered brain function precedes atrophy in aMCI, and at the same time the areas where the earliest atrophy is observed are not those where disconnection is most pronounced. These data may support models of AD pathophysiology which propose that in early AD the accumulation of extracellular amyloid pathology in cortical hubs proceeds separately from tau pathology, which is more closely associated to medial temporal atrophy (Buckner et al., 2009; de Haan et al., 2012; Tijms et al., 2013). The distribution of functional disconnection has a clear correspondence to the localization of gray matter atrophy in AD patients as reported in a previous study (Gili et al., 2011), involving the precuneus, inferior temporal gyrus, fusiform gyrus, orbitofrontal and medial frontal cortex, angular gyrus and insula.

Receiver operating characteristic curves confirmed that node degree was superior to ICA DMN in discriminating aMCI patients and controls. While ICA revealed significant DMN connectivity differences in a localized cluster in the posterior cingulate cortex, the effect vanished when averaging over the whole anatomical region, and discrimination accuracy was at chance level; by contrast, discrimination based on node degree was clearly above chance level, though the accuracy was relatively modest.

Decreased network completeness in patients and the fact that node degree differences were much weaker in the equi-completeness analysis indicate that the observed effects are primarily driven by diffuse reduction in connectivity strength, rather than by focal topological changes. While marked alterations in

network topology and connectivity of hub regions have been previously demonstrated in equi-completeness analyses, these are primarily found in moderate to severe AD; it appears plausible that in MCI, such architecture changes are not strong enough to survive normalization of the number of connections (Liu et al., 2013).

Indeed, a recent study on aMCI found that the best discriminant between patients and controls was the mean functional connectivity strength (Wang et al., 2013). Even though compensatory changes cannot be ruled out, we ascribe the apparent increase in connectivity observed mainly in frontal regions to the effect of completeness normalization; in these areas, functional connectivity is better preserved in comparison to others, hence their degree increases when overall connectivity is normalized. In summary, aMCI is associated with disrupted functional connectivity not only involving the cortical hub regions constituting the DMN and known to be associated with early amyloid deposition but also extending to regions where AD pathology is not observed until late stages of disease. The amplitude and topographical extent of these changes significantly exceed both the connectivity changes identified using ICA and the atrophy as determined using VBM. These data highlight the potential value of graph-based analyses of functional networks in network connectivity in the determination of biomarkers of early AD.

CHAPTER 4

FUNCTIONAL ANATOMY OF THE THALAMUS AS A MODEL OF INTEGRATED STRUCTURAL AND FUNCTIONAL CONNECTIVITY OF THE HUMAN BRAIN IN VIVO.

This chapter reports on a study where thalamo-cortical circuits were used as a model to infer the correspondence between anatomical (as measured by DTI) and functional (as measured by RS-fMRI) connectivity in a group of healthy subjects, and to mutually validate these 2 methods. Other researchers collaborated to the present work.

INTRODUCTION

It is becoming increasingly clear that complex networks rather than isolated cortical areas sub-serve specific brain functions in the human brain, such as, for instance, movement, memory, or attention (Bressler and Menon, 2010; Bullmore and Sporns, 2009; Lang et al., 2012; Sporns et al., 2005; van den Heuvel and Hulshoff Pol). Against this background, RS-fMRI has emerged as a non-invasive tool able to measure the correlation between the spontaneous neural activity of different brain areas. In parallel, DTI and tractography (Basser and Pierpaoli, 1996; Parker et al., 2003; Pierpaoli et al., 1996) has allowed the identification of white matter connections that link these functional nodes. Based on this model of brain connectivity, it is conceivable

that regions that appear to be functionally connected should be directly or indirectly structurally connected to each other.

Therefore, the combination of connectivity measures obtained using RS-fMRI and DTI should provide a more complete picture of brain networks than one single connectivity analysis. To date, however, attempts to integrate the two techniques have produced only partially convincing results.

One way of addressing this issue is to apply this model of connectivity to a brain structure with many, well characterized structural connections, such as the thalamus. The characterization of the thalamic structure has been performed across different species and through different methods. It was once thought that only the principal sensory nuclei of the thalamus received subcortical input and projected to the cerebral cortex, with the other nuclei not projecting to it. It is now known that every nucleus in the dorsal thalamus receives subcortical inputs and projects to the cerebral cortex (Jones, 2009). Post-mortem and lesion studies have also established that the thalamus is topographically organized into distinct nuclei from which parallel projections reach different regions of the cortex (Alexander et al., 1986; Haber, 2003). Electrophysiological and connectivity studies, conducted mainly in experimentally-accessible nuclei such as the somatic ventro-posterior nucleus or visual dorsal lateral geniculate nucleus, reinforced the notion of a rather strict point-by-point spatial correspondence between neuron soma location in the thalamus and axon distribution to the cortex. Overall, these observations led to the concept of thalamic nuclei being cytoarchitectonically-

circumscribed regions receiving a specific set of afferent fibers and projecting topographically within the borders of a specific set of cortical fields (Clasca et al., 2012).

The structural features of the thalamus make it possible to identify the thalamic nuclei based on the use of DTI. The first attempt in this direction exploited just the information derived from the local orientational features of the diffusion tensor in every voxel (Wiegell et al., 2002). An alternative method was introduced by Behrens and collaborators (Behrens et al., 2003): instead of relying only on the local information about diffusion, connectivity-based parcellation was used to segregate a grey matter region on the basis of information about remote connectivity derived from tractography, effectively enabling a segmentation of the thalamus based on this connectivity pattern (Behrens et al., 2003). A study conducted by the same group revealed that thalamic functional activations during motor and executive tasks co-localize with the thalamic regions with the highest probability of connectivity with motor and prefrontal cortical areas, respectively (Johansen-Berg et al., 2005).

Using RS-fMRI, Zhang and collaborators (Zhang et al., 2008) parcellated the thalamus into nuclear groups, examining patterns of functional connectivity within the thalamocortical system derived. In 2010 they then compared these results with those obtained by tractography parcellation, finding a general good overall concordance among structural and functional and histological results, thus suggesting that a simple model of direct anatomical connectivity between the cerebral cortex and the thalamus is capable of explaining much of

the observed correlations in neuronal activity (Zhang et al., 2010). A limitation of this study was that structural and functional connectivity were assessed in 2 separate groups of healthy participants.

The aim of the present study is to compare structural (as measured by DTI) and functional (as measured by RS-fMRI) connectivity between the thalamus and the cerebral cortex in the same cohort of healthy participants, and to mutually validate these 2 methods. We used DTI tractography to define distinct thalamic regions structurally connected to different cortical areas. This parcellation was then compared with information derived from RS-fMRI. Seed-based analysis (SBA) was performed, using the thalamic regions (formerly classified by DTI connectivity) as seeds, to identify the cortical areas more strongly connected, from a functional point of view, to each specific thalamic region.

METHODS

We recruited a group of 38 right-handed healthy volunteers [M/F =18/20; mean (SD) age=50.36 (13.74) years] with no history of medical or psychiatric disorders, autonomic dysfunction, or other major clinical conditions. The study was approved by the ethical committee of Santa Lucia Foundation, and written informed consent was obtained from all subjects before study initiation.

All imaging was obtained using a head-only 3.0T MRI scanner (Siemens Magnetom Allegra, Siemens Medical Solutions, Erlangen, Germany),

equipped with a circularly polarized transmit-receive coil. The acquisition protocol included the following sequences: 1) 3D Modified Driven Equilibrium Fourier Transform (MDEFT) scan (TR=1338 ms, TE=2.4ms, Matrix=256x224x176, in–plane FOV=250x250 mm^2, slice thickness=1 mm); 2) Diffusion tensor images (DTI) twice-refocused SE EPI (TR=7000 ms, TE=85 ms, maximum b factor=1000 smm^{-2}, isotropic resolution 2.3 mm^3). This sequence collects 7 images with no diffusion weighting (b_0) and 61 images with diffusion gradients applied in 61 non-collinear directions. 3) T2-weighted EPI sensitized to BOLD contrast (TR=2080 ms, TE=30 ms, 32 axial slices parallel to AC-PC line). BOLD EPIs were collected during rest for 7'and 20", resulting in a total of 220 volumes. During this acquisition, subjects were instructed to keep their eyes closed, not to think of anything in particular, and not to fall asleep.

DTI MRI ANALYSIS

After correction for eddy current distortions as described in (Cercignani et al. 2012), DTI images were processed using the Camino toolkit (www.camino.org.uk). The diffusion tensor was estimated in every voxel, and maps of fractional anisotropy (FA) were obtained for each subject.

Following the procedure described by (Behrens et al. 2003), thalamic parcellation was obtained by defining the seed region (thalamus) and the target regions (cortex areas labelled as explained below). Then, probabilistic tractography was used to assign to each voxel in the seed some probability of being connected to each of the targets. The seed voxels were thus classified as

connecting to the target with maximum probability (winner-takes-all strategy), and each cluster of voxels connecting to the same target was labelled as belonging to the same substructure.

A mask of the thalamus (seed region) in MNI coordinates was obtained by binarizing the Oxford Thalamic Connectivity Atlas (http://www.fmrib.ox.ac.uk/connect/), thresholded at 25% probability, while the target areas were defined on the MNI T1-weighted template provided with FSL as in (Behrens et al., 2003), identifying 7 exclusive cortical regions: prefrontal (PFC), primary motor (M1), premotor (lateral and medial) (PMC), primary and secondary somatosensory (S1/S2), posterior parietal (PPC), occipital and temporal cortices (Fig. 1).

The transformation matching the seed and target masks to every subject's DTII data was obtained by first co-registering the template with each participant's T1-weighted volume, and then registering the T1-weighted volume with their FA map. The transformation matrices were combined. All registrations were performed using FLIRT (http://fsl.fmrib.ox.ac.uk/fsl/).

Thalamic parcellation was obtained by running the probabilistic index of connectivity (PICo) algorithm (Parker et al., 2003) from each voxel in the thalamic mask, and labeling each voxel based on the most likely cortical region it was connected to. We will refer hereafter to the clusters identified by this segmentation as 'DTI thalamic segments'. The parcellated thalamic masks were transformed into standard space and averaged across subjects (Fig. 1-2).

FMRI PREPROCESSING

The RS-fMRI data were processed using MATLAB R2007B (Math-Work, Natick, MA) and SPM8 (http://www.fil.ion.ucl.ac.uk/spm/). The first 4 volumes of the functional images were discarded for signal equilibrium and adaptation of participant to scanning noise. Next, slice timing and head motion correction were performed, and the mean functional image was obtained for each participant. No participant exhibited head motion of >2 mm maximum translation or 2° rotation throughout the course of scan. The images were then normalized using the EPI template provided with SPM8.

In-house software was used to remove, using a 3rd order polynomial fit, the global temporal drift, the realignment parameters, and the signal averaged over whole brain voxels. Data were band-pass filtered (0.01-0.08 Hz) to remove high frequency variations.

SEED BASED FUNCTIONAL CONNECTIVITY ANALYSIS

Using seed based analysis, the mean time series from each DTI thalamic segment were extracted for every subject. They were then used as regressors in a first-level analysis in SPM8, in order to identify the degree of correlation, for every voxel in the brain, with each specific thalamic cluster, adding the motion parameters as nuisance variables. Contrast images for positive correlation were fed into a 2nd level analysis in SPM8, using a one-sample T-Test model. Results were considered significant for $p<0.05$ FWE corrected at voxel level, and masked to retain only cortical results.

QUANTITATIVE COMPARISON

In order to estimate the amount of overlap between structural and functional thalamo-cortical connections, we computed the number of cortical voxels resulting functionally connected to the thalamic clusters using SBA that overlapped with the cortical labels used for tractographic parcellation. We then computed: 1) the ratio between the overlapping voxels and the total number of voxels in each cortical label; and 2) the ratio between the overlapping voxels and the total number of voxels showing functional connectivity with the corresponding thalamic cluster. Both quantities were expressed as a percentage.

RESULTS

DTI THALAMIC PARCELLATION

The thalamic parcellation yielded results comparable with those reported by Behrens et al. (Behrens et al., 2003). As shown in Figures 1 and 2, each cortical region was specifically connected with distinct, spatially restricted zones within the thalamus. Each DTI thalamic segment obtained by this parcellation is color-coded as the corresponding connected cortex (Fig. 1-2). Moreover, we visually compared our parcellation with the one obtained by Wiegell and collegues (Wiegell et al., 2003). We found a consistent correspondence between the DTI thalamic segments that we obtained, the automatic segmentation that they performed using an anatomic clustering algorithm, and the thalamo-cortical pathways known from previous histological studies (Niemann et al., 2000).

According to our segmentation, the area of the thalamus preferentially connected with the prefrontal cortex (in green in Fig. 1-2) includes a large portion of the anterior complex, with part of the anterior ventral (AV), the ventral anterior (VA) and the ventro lateral (VL) nuclei, the medial-dorsal (MD) nucleus and the parafascicular (PF) and centromedian (CM) nuclei. Moreover, prefrontal connections were also found in a more posterior area corresponding with a portion of the pulvinar (Pu). Both MD and PF nuclei are known to project to the prefrontal association cortex, while the ventrolateral nucleus is known to be connected to the premotor cortex (Wiegell et al., 2003).

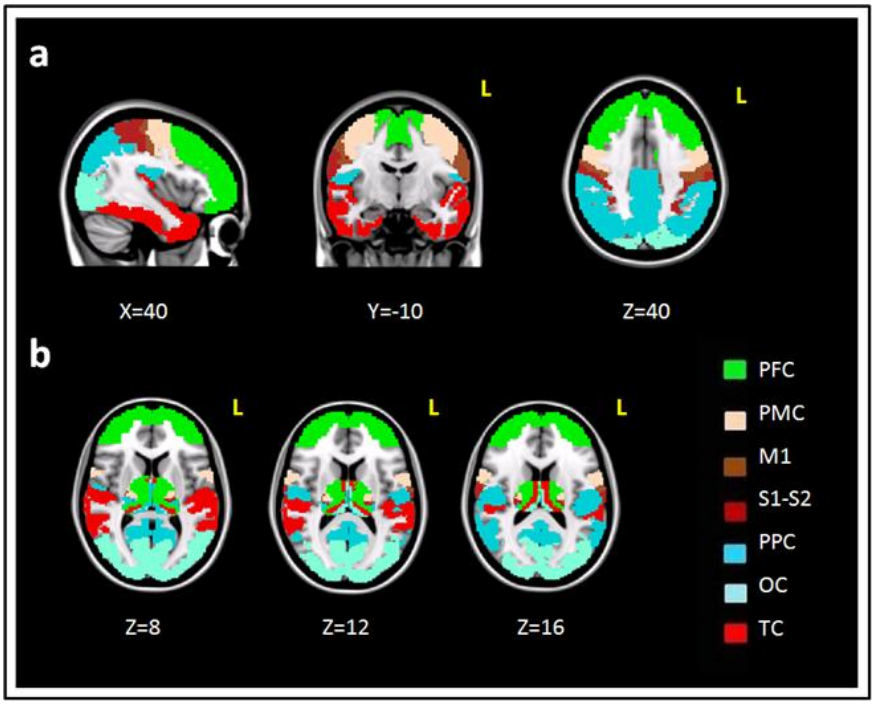

Fig. 1 DTI mri parcellation of the thalamus. A) for the DTI mri parcellation of the thalamus 7 exclusive cortical regions defined on the MNI t1-weighted template were used: prefrontal (PFC), primary motor (m1), lateral and medial premotor (PMC), temporal (TC), posterior parietal (PPC), primary and secondary somatosensory (s1/s2) and occipital cortex (OC). B) the resulting DTI thalamic segments obtained by DTI mri parcellation are overlaid onto a t1-weighted template provided with fsl. Each segment is color-coded as the corresponding connected cortex. See text for further details.

Posterior to this cluster, the segmentation identified a region connected to the temporal lobe (in red in Fig. 1-2), overlapping with the medial geniculate nucleus (MGN), the lateral geniculate nucleus (LGN) (bottom right in coronal slice section, Fig. 2), part of medial and inferior Pu and the supero-medial parts of the anterior complex that projects to limbic areas in the medial temporal regions (Behrens et al., 2003). Interestingly, from the existing literature, we know the MGN is involved in hearing function and its main

cerebral outputs are the primary auditory cortex and the superior temporal gyrus, while Pu projects mainly to parietal, temporal and occipital association cortices. The thalamic region connected to the premotor cortex is coloured in pink in Figures 1-2, and it shows a strong correspondence with the posterior part of VL nucleus (which is known to project to premotor and primary motor cortices). A correspondence with the lateral portion of CM (connected to motor cortex) and the anterior part of ventral posterolateral (VPL) nucleus (connected with primary somatosensory cortex) is also detectable.

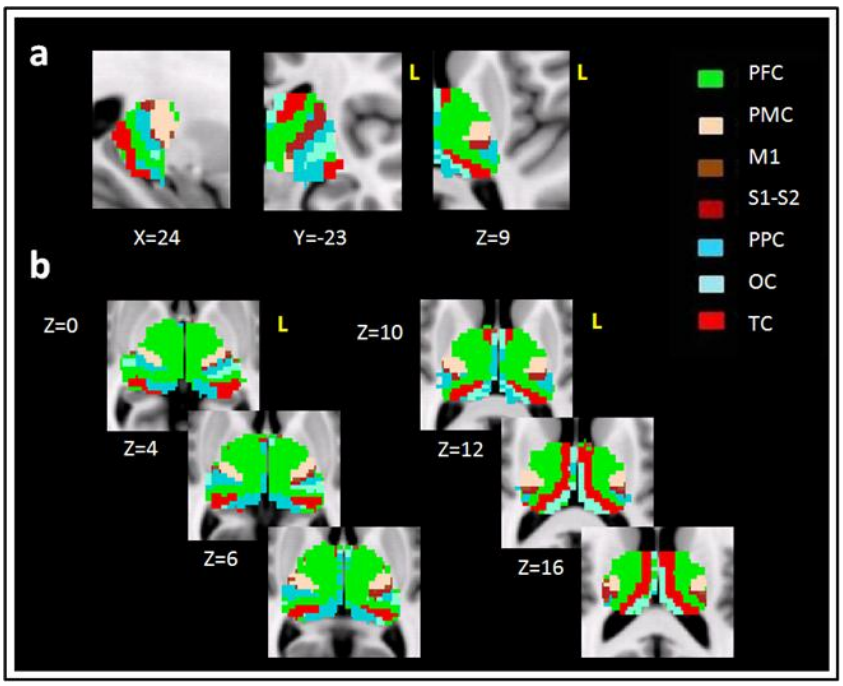

Fig. 2 Enlarged view of the DTI thalamic segments. A) sagittal, coronal and axial views of the segmented thalamus. Coordinates are in MNI space. B) zoomed axial views of the DTI thalamic segments. Colours correspond to the cortical labels listed in the legend, and shown in fig. 1. The thalamic parcellation yielded results comparable with those reported in (behrens et al., 2003). Abbreviations: PFC=prefrontal, M1=primary motor, PMC=Premotor, TC=temporal cortex, PPC=posterior parietal, S1/S2=primary and secondary somatosensory, OC=occipital cortices.

Because of the small size of motor and somatosensory cortex masks, voxels that show structural connections with these regions are not well delimited after thalamic parcellation. However, the voxels connected to the motor cortex (in brown in Fig. 1-2) are placed anteriorly with respect to those connected to somatosensory cortex (purple). Despite the small size, we identify a correspondence between these 2 thalamic regions and the posterior part of VPL and with a little portion of ventral posteromedial (VPM) nucleus. Both of them are known to act as relay stations for proprioceptive, vibration and touch information pathways, the former from the medial lemniscus, the latter from the trigeminal nerve. Moreover, VPL and VPM are known to be involved in movement through projections to somatosensory cortex and primary motor cortex.

The remaining 2 clusters are connected, respectively, with the posterior parietal cortex (darker blue), and with the occipital cortices (lighter blue). These regions are mainly distributed in the posterior and inferior parts of the thalamus including the lateral and medial part of Pu and the lateral posterior (LP) nucleus. A correspondence between a portion of the thalamus connected with parietal cortex and VPL is also noticeable. As reported above, Pu is well known to be involved in associative functions and it is mainly connected with parietal, temporal and occipital cortices. Also the LP nucleus plays a role in the associative functions and projects to posterior parietal cortex.

Overall, there is consistency between the results of our segmentation and the existing literature on thalamic nuclei. Table 1 summarizes the correlations

between our results, the corresponding thalamic nuclei and their known connections with the cortex.

SEED BASED FMRI CONNECTIVITY ANALYSIS

The RS-fMRI data showed significant ($p<0.05$ FWE corrected) patterns of connectivity in the cortex for all the DTI thalamic segments, with the exception of the thalamic region structurally connected to M1, whose fMRI connectivity pattern did not survive FWE correction. In order to assess the consistency between structural and functional connections, we compared the cortical areas functionally connected to each DTI thalamic region with the cortical mask originally used as targets to drive the DTI segmentation. As reported in Figures 3-7 (panel A), the thalamic portion structurally connected to PFC, S1-S2, PMC, TC and PPC, showed a partial overlap (in yellow) between functional connectivity and original masks used to assess structural thalamo-cortical connections. Not overlapping regions were found between functional connection with PFC-structurally-connected thalamic portion and original OC mask used to assess structural thalamo-cortical connections. Every DTI thalamic region also showed functional connectivity to regions of the cortex outside the target mask used for tractography (in blue in Fig. 3-7, panel B). Table 2 lists all the functional connections found for each DTI thalamic segment.

QUANTITATIVE COMPARISON

Figure 8 shows the results of the quantitative comparison, confirming that the overlap between functional and structural connectivity to the thalamus is modest.

DTI thalamic segment connected to	Thalamic nuclei included in DTI segment		KNOWN CONNECTIONS
PREFRONTAL CORTEX	**AV** anterior ventral	**X**	cinglate gyrus, limbic association cortex
	VA Ventral anterior	**X**	prefrontal association cortex
	VL ventro lateral		premotor and primary motor cortex
	MD media dorsal	**X**	prefrontal association cortex
	PF parafascicular	**X**	prefrontal cortex, caudate nucleus
	CM centromedian		motor cortex and putamen
	Pu pulvinar		parietal, temporal, occipital association cortex
PREMOTOR CORTEX	**VL** ventral lateral	**X**	premotor and primary motor cortex
	VPL ventral postero lateral		primary somatosensory
MOTOR CORTEX	**VPL** ventral postero lateral		primary somatosensory
	VPM ventral postero medial		primary somatosensory, insula
	CM centromedian	**X**	motor cortex and putamen
SOMATOSENSORY CORTEX	**VPL** ventral postero lateral		primary somatosensory
	PM ventral postero media	**X**	primary somatosensory, insula
	CM centromedian		motor cortex and putamen
PARIETAL POSTERIOR CORTEX	**Pu** pulvinar **X**		parietal, temporal, occipital association cortex
	LP Lateral posterior nucleus	**X**	posterior parietal association
	VPL ventral postero lateral	**X**	primary somatosensory
OCCIPITAL CORTEX	**Pu** pulvinar	**X**	parietal, temporal, occipital association cortex
	LP Lateral posterior nucleus	**X**	posterior parietal association
TEMPORAL CORTEX	**MGN** medial geniculate	**X**	primary auditory cortex, superior temporal gyrus
	LGN lateral geniculate nucleus		primary visual cortex, calcarine gyrus
	VA Ventral anterior		prefrontal association cortex
	VL ventral lateral		premotor and primary motor cortex
	MD media dorsal		prefrontal association cortex

Table 1. Comparison of DTI segmentation and anatomical properties of the thalamus. The first column lists the cortical regions each DTI thalamic segment was mostly connected to. The middle column lists the thalamic nuclei identified within each DTI Thalamic segment. The right column lists the connections that have been documented for the nuclei listed in the central column. A cross indicates a matching between tractographic and known connections. To ease the comprehension, each segment is coloured with the same shade as in Figures 1-2.

DTI thalamic segment connected to	Functional connections overlapping with cortical masks*	Functional connections not overlapping with cortical masks*
PREFRONTAL CORTEX	Superior frontal gyrus L	Precentral gyrus R L
	Middle frontal gyrus R	Temporal pole R L
	Frontal pole R L	Cyngulate gyrus
		Supramarginal Gyrus R L
		Planum polare R
PREMOTOR CORTEX	Precentral gyrus R L	Post central gyrus L
		Lingual gyrus R
		Planum polare R L
		Insular cortex R L
MOTOR CORTEX	None	None
SOMATOSENSORY CORTEX	Superior lateral lobe L	Precuneus cortex L
	Posterior central gyrus R	Precentral gyrus R
		Parietal operculum cortex R L
PARIETAL POSTERIOR CORTEX	Precuneus cortex R L	Temporal pole R
	Central operculum cortex R	Temporal fusiform cortex R L
	Cingulate gyrus R L	Lyngual gyrus R L
OCCIPITAL CORTEX	None	Cyngulate gyrus R L
TEMPORAL CORTEX	Temporal fusiform cortex R L	Lyngual gyrus R L
	Temporal pole R L	Intracalcarin cortex R L
	Inferior temporal gyrus R L	Precuneus Cortex R L

* By “cortical masks” here we refer to the cortical labels used to segment the thalamus in the DTI analysis.

Table 2. Functional connections to every DTI thalamic segment The first column lists the cortical regions each DTI thalamic segment was mostly connected to. The middle and right column lists the cortical areas found to be functionally connected to each of them, based on RS-fMRI analysis, classified as being overlapping or non-overlapping with structural connections. To ease the comprehension, each segment is coloured with the same shade as in Figures 1-2.

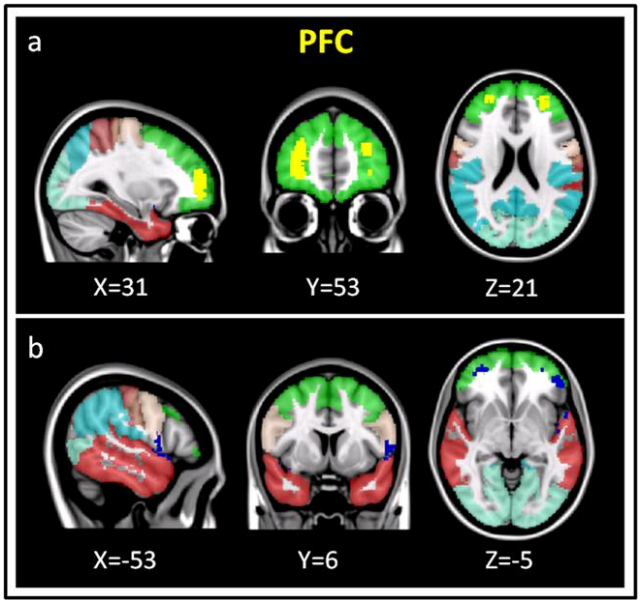

Fig. 3 Prefrontal cortex (PFC) connections: overlap and mismatch between functional and structural thalamic connections. A) overlapping regions (yellow) between functional connection with pfc-structurally-connected thalamic portion and original PFC mask (green) used to assess structural thalamo-cortical connections. B) functional connections (blue) to pfc structurally connected thalamic portion that fall outside the target pfc mask used for tractography.

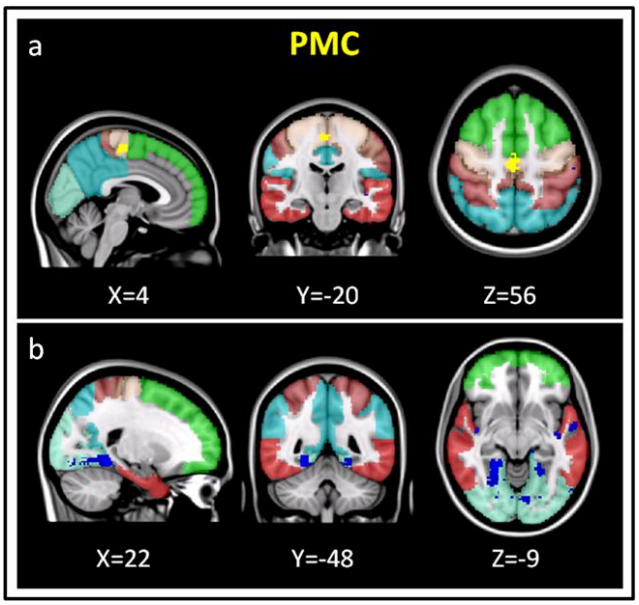

Fig. 4 Premotor cortex (PMC) connections.h between functional and structural thalamic connections. A) overlapping regions (yellow) between functional connection with PMC-structurally-connected thalamic portion and original PMC mask (pink) used to assess structural thalamo-cortical connections. B) functional connections (blue) to pmc structurally connected thalamic portion that fall outside the target pmc mask used for tractography

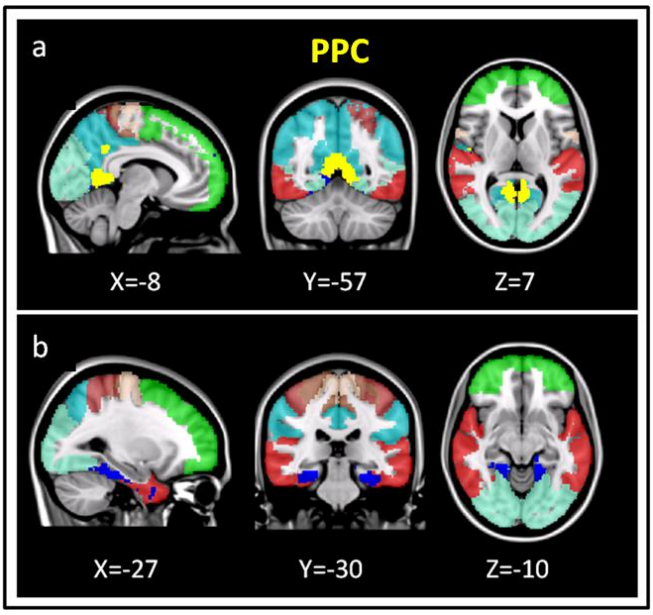

Fig. 5 Parietal cortex (PC) connections: overlap and mismatch between functional and structural thalamic connections. A) overlapping regions (yellow) between functional connection with pc-structurally-connected thalamic portion and original PC mask (medium blue) used to assess structural thalamo-cortical connections. B) functional connections (dark blue) to PC structurally connected thalamic portion that fall outside the target pc mask used for tractography.

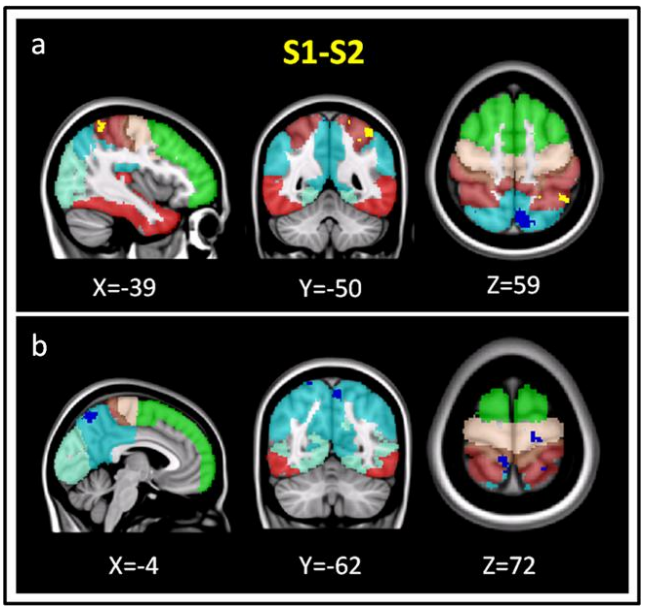

Fig. 6 Somatosensory cortex (s1/s2) connections: overlap and mismatch between functional and structural thalamic connections. A) overlapping regions (yellow) between functional connection with s1/s2-structurally-connected thalamic portion and original s1/s2 mask (brown) used to assess structural thalamo-cortical connections. (yellow voxels). B) regions functional connections to s1/s2 structurally connected thalamic portion that fall outside the target s1/s2 mask used for tractography.

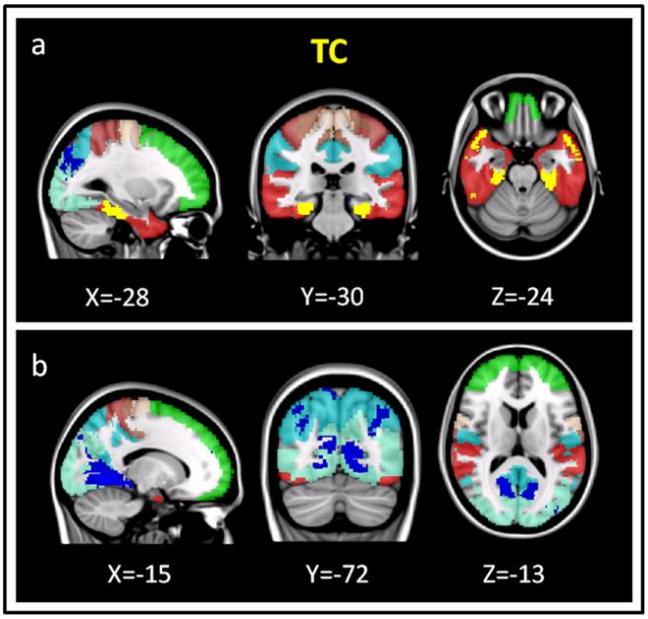

Fig. 7 Temporal Cortex (TC) Connections: overlap and mismatch between functional and structural thalamic connections. A) Overlapping regions (yellow) between functional connection with TC-structurally-connected thalamic portion and original TC mask used to assess structural thalamo-cortical connections (red). B) Functional connections (dark blue) to TC structurally connected thalamic portion that fall outside the target TC mask used for tractography.

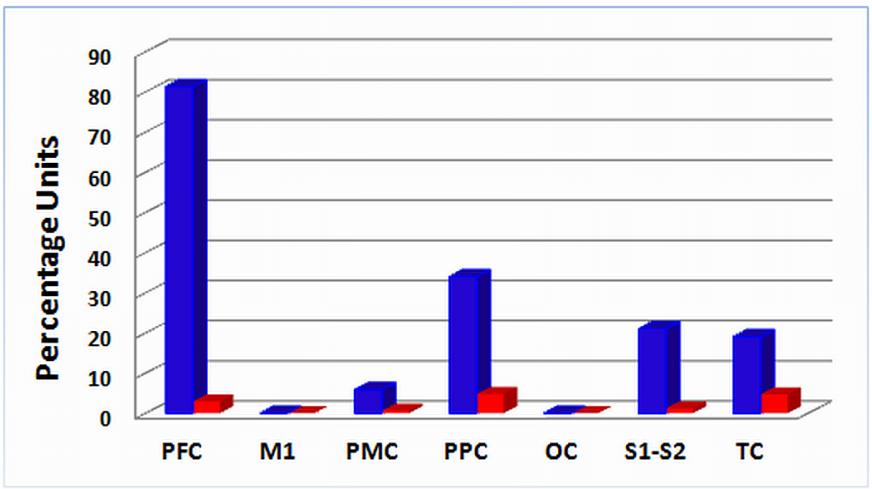

Fig.8 percentage overlap between structural and functional connections, obtained with probabilistic tractography and seed-based analysis, respectively. Percentage are computed a) over the total number of voxels in the corresponding corticallabel, and b) over the total number of voxels found to be connected to each thalamic cluster by sba. Abbreviations: PFC=prefrontal, M1=primary motor, PMC=premotor, TC=temporal cortex, PPC=posterior parietal, s1/s2=primary and secondary somatosensory, OC=occipital cortices.

DISCUSSION

This work attempts for the first time to characterize and compare structural and functional thalamo-cortical connections in the same group of individuals. The purpose was to use the thalamus as a model for integrating structural connectivity measures derived from DTI and functional connectivity measures derived from RS-fMRI. This fits with the concept that the anatomical specialization of a brain region determines its functional specialization (Passingham et al., 2002). Therefore, mapping the anatomical connections of a region should allow us to define functional-anatomical boundaries (Beherens et al., 2011). Despite functionally connected regions are expected to be also connected in structure, the extent to which functional and anatomical MRI-derived connectivities express each other is still largely unknown.

Several interesting observations can be drawn from our results. First, this study confirms the reproducibility of thalamic parcellation using probabilistic tractography: our results are consistent with those obtained by previous work by other groups (Behrens et al., 2003; Johansen-Berg et al., 2005; Zhang et al., 2010). Taken together, all these studies suggest that there is a good correspondence between the segmentation based on cortical connectivity and predictions based on invasive tract tracing studies on thalamo-cortical and cortico-thalamic connectivity in non-human animals (Darian-Smith et al., 1990; Darian-Smith et al., 1996; Goldman-Rakic and Porrino, 1985; Yeterian

and Pandya, 1985; Yeterian and Pandya, 1988; Yeterian and Pandya, 1989; Yeterian and Pandya, 1991; Yeterian and Pandya, 1997).

To provide a better understanding of the relationship between functional and anatomical connectivity, we used SBA of RS-fMRI data. The results showed only a partial overall correspondence between structural and functional connections, thus suggesting that the two approaches are likely to provide complementary information. Indeed, structural connectivity as measured by tractography can only detect mono-synaptic connections, while functional connectivity is likely to rely on poly-synaptic pathways too. For example, a number of thalamo-cortical connections are known to be non-direct, but mediated by the basal ganglia (Haber et al., 2009). This finding of non overlapping functional and anatomical connections is consistent with the results of a study conducted by Honey and collaborators demonstrating that robust functional connectivity can be found between regions not structurally linked by direct pathways, and that functional networks continuously reconfigure around the underlying anatomical skeleton. Moreover, although the presence of strong anatomical connections is predictive of strong RS functional connections, the reverse inference is less reliable (Honey et al., 2009). Another important observation is that we are only considering functional connectivity at rest. As it is conceivable that some level of modulation is introduced by task performance (Albert et al., 2009; Hasson et al., 2009), functional connectivity at rest may differ from functional connectivity during the performance of an active task.

Finally, some other methodological issues should be considered. As many authors before us, we have used a winner-takes-all strategy to define the DTI thalamic segments. This approach increases specificity to selected pathways, but reduces sensitivity, as some nuclei show connections to multiple cortical sites. For example the thalamic portion found to be connected with PFC by DTI (green in Fig. 1-2) includes part of Pu, which is known to be anatomically connected to the temporal pole (Chabardes et al., 2002; Niemann et al., 2000). Consistently, the seed-based functional connectivity analysis highlighted a correlation between the BOLD time series extracted from this segment and the insular cortex and planum polare (Table 2).

The between-region distance could also play an important role in the localization of functional correlation (Honey et al., 2009): those regions that are closer to the thalamic nucleus used as seed are more likely to show a correlation with it because of the proximity influence. Finally, the variable size of each DTI thalamic segment could influence the detection of functional connections through RS seed based analysis.

Additional factors might be responsible, at least partially, for our results. First, different spatial sensitivity of the two techniques could arise from different image resolutions, different preprocessing steps (e.g fMRI data were smoothed while DTI data were not), and different kind of artifacts (e.g. susceptibility). Second, specific limitations of each approach could also play a role, such as the inability of the tensor model used to analyze DTI to account

for multiple directions within a voxel. Future studies should thus be designed to address at least some of these limitations.

In conclusion, this is the first study that attempts to cross validate two different methodologies for the investigation of thalamo-cortical correlations in the same group of subjects, showing only a partial correspondence. While some methodological aspects might account for this mismatch, we propose that these two approaches offer complementary information on brain connectivity. Future studies are warranted to extend the results we obtained in the thalamus to other structures, and to confirm that the mechanisms behind functional connectivity are more complex than just expressing structural connectivity.

CHAPTER 5

NETWORK BASED STATISTICAL ANALYSIS DETECTS CHANGES INDUCED BY CONTINUOUS THETA BURST STIMULATION ON BRAIN ACTIVITY AT REST

In this study I combined RS-fMRI with TMS to evaluate the influence of inhibitory effect of cTBS on the functional connectivity in a group of healthy controls. The study was performed in collaboration with other reasearechers.

INTRODUCTION

As already mentioned in Chapter 1, as RS-fMRI is becoming one of the most popular techniques for assessing functional connectivity and non invasive brain stimulation methods such as TMS can be used to probe response to perturbation/stimulation, the combination of these techniques holds great promise for the characterization of brain networks and for addressing several important clinical issues (Deco et al., 2011; Fox and Raichle, 2007; van den Heuvel and Hulshoff Pol, 2010).

To date, different approaches have been used to investigate the effect of a perturbation on fMRI functional connectivity: some studies have been performed to assess the influence of tDCS on RS-fMRI data (Keeser et al., 2011; Meinzer et al., 2012; Pena-Gomez et al., 2011; Polania et al., 2011). Other work focused on the influence of TMS on task-based effective connectivity (Grefkes et al., 2008; Lee et al., 2003b; O'Shea et al., 2007;

Pleger et al., 2006). Just few studies investigated so far the effects of repetitive TMS (rTMS) on RS-fMRI (Eldaief et al., 2011; van der Werf et al., 2010; Vercammen et al., 2010b). In one study rTMS was applied over the left dorsolateral prefrontal cortex (DLPFC) resulting in distal changes of neural activity within the DMN (van der Werf et al., 2010). Similarly Eldaief and collaborators tested two different frequencies of rTMS applied over the left posterior inferior parietal lobule (IPL) to evaluate the effect on the DMN: high-frequency rTMS decreased functional correlations between cortical DMN nodes, but not between these nodes and the hippocampal formation. In contrast, low frequency rTMS increased functional correlations between IPL and the hippocampal formation (Eldaief et al., 2011). Another study tested the effects of 5 Hz rTMS on prefrontal-hippocampal coupling during both a working memory task and at rest. Finally, seeded functional connectivity analyses demonstrated significant effects of rTMS on the prefrontal network dynamics in the n-back task that were not evident during rest (Bilek et al., 2013). All these studies were performed with a strong working hypothesis, either testing only one Resting State Network (RSN) (Eldaief et al., 2011; van der Werf et al., 2010) or using coupling analyses within a specified connection (Bilek et al., 2013). Moreover all of them compared the effects of rTMS in two separate sessions performed on different days, which could have increased the intrinsic variability of the functional connectivity measured by fMRI.

Here, for the first time we compared RS-fMRI data recorded before and after real continuous theta-burst repetitive stimulation (cTBS), a powerful protocol resulting in long-lasting decreases of cortical excitability (Huang et al., 2005), which I have described in detail in Chapter 1. An additional element of novelty is that we used a network analysis based on network based statistics (NBS) (Zalesky et al., 2010) (see Chapter1) to include all the most relevant nodes of the areas interconnected with the stimulated site (the right DLPFC). We chose to stimulate the right DLPFC, since TMS of this area is known to modulate several cognitive functions and has a potential role in treating various clinical conditions such as depression and Parkinson's disease (Chen et al., 2013; George et al., 2013).

METHODS

The study was approved by the ethics committee of Santa Lucia Foundation, and written informed consent was obtained from all subjects before study initiation.

We recruited 36 healthy volunteers [m/f =18/18; mean (SD) age=26.88 (3.5) years] with no history of medical or psychiatric disorders, autonomic dysfunction, or other major clinical conditions. The experimental session included an MRI scan, followed by either cTBS or sham stimulation, and a post-intervention MRI scan (Fig. 1). Each participant was randomly assigned to either group, resulting in 18 participants receiving cTBS, and 18 receiving the sham.

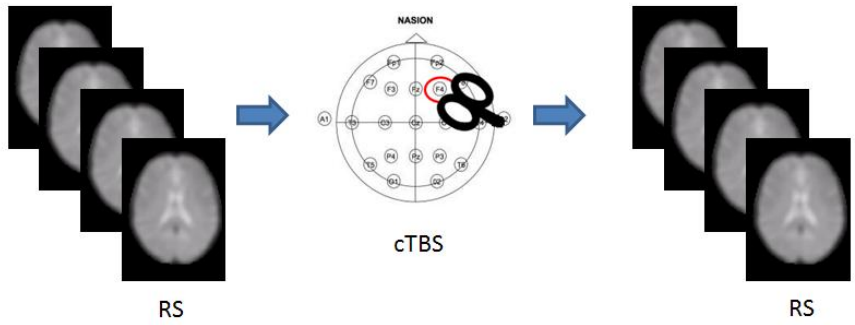

Fig. 1 Experimental set up. RS-fMRI was acquired before and after cTBS stimulation in half of the participants. The remaining 18 participants received sham stimulation instead.

MRI ACQUISITION PROTOCOL

All imaging was obtained using a head-only 3.0T MR scanner (Siemens Magnetom Allegra, Siemens Medical Solutions, Erlangen, Germany). The acquisition protocol included the following sequences: 1) a magnetization-prepared rapid gradient echo (MPRAGE) sequence (TR = 2500ms; TE = 2.74 ms; TI = 900 ms; Flip angle = 8°; matrix = 256×208×176; slab thickness = 1mm; FOV = 256×208×176mm^3). 2) a series of T2* weighted echo planar imaging (EPI) scans, sensitized to blood oxygenation level dependent contrast (BOLD) (TR:2080 ms, TE:30 ms, 32 axial slices parallel to AC-PC line, matrix:64×64, pixel size:3×3 mm^2, slice thickness:2.5 mm, flip angle:70°) for resting state fMRI. BOLD EPIs were collected during rest for a 7 min and 20 s period, resulting in a total of 220 volumes.

cTBS PROTOCOL

A MagStim Super Rapid magnetic stimulator (Magstim Company, Whitland, Wales, UK), connected with a figure-of-eight coil with a diameter of 90 mm was used to deliver cTBS over the scalp site corresponding to the right

prefrontal cortex (F4 electrode International 10-20 system). The magnetic stimulus had a biphasic waveform with a pulse width of about 300 μs. Three-pulse bursts at 50 Hz repeated every 200 ms for 40 s were delivered at 80% of the Active Motor Threshold (AMT) over right prefrontal cortex (600 pulses). AMT was tested over the motor cortex of the right hemisphere. AMT was defined as the lowest intensity that produced MEPs of >200 μV in at least five out of 10 trials when the subject made a 10% of maximum contraction using visual feedback (Rothwell, 1997). The coil was positioned tangentially to the scalp, with the handle pointing superiorly. For sham cTBS the coil was positioned over the same scalp site, but angled away so that no current was induced in the brain.

DLPFC was targeted using a neuronavigation system (Softaxic) to precisely position the coil over the cortical site, using individual T1-weighted magnetic resonance imaging volumes as anatomical reference; this technique has been previously described in detail (Koch et al., 2009; Koch et al., 2007). The stimulation points were determined before the experiment and were marked on the adherent plastic cap worn by the subject. To target DLPFC, the coil was positioned over the middle of the line separating the anterior and middle thirds of this gyrus, following the algorithm proposed by Mylius and collaborators (Mylius et al., 2013). According to the anatomical data reported by Rajkowska and Goldman-Rakic (Rajkowska and Goldman-Rakic, 1995), this target is localized at the junction between BA9 and BA46. This location is in agreement with meta-analyses of neuroimaging studies on working

memory (Fitzgerald et al., 2006; Glahn et al., 2005). The center of the coils was positioned tangentially to the skull with the handle pointing backward angled at 45° (Fig. 1).

RS-FMRI PREPROCESSING

The RS-fMRI data were processed using MATLAB R2007B (Math-Work, Natick, MA) and SPM8 (http://www.fil.ion.ucl.ac.uk/spm/software/spm8/) .

The first 4 volumes of the functional images were discarded for signal equilibrium and adaptation of participant to scanning noise. Next, slice timing and head motion correction were performed. Participants exhibiting head motion of >2 mm maximum translation of 2° rotation throughout the course of scan were excluded. The images were then normalized using the EPI template provided with SPM8.

In-house software was used to remove the global temporal drift using a 3rd order polynomial fit, the realignment parameters, and the signal averaged over whole brain voxels. Data were band-pass filtered (between 0.01 and 0.08 Hz)

SEED BASED CONNECTIVITY ANALYSIS (SBA)

SBA was performed to identify the cortical areas functionally connected with the stimulated region. For each subject the mean time course (TC) of the right DLPFC was extracted for each subject using the prefrontal cortex region defined in Harvard Oxford atlas (http://www.cma.mgh.harvard.edu/), available with FSL.

Each participant's TC was then used as regressor in a first-level analysis in SPM8, in order to identify the degree of correlation, for every voxel in the brain, with the prefrontal region, adjusting for the motion parameters.

Contrast images for positive correlation were fed into a 2nd level analysis using a one-sample T-Test. Results were considered significant for $p<0.05$ FWE corrected at voxel level.

NETWORK BASED STATISTIC (NBS)

The clusters that resulted to be significantly connected to the right prefrontal cortex (Fig.2) were then defined as the nodes of the network of interest. Using marsbar (http://marsbar.sourceforge.net/), we created 29 spheres, with a diameter of 8 mm each (see Table I, Fig.3), centered at the centre of gravity of each of the nodes, from which mean TCs were extracted to estimate a connectivity matrix for each subject. The number of rows and columns in this matrix is the total number of nodes in the network, and the elements are defined as the correlation coefficient between the TC of each pair of nodes.

Once each participant connectivity matrix was obtained, we used the NBS toolbox (Zalesky et al., 2010) (http://www.cmtk.org/viewer/documentation/users/tutorials/tut_nbs.html) to compare the correlation between each node of the network before and after cTBS, using a paired T-test design. The false discovery rate (FDR) was used to adjust for multiple comparisons, with 25000 permutations. Results were considered significant for $p<0.05$. The same analysis was performed on the data acquired before and after sham stimulation.

RESULTS

Four participants who received sham stimulation were excluded due to excessive motion during fMRI, thus resulting in the following 2 groups: 18

subjects receiving cTBS [m/f =9/9; mean (SD) age=26.72 (3.8) years], and 14 receiving sham stimulation [m/f =6/8; mean (SD) age=27.07(3.6) years].

SBA revealed a specific pattern of correlation between right DLPFC and several brain regions, including the right and left prefrontal, parietal, temporal cortex, precuneus, posterior cingulated cortex, thalamus, caudate nucleus and cerebellum (Fig. 2). The corresponding network nodes are shown in Table I and Fig.3.

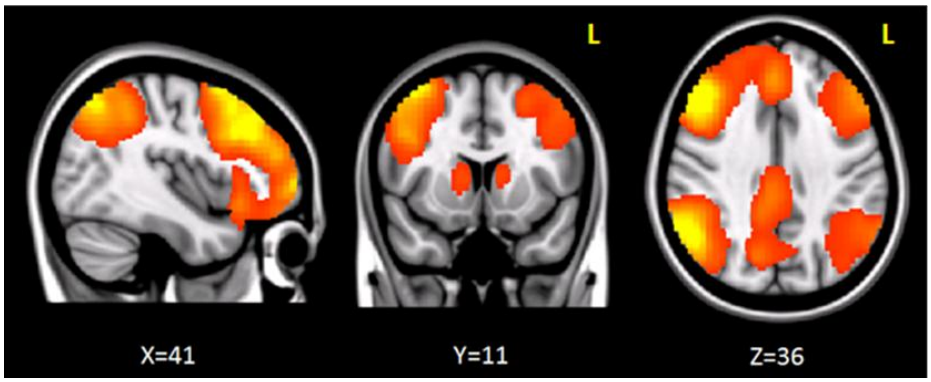

Fig. 2 Brain regions functionally correlated to the right prefrontal cortex used as seed in seed-based analysis.

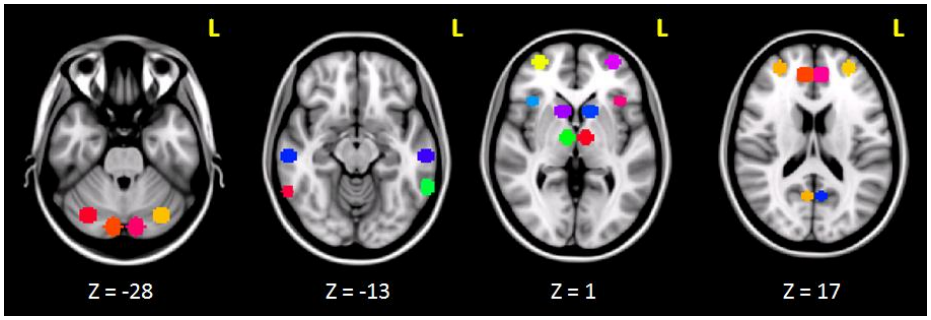

Fig. 3 Spherical rois (radius=8mm) defining the nodes of the network investigated before and after cTBS.

We detected a striking decreased correlation between the right DLPFC and the right posterior parietal cortex (Brodmann areas 10 and 40 respectively) after stimulation ($p<0.05$) (Fig. 4). The same analysis performed on the data acquired before and after sham stimulation did not show any difference among the tested connectivity matrices.

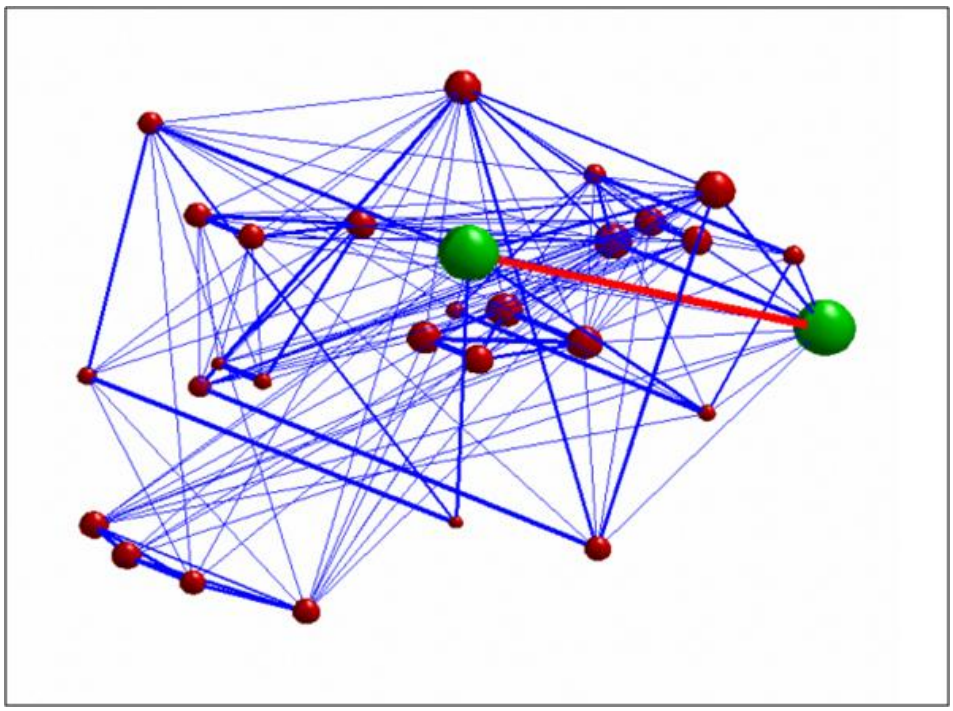

Fig. 4 3d graph representing the investigated network. The green nodes indicate the rois whose connectivity (represented by the red edge) was decreased after stimulation. The radius of each of the red nodes reflects the node strength (i.e., the sum of the weights of each edge connected to the node). The thickness of the edges reflect the strength of correlation between each node. Only connections with correlation coefficient > 0.3 are displayed.

DISCUSSION

In this study we provide new evidence for the role of RS-fMRI in detecting changes in brain activity associated with TMS. Through RS-fMRI it is possible to identify functional connections that reflect temporal coupling

between distant regions. Thus, characterizing the covariance of the BOLD signal in anatomically distant areas of the brain can be useful to measure the degree to which the network properties are affected by TMS. Here, RS-fMRI was carried out before and immediately after TMS to provide direct measures of the functional organization of the DLPFC-correlated network and its plastic reorganization induced by stimulation.

To assess the influence of the perturbation induced by TMS on FC, we used NBS. It is a novel network based approach to identify functional correlations between different brain regions known to be part of a specific pattern of co-activation. This methodology is based on graph theory that provides a theoretical framework to examine complex networks, thus revealing important information about their local and global organization (Eldaief et al., 2011; van den Heuvel and Hulshoff Pol, 2010). NBS was used after the identification of a specific network of right DLPFC correlated regions, in order to restrict the analysis to the nodes showing functional connections to the stimulation site. Such network was identified using SBA, and it strictly resembles a network previously described as the right fronto-parietal network (FPN) by several groups (Beckmann CF, 2005; Calhoun et al., 2008; Damoiseaux et al., 2006; Jeong et al., 2012; van den Heuvel and Hulshoff Pol, 2010). Accordingly, we found that DLPFC cTBS induced a selective modulation of the ipsilateral posterior parietal cortex. This finding could be interpreted on the basis of the well known functional interactions strongly linking the activity of the DLPFC with that of the PPC (Koch et al. 2012a). These two areas are jointly

implicated in a variety of cognitive functions and are thereby considered two main nodes of the FPN. Indeed, throughout the literature, two strongly lateralized RSNs have consistently been reported, one predominantly in the right hemisphere and the other in the left hemisphere usually with a specular pattern involving the middle frontal and orbital cortex (BA 6/9/10), the superior parietal cortex (BA 7/40), the middle temporal gyrus (BA 21), and the posterior cingulate cortex (BA 23/31) (Damoiseaux et al., 2006). These two networks are known to be closely coupled in a wide range of cognitive processes, such as working memory, both in adults (D'Esposito et al., 1998; Damoiseaux et al., 2006; van Asselen et al., 2006; Wager and Smith, 2003) and in children and adolescents (Finn et al., 2010; Kwon et al., 2002; Thomason et al., 2009), language (Smith et al., 2009), attention (Corbetta et al., 1998; Dosenbach et al., 2007; Fink et al., 2001; Vannini et al., 2007) and visual processes (De Luca et al., 2006).

Consistently, recent tDCS literature suggests that low-intensity electrical stimulation over the DLPFC can result in transient improvements in a variety of cognitive functions including declarative (Floel et al., 2008) and working memory (Fregni et al., 2005; Zaehle et al., 2011), planning (Dockery et al., 2009), language learning (Floel et al., 2008), attention (Boggio et al., 2007) and decision making (Boggio et al., 2010).

To better understand the substrate of these changes, the interaction between the nodes of the FPNs has been investigated using tDCS. A previous study (Pena-Gomez et al., 2011) examined how active tDCS over the left or right

DLPFC in comparison with sham tDCS modulates time course fluctuations within and across the DMN and the anti-correlated network (AN) on RS-fMRI. One of the main results emerging from this work is that active anodal tDCS over the DLPFC results in a stronger temporal functional connectivity between prefrontal and parietal regions, supporting our current findings. Similar results were obtained by Keeser et al. (Keeser et al., 2011), who measured significant changes in regional brain connectivity for nodes of the DMN and the right and left FPNs. Such changes were detected after DLPFC-tDCS both, close to the primary stimulation site, and in connected brain regions.

On the other hand, the effects of TMS (as opposed to tDCS) have been mainly evaluated in combination with task-active fMRI, instead of RS-fMRI. Only recently, a number of studies attempted to assess the effect of TMS on functional connectivity at rest (Eldaief et al., 2011; Grefkes et al., 2008; Lee et al., 2003b; O'Shea et al., 2007; Padberg and George, 2009; van der Werf et al., 2010; Vercammen et al., 2010b). Most of these works were performed with a strong working hypothesis, either testing only one RSN (Eldaief et al., 2011; van der Werf et al., 2010) or using coupling analyses within a specified connection (Bilek et al., 2013). Crucially, all of them evaluated the effects of rTMS by comparing post-stimulation vs post-sham data recorded on separate days, introducing a bias due to the intrinsic variability of RS-fMRI. By contrast, in order to reduce the effect of intrinsic individual variability, we

compared for the first time RS-fMRI data recorded within the same session before and after TMS, with a short interval between MRI sessions.

Our data indicate a selective influence of right DLPFC-cTBS on the ipsilateral posterior parietal cortex, while no connectivity change was detected after sham stimulation. As it is known that cTBS is able to induce prolonged cortical inhibition (Huang et al., 2005), the decreased correlation between BA10 and BA40 we observed after stimulation could be explained by two alternative hypotheses: i) cTBS is able to induce cortical inhibition just in the stimulated site with a consequent disruption of the co-activation of the two areas; ii) the inhibition of cortical activity occurs immediately in the stimulation site, subsequently spreading to distant connected area. The propagation of inhibitory signal at microscopic level induces a de-synchronization of normal coupling activity of the areas involved. So the de-coupling of neuronal activity we observed through the BOLD signal could reflect an undergoing mechanism of signal propagation. Thus, we hypothesize that cTBS does not solely produce focal effects by selectively affecting an isolated patch of cortex. Rather, target sites should be considered as nodes within a widespread network of interacting brain regions, where perturbing or boosting processing of one element can also influence several others. We can only speculate on why we found a selective modulation of the DLPFC-PPC connection. The DLPFC and PPC neuronal assemblies have a strong functional coupling that could be more sensitive to an external perturbation such as that induced by the low intensity cTBS protocol applied in the current

study (Koch et al. 2012a). However, it is likely that by simply increasing the intensity of the magnetic field or changing the frequency of stimulation it could be possible to affect the coupling among other interconnected nodes. Notably, recent evidence suggests that an individual approach based on functional connectivity MRI could provide the most reliable approach to detect the effects of DLPFC TMS (Fox et al. 2012a, Fox et al. 2012b).

Our results could also have several implications for clinical applications, as it has been demonstrated by the role of rTMS of the DLPFC in the treatment of major depressive disorder (MDD). This therapeutic effect can be achieved by either excitatory stimulation of the left (George and Post, 1995; O'Reardon et al., 2007; Padberg and George, 2009; Pascual-Leone et al., 1996) or inhibitory stimulation of the right DLPFC (Isenberg et al., 2005; Pallanti et al., 2010; Rossini et al., 2010). A recent meta-analysis study conducted by Chen and collaborators (Chen et al., 2013), demonstrated that, despite the comparable efficacy of both methodology, the latter (inhibitory TMS) may be a more acceptable treatment for MDD than the former (excitatory TMS), based on patients reporting less headaches, and on the decrease risk of inducing adverse events such as seizures (Schutter, 2010). The present results could also be important for other conditions in which the non invasive modulation of the FPN can provide notable clinical improvements, such as the case of post-stroke hemispatial neglect (Koch et al. 2012b).

In conclusion, our findings provide new insights into the mechanisms of stimulation-induced brain plasticity by demonstrating that the network

communication at rest shapes the brain reorganization induced by cTBS. The use of TMS and RS-fMRI allows to characterize both local (i.e., in the cortical tissue directly under the TMS coil) and remote (i.e., distant from the original cortical target site) effects of TMS in more detail, leading to a better understanding of TMS-induced modulations in neural processing.

CONCLUSIONS

The experiments described in this thesis generated a number of results, as well as some ground for further investigations. Here the main findings are briefly summarized.

ROLE OF DISCONNECTION IN NEUROLOGICAL DISORDERS

In the first work DTI data were analyzed using TBSS. Comparing right-hemisphere stroke patients with neglect and healthy subject, subtle abnormal changes in the FA values were found along several WM tracts of the left (non lesioned) hemisphere of neglect patients. Moreover, a correlation was demonstrated between these alterations and the severity of neglect observed in our patients. In the present work our data support the hypothesis that the main damage occurring in the left hemisphere of these patients is dominated by demyelination in the context of Wallerian degeneration phenomena. While the occurrence of Wallerian degeneration in one hemisphere can be expected in cases of macroscopic damage in the other hemisphere, an intriguing result of this study is that FA changes in the ‘‘healthy’’ hemisphere also accounted for the severity of neglect symptoms observed in our patients. These results provide new anatomical evidence supporting the idea that changes in right-left balance rather than an isolated involvement of the right hemisphere can be critical for the occurrence of neglect symptoms.

When looking at the general porpoise of the thesis, the present work yields two main conclusions. First, the characterization of anatomical connectivity is crucial to understand the pathological mechanisms at the basis of functional and behavioral changes that occur in several neurologic disorders. Second, diffusion weighted structural imaging has been demonstrated to be a powerful tool to assess the alteration in anatomical connectivity and its correlation with neuropsychological indices, thus providing new evidence of the importance of neuroimaging in the detection of abnormal brain structure and functioning.

The second study was conducted in order to characterize functional connectivity in a group of aMCI using RS-fMRI analysis using network analysis. We have shown a marked disconnection of the precuneus, parietal and temporal areas, regions representing densely interconnected cortical hubs, within which early deposition of extracellular amyloid is observed (Buckner et al., 2009; Liu et al., 2013; Wang et al., 2013). However, our analyses also demonstrate disruption of network connectivity in brain regions where AD pathology is not manifest until late disease stages, such as the sensorimotor cortex and the insula, the thalamus and the basal ganglia. Comparing these results and those obtained by VBM to asses volume loss, it was hypothesized that changes in functional network architecture precedes the cortical atrophy that characterize AD patients.

From a more general prospective, this work highlights the potential value of the detection of changes in functional connectivity in aMCI patients: the abnormal pattern of functional connections revealed in these subjects could

represent a biomarker of AD development, providing an important tool for an early diagnosis of the disease. In this context, network analysis appears particularly promising, as we have shown it can be more sensitive than more standard approaches such as ICA. Together, the results of these 2 chapters highlight the role of disconnection in the development of neurological symptoms. Future work in this area should include longitudinal designs able to clarify the prognostic value of disconnection measures.

STRUCTURAL VS FUNCTIONAL CONNECTIVITY

The third analysis was carried out in a group of healthy subjects. We attempt for the first time to characterize the thalamo-cortical connections in the same group of individuals from both, a structural (derived from DTI) and a functional (derived from RS-fMRI) point of view. Despite functionally connected regions are expected to be also connected in structure, the extent to which functional and anatomical MRI-derived connectivities express each other is still largely unknown. Using parcellation based on tractography and SBA on RS-fMRI data, only a partial overall correspondence between structural and functional connections was found. Taking into account that some methodological issues should be considered (winner-takes-all strategy that reduces sensitivity; between-region distance; different spatial sensitivity; tensor model accounting only for one direction), I speculate that the two approaches are likely to provide complementary information. In fact, it is likely that, while structural connectivity as measured by tractography can only

detect mono-synaptic connections, functional connectivity is likely to rely on poly-synaptic pathways too.

The study highlights that the correspondence between anatomical and functional connectivity needs further investigation. In these prospective one of the main issue is to evaluate the impact of the methodological limitations that could affect the results. To do that several aspect can be modified: the analysis should be carried out in a bigger group of healthy subject; anatomical connectivity could be assess using diffusion models that account for multiple direction, increasing the possibility to detect more specific anatomical connections; other structures can be examined with the same approach (for example cerebello-thalamic or basal ganglia-cortical connections).

In order to better understand this correspondence between functional and anatomical connectivity, I started to analyze data from the same group of subjects using a different approach: the idea is to segment the thalamus into functional components using ICA, that can be then used to parcellate the cortex on the base of functional (using SBA) and anatomical connection (using diffusion tractography) with each component. In that way a direct comparison of the two approaches can be carried out.

COMBINING NEUROIMAGING AND NEUROPHYSIOLOGY

The study described in chapter 5 provides new evidence for the role of RS-fMRI in detecting changes in brain activity associated with TMS. Our findings support the idea that cTBS induce a functional discoupling between the

stimulated DLPFC (BA10) and a region (BA40) that is known to be connected to DLPFC.

From these results we hypothesize that the effect of cTBS does not affect a selective part of the cortex, rather, target sites should be considered as nodes within a widespread network of interacting brain regions, where perturbing or boosting processing of one element can also influence several others. Thus, first, we provide new evidence of the possibility to induce cortical changes using TMS; second, we underline the crucial role that the combination of TMS and RS-fMRI has in the characterization of both local and remote effects of TMS, providing new insight into a better understanding of functional connectivity of the human brain.

The mechanisms that it is important to consider is whether an observed change in connectivity actually reflects a change in connection strength between remote areas or whether it could be explained by local effects of the rTMS alone.

However, because the mechanisms leading to functional connectivity changes induced by TMS remain unclear, further studies are necessary. Several issues have to be considered in the setup of future experiments.

First of all, it should be useful to assess functional connectivity alteration at single subject level, further decreasing the influence of inter-subject variability. Another important aspect that should be considered is the duration of the effect of TMS: increasing the number of RS-fMRI data acquisition sessions after the stimulation could be very important to clarify how for how

long the effect of the stimulation lasts and how it changes over time. Also, another interesting question is to understand how and how much the degree of functional connection detected with RS-fMRI varies in a short or long time. Follow-up experiments should be planned in order to clarify this aspect.

A more precise localization of the stimulated site is another important challenge to ameliorate these kind of experiments. In order to address this issue, I am going to take part in a new project, aiming to clarify the role of the precuneus in AD patients. The experimental design includes a preliminary phase in which RS-fMRI data will be acquired in a group of healthy volunteers before and after precuneus stimulation with cTBS. In order to stimulate the correct region, a RS-fMRI scan will be first performedto extract the DMN of each subject and identify the functional activation in the precuneus. The coordinates for each subject will be used to identify the right region to stimulate in the following scan sessions, thus improving the specificity of the target area.

GENERAL CONCLUSIONS AND FUTURE WORK

Finally, from a general prospective, an important issue that should be addresses in future studies is the combination of functional and structural MRI and TMS: for example, the characterization of subjective anatomical connection could be used as a reference to plan experiment designs for subjective investigation, further reducing the bias due to inter-subject variability.

To concluede, all these studies demonstrate the validity of neuroimaging techniques to characterize functional and anatomical connections and their changes in pathological conditions, and they confirm the importance of combining different techniques in order to improve the characterisation of brain networks.

REFERENCES

Albert, N. B., Robertson, E. M., and Miall, R. C. (2009). The resting human brain and motor learning. Curr Biol 19, 1023-1027.

Alexander, G. E., DeLong, M. R., and Strick, P. L. (1986). Parallel organization of functionally segregated circuits linking basal ganglia and cortex. Annu Rev Neurosci 9, 357-381.

Anwander, A., Tittgemeyer, M., von Cramon, D. Y., Friederici, A. D., and Knosche, T. R. (2007). Connectivity-Based Parcellation of Broca's Area. Cereb Cortex 17, 816-825.

Attwell, D., and Laughlin, S. B. (2001). An energy budget for signaling in the grey matter of the brain. J Cereb Blood Flow Metab 21, 1133-1145.

Barker, A. T., Jalinous, R., and Freeston, I. L. (1985). Non-invasive magnetic stimulation of human motor cortex. Lancet 1, 1106-1107.

Basser, P. J., and Pierpaoli, C. (1996). Microstructural and physiological features of tissues elucidated by quantitative-diffusion-tensor MRI. J Magn Reson B 111, 209-219.

Basser, P. J., Mattiello, J., and LeBihan, D. (1994). Estimation of the effective self-diffusion tensor from the NMR spin echo. J Magn Reson B 103, 247-254.

Batchelor, P. G., Calamante, F., Tournier, J. D., Atkinson, D., Hill, D. L., and Connelly, A. (2006). Quantification of the shape of fiber tracts. Magn Reson Med 55, 894-903.

Beckmann CF, D. M., Devlin JT, Smith SM (2005). Investigations into resting-state connectivity using independent component analysis. Philos Trans R Soc Lond B Biol Sci 360, 1001–1013.

Beckmann, M., Johansen-Berg, H., and Rushworth, M. F. (2009). Connectivity-based parcellation of human cingulate cortex and its relation to functional specialization. J Neurosci 29, 1175-1190.

Behrens, T. E., Berg, H. J., Jbabdi, S., Rushworth, M. F., and Woolrich, M. W. (2007). Probabilistic diffusion tractography with multiple fibre orientations: What can we gain? Neuroimage 34, 144-155.

Behrens, T. E., Johansen-Berg, H., Woolrich, M. W., Smith, S. M., Wheeler-Kingshott, C. A., Boulby, P. A., Barker, G. J., Sillery, E. L., Sheehan, K., Ciccarelli, O., et al. (2003). Non-invasive mapping of connections between human thalamus and cortex using diffusion imaging. Nat Neurosci 6, 750-757.

Bien, N., Roebroeck, A., Goebel, R., and Sack, A. T. (2009). The brain's intention to imitate: the neurobiology of intentional versus automatic imitation. Cereb Cortex 19, 2338-2351.

Bilek, E., Schafer, A., Ochs, E., Esslinger, C., Zangl, M., Plichta, M. M., Braun, U., Kirsch, P., Schulze, T. G., Rietschel, M., et al. (2013). Application of high-frequency repetitive transcranial magnetic

stimulation to the DLPFC alters human prefrontal-hippocampal functional interaction. J Neurosci 33, 7050-7056.

Bisiach, E., Perani, D., Vallar, G., and Berti, A. (1986). Unilateral neglect: personal and extra-personal. Neuropsychologia 24, 759-767.

Biswal, B., Yetkin, F. Z., Haughton, V. M., and Hyde, J. S. (1995). Functional connectivity in the motor cortex of resting human brain using echo-planar MRI. Magn Reson Med 34, 537-541.

Boggio, P. S., Bermpohl, F., Vergara, A. O., Muniz, A. L., Nahas, F. H., Leme, P. B., Rigonatti, S. P., and Fregni, F. (2007). Go-no-go task performance improvement after anodal transcranial DC stimulation of the left dorsolateral prefrontal cortex in major depression. J Affect Disord 101, 91-98.

Boggio, P. S., Campanha, C., Valasek, C. A., Fecteau, S., Pascual-Leone, A., and Fregni, F. (2010). Modulation of decision-making in a gambling task in older adults with transcranial direct current stimulation. Eur J Neurosci 31, 593-597.

Bookheimer, S. Y., Strojwas, M. H., Cohen, M. S., Saunders, A. M., Pericak-Vance, M. A., Mazziotta, J. C., and Small, G. W. (2000). Patterns of brain activation in people at risk for Alzheimer's disease. N Engl J Med 343, 450-456.

Bozzali, M., Filippi, M., Magnani, G., Cercignani, M., Franceschi, M., Schiatti, E., Castiglioni, S., Mossini, R., Falautano, M., Scotti, G., et al. (2006). The contribution of voxel-based morphometry in

staging patients with mild cognitive impairment. Neurology 67, 453-460.

Bressler, S. L., and Menon, V. (2010). Large-scale brain networks in cognition: emerging methods and principles. Trends Cogn Sci 14, 277-290.

Broser, P., Vargha-Khadem, F., and Clark, C. A. (2011). Robust subdivision of the thalamus in children based on probability distribution functions calculated from probabilistic tractography. Neuroimage 57, 403-415.

Buckner, R. L., Andrews-Hanna, J. R., and Schacter, D. L. (2008). The brain's default network: anatomy, function, and relevance to disease. Ann N Y Acad Sci 1124, 1-38.

Buckner, R. L., Sepulcre, J., Talukdar, T., Krienen, F. M., Liu, H., Hedden, T., Andrews-Hanna, J. R., Sperling, R. A., and Johnson, K. A. (2009). Cortical hubs revealed by intrinsic functional connectivity: mapping, assessment of stability, and relation to Alzheimer's disease. J Neurosci 29, 1860-1873.

Bullmore, E., and Sporns, O. (2009). Complex brain networks: graph theoretical analysis of structural and functional systems. Nat Rev Neurosci 10, 186-198.

Burt, T., Lisanby, S. H., and Sackeim, H. A. (2002). Neuropsychiatric applications of transcranial magnetic stimulation: a meta analysis. Int J Neuropsychopharmacol 5, 73-103.

Busch, D., Hagemann, N., and Bender, N. (2010). The dimensionality of the Edinburgh Handedness Inventory: An analysis with models of the item response theory. Laterality 15, 610-628.

Calhoun, V. D., Adali, T., Pearlson, G. D., and Pekar, J. J. (2001). A method for making group inferences from functional MRI data using independent component analysis. Hum Brain Mapp 14, 140-151.

Calhoun, V. D., Kiehl, K. A., and Pearlson, G. D. (2008). Modulation of temporally coherent brain networks estimated using ICA at rest and during cognitive tasks. Hum Brain Mapp 29, 828-838.

Cassidy, T. P., Lewis, S., and Gray, C. S. (1998). Recovery from visuospatial neglect in stroke patients. J Neurol Neurosurg Psychiatry 64, 555-557.

Chabardes, S., Kahane, P., Minotti, L., Hoffmann, D., and Benabid, A. L. (2002). Anatomy of the temporal pole region. Epileptic Disord 4 Suppl 1, 9-15.

Chen, J., Zhou, C., Wu, B., Wang, Y., Li, Q., Wei, Y., Yang, D., Mu, J., Zhu, D., Zou, D., and Xie, P. (2013). Left versus Right Repetitive Transcranial Magnetic Stimulation in Treating Major Depression: a Meta-Analysis of Randomised Controlled Trials. Psychiatry Res.

Clasca, F., Rubio-Garrido, P., and Jabaudon, D. (2012). Unveiling the diversity of thalamocortical neuron subtypes. Eur J Neurosci 35, 1524-1532.

Cloutman, L. L., and Lambon Ralph, M. A. (2012). Connectivity-based structural and functional parcellation of the human cortex using diffusion imaging and tractography. Front Neuroanat 6, 34.

Cole, D. M., Smith, S. M., and Beckmann, C. F. (2010). Advances and pitfalls in the analysis and interpretation of resting-state FMRI data. Front Syst Neurosci 4, 8.

Corbetta, M., Akbudak, E., Conturo, T. E., Snyder, A. Z., Ollinger, J. M., Drury, H. A., Linenweber, M. R., Petersen, S. E., Raichle, M. E., Van Essen, D. C., and Shulman, G. L. (1998). A common network of functional areas for attention and eye movements. Neuron 21, 761-773.

Corbetta, M., Miezin, F. M., Shulman, G. L., and Petersen, S. E. (1993). A PET study of visuospatial attention. J Neurosci 13, 1202-1226.

Cordes, D., Haughton, V. M., Arfanakis, K., Carew, J. D., Turski, P. A., Moritz, C. H., Quigley, M. A., and Meyerand, M. E. (2001). Frequencies contributing to functional connectivity in the cerebral cortex in "resting-state" data. AJNR Am J Neuroradiol 22, 1326-1333.

Damoiseaux, J. S., Rombouts, S. A., Barkhof, F., Scheltens, P., Stam, C. J., Smith, S. M., and Beckmann, C. F. (2006). Consistent resting-

state networks across healthy subjects. Proc Natl Acad Sci U S A 103, 13848-13853.

Darian-Smith, C., Darian-Smith, I., and Cheema, S. S. (1990). Thalamic projections to sensorimotor cortex in the newborn macaque. J Comp Neurol 299, 47-63.

Darian-Smith, I., Galea, M. P., Darian-Smith, C., Sugitani, M., Tan, A., and Burman, K. (1996). The anatomy of manual dexterity. The new connectivity of the primate sensorimotor thalamus and cerebral cortex. Adv Anat Embryol Cell Biol 133, 1-140.

de Graaf, T. A., Jacobs, C., Roebroeck, A., and Sack, A. T. (2009). FMRI effective connectivity and TMS chronometry: complementary accounts of causality in the visuospatial judgment network. PLoS One 4, e8307.

de Haan, W., Mott, K., van Straaten, E. C., Scheltens, P., and Stam, C. J. (2012). Activity dependent degeneration explains hub vulnerability in Alzheimer's disease. PLoS Comput Biol 8, e1002582.

De Luca, M., Beckmann, C. F., De Stefano, N., Matthews, P. M., and Smith, S. M. (2006). fMRI resting state networks define distinct modes of long-distance interactions in the human brain. Neuroimage 29, 1359-1367.

Deco, G., Jirsa, V. K., and McIntosh, A. R. (2011). Emerging concepts for the dynamical organization of resting-state activity in the brain. Nat Rev Neurosci 12, 43-56.

D'Esposito, M., Aguirre, G. K., Zarahn, E., Ballard, D., Shin, R. K., and Lease, J. (1998). Functional MRI studies of spatial and nonspatial working memory. Brain Res Cogn Brain Res 7, 1-13.

Di Lazzaro, V., Pilato, F., Dileone, M., Profice, P., Oliviero, A., Mazzone, P., Insola, A., Ranieri, F., Meglio, M., Tonali, P. A., and Rothwell, J. C. (2008). The physiological basis of the effects of intermittent theta burst stimulation of the human motor cortex. J Physiol 586, 3871-3879.

Dockery, C. A., Hueckel-Weng, R., Birbaumer, N., and Plewnia, C. (2009). Enhancement of planning ability by transcranial direct current stimulation. J Neurosci 29, 7271-7277.

Dosenbach, N. U., Fair, D. A., Miezin, F. M., Cohen, A. L., Wenger, K. K., Dosenbach, R. A., Fox, M. D., Snyder, A. Z., Vincent, J. L., Raichle, M. E., et al. (2007). Distinct brain networks for adaptive and stable task control in humans. Proc Natl Acad Sci U S A 104, 11073-11078.

Eldaief, M. C., Halko, M. A., Buckner, R. L., and Pascual-Leone, A. (2011). Transcranial magnetic stimulation modulates the brain's intrinsic activity in a frequency-dependent manner. Proc Natl Acad Sci U S A 108, 21229-21234.

Esposito, F., Aragri, A., Pesaresi, I., Cirillo, S., Tedeschi, G., Marciano, E., Goebel, R., and Di Salle, F. (2008). Independent component model

of the default-mode brain function: combining individual-level and population-level analyses in resting-state fMRI. Magn Reson Imaging 26, 905-913.

Fink, G. R., Marshall, J. C., Weiss, P. H., and Zilles, K. (2001). The neural basis of vertical and horizontal line bisection judgments: an fMRI study of normal volunteers. Neuroimage 14, S59-67.

Finn, A. S., Sheridan, M. A., Kam, C. L., Hinshaw, S., and D'Esposito, M. (2010). Longitudinal evidence for functional specialization of the neural circuit supporting working memory in the human brain. J Neurosci 30, 11062-11067.

Fitzgerald, P. B., Oxley, T. J., Laird, A. R., Kulkarni, J., Egan, G. F., and Daskalakis, Z. J. (2006). An analysis of functional neuroimaging studies of dorsolateral prefrontal cortical activity in depression. Psychiatry Res 148, 33-45.

Floel, A., Suttorp, W., Kohl, O., Kurten, J., Lohmann, H., Breitenstein, C., and Knecht, S. (2008). Non-invasive brain stimulation improves object-location learning in the elderly. Neurobiol Aging 33, 1682-1689.

Fox, M. D., and Greicius, M. (2010). Clinical applications of resting state functional connectivity. Front Syst Neurosci 4, 19.

Fox, M. D., and Raichle, M. E. (2007). Spontaneous fluctuations in brain activity observed with functional magnetic resonance imaging. Nat Rev Neurosci 8, 700-711.

Fox, M. D., Halko, M. A., Eldaief, M. C., and Pascual-Leone, A. (2012). Measuring and manipulating brain connectivity with resting state functional connectivity magnetic resonance imaging (fcMRI) and transcranial magnetic stimulation (TMS). Neuroimage 62, 2232-2243.

Fox, M. D., Snyder, A. Z., Vincent, J. L., Corbetta, M., Van Essen, D. C., and Raichle, M. E. (2005). The human brain is intrinsically organized into dynamic, anticorrelated functional networks. Proc Natl Acad Sci U S A 102, 9673-9678.

Fregni, F., Boggio, P. S., Nitsche, M., Bermpohl, F., Antal, A., Feredoes, E., Marcolin, M. A., Rigonatti, S. P., Silva, M. T., Paulus, W., and Pascual-Leone, A. (2005). Anodal transcranial direct current stimulation of prefrontal cortex enhances working memory. Exp Brain Res 166, 23-30.

Friston, K. J., Frith, C. D., and Frackowiak, R. S. (1993a). Principal component analysis learning algorithms: a neurobiological analysis. Proc Biol Sci 254, 47-54.

Friston, K. J., Frith, C. D., Liddle, P. F., and Frackowiak, R. S. (1993b). Functional connectivity: the principal-component analysis of large (PET) data sets. J Cereb Blood Flow Metab 13, 5-14.

Gauthier, S., Reisberg, B., Zaudig, M., Petersen, R. C., Ritchie, K., Broich, K., Belleville, S., Brodaty, H., Bennett, D., Chertkow, H., et al. (2006). Mild cognitive impairment. Lancet 367, 1262-1270.

George, M. S., and Post, R. M. (1995). Daily left prefrontal repetitive transcranial magnetic stimulation for acute treatment of medication-resistant depression. Am J Psychiatry 168, 356-364.

George, M. S., Taylor, J. J., and Short, E. B. (2013). The expanding evidence base for rTMS treatment of depression. Curr Opin Psychiatry 26, 13-18.

Gili, T., Cercignani, M., Serra, L., Perri, R., Giove, F., Maraviglia, B., Caltagirone, C., and Bozzali, M. (2011). Regional brain atrophy and functional disconnection across Alzheimer's disease evolution. J Neurol Neurosurg Psychiatry 82, 58-66.

Gitelman, D. R., Nobre, A. C., Parrish, T. B., LaBar, K. S., Kim, Y. H., Meyer, J. R., and Mesulam, M. (1999). A large-scale distributed network for covert spatial attention: further anatomical delineation based on stringent behavioural and cognitive controls. Brain 122 (Pt 6), 1093-1106.

Glahn, D. C., Ragland, J. D., Abramoff, A., Barrett, J., Laird, A. R., Bearden, C. E., and Velligan, D. I. (2005). Beyond hypofrontality: a quantitative meta-analysis of functional neuroimaging studies of working memory in schizophrenia. Hum Brain Mapp 25, 60-69.

Goldman-Rakic, P. S., and Porrino, L. J. (1985). The primate mediodorsal (MD) nucleus and its projection to the frontal lobe. J Comp Neurol 242, 535-560.

Grefkes, C., Eickhoff, S. B., Nowak, D. A., Dafotakis, M., and Fink, G. R. (2008). Dynamic intra- and interhemispheric interactions during unilateral and bilateral hand movements assessed with fMRI and DCM. Neuroimage 41, 1382-1394.

Grefkes, C., Nowak, D. A., Wang, L. E., Dafotakis, M., Eickhoff, S. B., and Fink, G. R. (2010). Modulating cortical connectivity in stroke patients by rTMS assessed with fMRI and dynamic causal modeling. Neuroimage 50, 233-242.

Greicius, M. D., Flores, B. H., Menon, V., Glover, G. H., Solvason, H. B., Kenna, H., Reiss, A. L., and Schatzberg, A. F. (2007). Resting-state functional connectivity in major depression: abnormally increased contributions from subgenual cingulate cortex and thalamus. Biol Psychiatry 62, 429-437.

Greicius, M. D., Krasnow, B., Reiss, A. L., and Menon, V. (2003). Functional connectivity in the resting brain: a network analysis of the default mode hypothesis. Proc Natl Acad Sci U S A 100, 253-258.

Greicius, M. D., Supekar, K., Menon, V., and Dougherty, R. F. (2009). Resting-state functional connectivity reflects structural connectivity in the default mode network. Cereb Cortex 19, 72-78.

Haber, S. N. (2003). The primate basal ganglia: parallel and integrative networks. J Chem Neuroanat 26, 317-330.

Hallett, M. (2007). Transcranial magnetic stimulation: a primer. Neuron 55, 187-199.

Hanley, J. A., and McNeil, B. J. (1982). The meaning and use of the area under a receiver operating characteristic (ROC) curve. Radiology 143, 29-36.

Hannula, H., Neuvonen, T., Savolainen, P., Hiltunen, J., Ma, Y. Y., Antila, H., Salonen, O., Carlson, S., and Pertovaara, A. (2010). Increasing top-down suppression from prefrontal cortex facilitates tactile working memory. Neuroimage 49, 1091-1098.

Haselgrove, J. C., and Moore, J. R. (1996). Correction for distortion of echo-planar images used to calculate the apparent diffusion coefficient. Magn Reson Med 36, 960-964.

Hasson, U., Nusbaum, H. C., and Small, S. L. (2009). Task-dependent organization of brain regions active during rest. Proc Natl Acad Sci U S A 106, 10841-10846.

Heilman, K. M., and Van Den Abell, T. (1980). Right hemisphere dominance for attention: the mechanism underlying hemispheric asymmetries of inattention (neglect). Neurology 30, 327-330.

Heilman, K. M., Valenstein, E., and Watson, R. T. (2000). Neglect and related disorders. Semin Neurol 20, 463-470.

Hier, D. B., Mondlock, J., and Caplan, L. R. (1983). Behavioral abnormalities after right hemisphere stroke. Neurology 33, 337-344.

Hill, A. J. (1978). First occurrence of hippocampal spatial firing in a new environment. Exp Neurol 62, 282-297.

Hoffman, R. E., Hampson, M., Wu, K., Anderson, A. W., Gore, J. C., Buchanan, R. J., Constable, R. T., Hawkins, K. A., Sahay, N., and Krystal, J. H. (2007). Probing the pathophysiology of auditory/verbal hallucinations by combining functional magnetic resonance imaging and transcranial magnetic stimulation. Cereb Cortex 17, 2733-2743.

Honey, C. J., Sporns, O., Cammoun, L., Gigandet, X., Thiran, J. P., Meuli, R., and Hagmann, P. (2009). Predicting human resting-state functional connectivity from structural connectivity. Proc Natl Acad Sci U S A 106, 2035-2040.

Hoogendam, J. M., Ramakers, G. M., and Di Lazzaro, V. (2011). Physiology of repetitive transcranial magnetic stimulation of the human brain. Brain Stimul 3, 95-118.

Horwitz, B. (2003). The elusive concept of brain connectivity. Neuroimage 19, 466-470.

Huang, H., Zhang, J., van Zijl, P. C., and Mori, S. (2004). Analysis of noise effects on DTI-based tractography using the brute-force and multi-ROI approach. Magn Reson Med 52, 559-565.

Huang, Y. Z., Chen, R. S., Rothwell, J. C., and Wen, H. Y. (2007). The after-effect of human theta burst stimulation is NMDA receptor dependent. Clin Neurophysiol 118, 1028-1032.

Huang, Y. Z., Edwards, M. J., Rounis, E., Bhatia, K. P., and Rothwell, J. C. (2005). Theta burst stimulation of the human motor cortex. Neuron 45, 201-206.

Isenberg, K., Downs, D., Pierce, K., Svarakic, D., Garcia, K., Jarvis, M., North, C., and Kormos, T. C. (2005). Low frequency rTMS stimulation of the right frontal cortex is as effective as high frequency rTMS stimulation of the left frontal cortex for antidepressant-free, treatment-resistant depressed patients. Ann Clin Psychiatry 17, 153-159.

Jack, C. R., Jr., Albert, M. S., Knopman, D. S., McKhann, G. M., Sperling, R. A., Carrillo, M. C., Thies, B., and Phelps, C. H. (2011). Introduction to the recommendations from the National Institute on Aging-Alzheimer's Association workgroups on diagnostic guidelines for Alzheimer's disease. Alzheimers Dement 7, 257-262.

Jenkinson, M., and Smith, S. (2001). A global optimisation method for robust affine registration of brain images. Med Image Anal 5, 143-156.

Jeong, B., Choi, J., and Kim, J. W. (2012). MRI study on the functional and spatial consistency of resting state-related independent components of the brain network. Korean J Radiol 13, 265-274.

Johansen-Berg, H., and Rushworth, M. F. (2009). Using diffusion imaging to study human connectional anatomy. Annu Rev Neurosci 32, 75-94.

Johansen-Berg, H., Behrens, T. E., Robson, M. D., Drobnjak, I., Rushworth, M. F., Brady, J. M., Smith, S. M., Higham, D. J., and Matthews, P. M. (2004). Changes in connectivity profiles define functionally distinct regions in human medial frontal cortex. Proc Natl Acad Sci U S A 101, 13335-13340.

Johansen-Berg, H., Behrens, T. E., Sillery, E., Ciccarelli, O., Thompson, A. J., Smith, S. M., and Matthews, P. M. (2005). Functional-anatomical validation and individual variation of diffusion tractography-based segmentation of the human thalamus. Cereb Cortex 15, 31-39.

Jones, D. K., and Cercignani, M. (2010). Twenty-five pitfalls in the analysis of diffusion MRI data. NMR Biomed 23, 803-820.

Jones, D. K., and Pierpaoli, C. (2005). Confidence mapping in diffusion tensor magnetic resonance imaging tractography using a bootstrap approach. Magn Reson Med 53, 1143-1149.

Jones, D. K., Catani, M., Pierpaoli, C., Reeves, S. J., Shergill, S. S., O'Sullivan, M., Golesworthy, P., McGuire, P., Horsfield, M. A.,

Simmons, A., et al. (2006). Age effects on diffusion tensor magnetic resonance imaging tractography measures of frontal cortex connections in schizophrenia. Hum Brain Mapp 27, 230-238.

Jones, E. G. (2009). Synchrony in the interconnected circuitry of the thalamus and cerebral cortex. Ann N Y Acad Sci 1157, 10-23.

Keeser, D., Meindl, T., Bor, J., Palm, U., Pogarell, O., Mulert, C., Brunelin, J., Moller, H. J., Reiser, M., and Padberg, F. (2011). Prefrontal transcranial direct current stimulation changes connectivity of resting-state networks during fMRI. J Neurosci 31, 15284-15293.

Kinsbourne, M. (1977). Hemi-neglect and hemisphere rivalry. Adv Neurol 18, 41-49.

Klimesch, W., Doppelmayr, M., Russegger, H., and Pachinger, T. (1996). Theta band power in the human scalp EEG and the encoding of new information. Neuroreport 7, 1235-1240.

Koch, G., and Rothwell, J. C. (2009). TMS investigations into the task-dependent functional interplay between human posterior parietal and motor cortex. Behav Brain Res 202, 147-152.

Koch, G., Bonni, S., Giacobbe, V., Bucchi, G., Basile, B., Lupo, F., Versace, V., Bozzali, M., and Caltagirone, C. (2012a). theta-burst

stimulation of the left hemisphere accelerates recovery of hemispatial neglect. Neurology 78, 24-30.

Koch, G., Cercignani, M., Bonni, S., Giacobbe, V., Bucchi, G., Versace, V., Caltagirone, C., and Bozzali, M. (2011). Asymmetry of parietal interhemispheric connections in humans. J Neurosci 31, 8967-8975.

Koch, G., Oliveri, M., and Caltagirone, C. (2009). Neural networks engaged in milliseconds and seconds time processing: evidence from transcranial magnetic stimulation and patients with cortical or subcortical dysfunction. Philos Trans R Soc Lond B Biol Sci 364, 1907-1918.

Koch, G., Oliveri, M., Cheeran, B., Ruge, D., Lo Gerfo, E., Salerno, S., Torriero, S., Marconi, B., Mori, F., Driver, J., et al. (2008). Hyperexcitability of parietal-motor functional connections in the intact left-hemisphere of patients with neglect. Brain 131, 3147-3155.

Koch, G., Oliveri, M., Torriero, S., Salerno, S., Lo Gerfo, E., and Caltagirone, C. (2007). Repetitive TMS of cerebellum interferes with millisecond time processing. Exp Brain Res 179, 291-299.

Koch, G., Veniero, D., and Caltagirone, C. (2012b). To the other side of the neglected brain: the hyperexcitability of the left intact hemisphere. Neuroscientist 19, 208-217.

Koch, M. A., Norris, D. G., and Hund-Georgiadis, M. (2002). An investigation of functional and anatomical connectivity using magnetic resonance imaging. Neuroimage 16, 241-250.

Kwon, H., Reiss, A. L., and Menon, V. (2002). Neural basis of protracted developmental changes in visuo-spatial working memory. Proc Natl Acad Sci U S A 99, 13336-13341.

Lang, E. W., Tome, A. M., Keck, I. R., Gorriz-Saez, J. M., and Puntonet, C. G. (2012). Brain connectivity analysis: a short survey. Comput Intell Neurosci 2012, 412512.

Larson, J., Wong, D., and Lynch, G. (1986). Patterned stimulation at the theta frequency is optimal for the induction of hippocampal long-term potentiation. Brain Res 368, 347-350.

Lazar, M., Jensen, J. H., Xuan, L., and Helpern, J. A. (2008). Estimation of the orientation distribution function from diffusional kurtosis imaging. Magn Reson Med 60, 774-781.

Lee, L., Harrison, L. M., and Mechelli, A. (2003a). A report of the functional connectivity workshop, Dusseldorf 2002. Neuroimage 19, 457-465.

Lee, L., Siebner, H. R., Rowe, J. B., Rizzo, V., Rothwell, J. C., Frackowiak, R. S., and Friston, K. J. (2003). Acute remapping within the motor system induced by low-frequency repetitive transcranial magnetic stimulation. J Neurosci 23, 5308-5318.

Lee, L., Siebner, H. R., Rowe, J. B., Rizzo, V., Rothwell, J. C., Frackowiak, R. S., and Friston, K. J. (2003b). Acute remapping within the motor system induced by low-frequency repetitive transcranial magnetic stimulation. J Neurosci 23, 5308-5318.

Leh, S. E., Ptito, A., Chakravarty, M. M., and Strafella, A. P. (2007). Fronto-striatal connections in the human brain: a probabilistic diffusion tractography study. Neurosci Lett 419, 113-118.

Liu, Y., Yu, C., Zhang, X., Liu, J., Duan, Y., Alexander-Bloch, A. F., Liu, B., Jiang, T., and Bullmore, E. (2013). Impaired Long Distance Functional Connectivity and Weighted Network Architecture in Alzheimer's Disease. Cereb Cortex.

Lowe, M. J., Beall, E. B., Sakaie, K. E., Koenig, K. A., Stone, L., Marrie, R. A., and Phillips, M. D. (2008). Resting state sensorimotor functional connectivity in multiple sclerosis inversely correlates with transcallosal motor pathway transverse diffusivity. Hum Brain Mapp 29, 818-827.

Lowe, M. J., Dzemidzic, M., Lurito, J. T., Mathews, V. P., and Phillips, M. D. (2000). Correlations in low-frequency BOLD fluctuations reflect cortico-cortical connections. Neuroimage 12, 582-587.

Margulies, D. S., Kelly, A. M., Uddin, L. Q., Biswal, B. B., Castellanos, F. X., and Milham, M. P. (2007). Mapping the functional connectivity of anterior cingulate cortex. Neuroimage 37, 579-588.

Mars, R. B., Sallet, J., Schuffelgen, U., Jbabdi, S., Toni, I., and Rushworth, M. F. (2011). Connectivity-based subdivisions of the human right "temporoparietal junction area": evidence for different areas participating in different cortical networks. Cereb Cortex 22, 1894-1903.

McIntosh, A. R. (1999). Mapping cognition to the brain through neural interactions. Memory 7, 523-548.

McKeown, M. J., Makeig, S., Brown, G. G., Jung, T. P., Kindermann, S. S., Bell, A. J., and Sejnowski, T. J. (1998). Analysis of fMRI data by blind separation into independent spatial components. Hum Brain Mapp 6, 160-188.

Meinzer, M., Antonenko, D., Lindenberg, R., Hetzer, S., Ulm, L., Avirame, K., Flaisch, T., and Floel, A. (2012). Electrical brain stimulation improves cognitive performance by modulating functional connectivity and task-specific activation. J Neurosci 32, 1859-1866.

Mesulam, M. M. (1981). A cortical network for directed attention and unilateral neglect. Ann Neurol 10, 309-325.

Minati, L., Nigri, A., Cercignani, M., and Chan, D. (2013). Detection of scale-freeness in brain connectivity by functional MRI: signal processing aspects and implementation of an open hardware co-processor. Med Eng Phys 35, 1525-1531.

Mori, S., and van Zijl, P. C. (2002). Fiber tracking: principles and strategies - a technical review. NMR Biomed 15, 468-480.

Mukherjee, P., Chung, S. W., Berman, J. I., Hess, C. P., and Henry, R. G. (2008). Diffusion tensor MR imaging and fiber tractography: technical considerations. AJNR Am J Neuroradiol 29, 843-852.

Murphy, K., Birn, R. M., Handwerker, D. A., Jones, T. B., and Bandettini, P. A. (2009). The impact of global signal regression on resting state correlations: are anti-correlated networks introduced? Neuroimage 44, 893-905.

Mylius, V., Ayache, S. S., Ahdab, R., Farhat, W. H., Zouari, H. G., Belke, M., Brugieres, P., Wehrmann, E., Krakow, K., Timmesfeld, N., et al. (2013). Definition of DLPFC and M1 according to anatomical landmarks for navigated brain stimulation: inter-rater reliability, accuracy, and influence of gender and age. Neuroimage 78, 224-232.

Niemann, K., Mennicken, V. R., Jeanmonod, D., and Morel, A. (2000). The Morel stereotactic atlas of the human thalamus: atlas-to-MR registration of internally consistent canonical model. Neuroimage 12, 601-616.

Nobre, A. C., Sebestyen, G. N., Gitelman, D. R., Mesulam, M. M., Frackowiak, R. S., and Frith, C. D. (1997). Functional localization of the system for visuospatial attention using positron emission tomography. Brain 120 (Pt 3), 515-533.

Oberman, L., Edwards, D., Eldaief, M., and Pascual-Leone, A. (2011). Safety of theta burst transcranial magnetic stimulation: a systematic review of the literature. J Clin Neurophysiol 28, 67-74.

Ogawa, S., Lee, T. M., Kay, A. R., and Tank, D. W. (1990). Brain magnetic resonance imaging with contrast dependent on blood oxygenation. Proc Natl Acad Sci U S A 87, 9868-9872.

Ogawa, S., Menon, R. S., Tank, D. W., Kim, S. G., Merkle, H., Ellermann, J. M., and Ugurbil, K. (1993). Functional brain mapping by blood oxygenation level-dependent contrast magnetic resonance imaging. A comparison of signal characteristics with a biophysical model. Biophys J 64, 803-812.

O'Reardon, J. P., Solvason, H. B., Janicak, P. G., Sampson, S., Isenberg, K. E., Nahas, Z., McDonald, W. M., Avery, D., Fitzgerald, P. B., Loo, C., et al. (2007). Efficacy and safety of transcranial magnetic stimulation in the acute treatment of major depression: a multisite randomized controlled trial. Biol Psychiatry 62, 1208-1216.

O'Shea, J., and Walsh, V. (2007). Transcranial magnetic stimulation. Curr Biol 17, R196-199.

O'Shea, J., Johansen-Berg, H., Trief, D., Gobel, S., and Rushworth, M. F. (2007). Functionally specific reorganization in human premotor cortex. Neuron 54, 479-490.

Padberg, F., and George, M. S. (2009). Repetitive transcranial magnetic stimulation of the prefrontal cortex in depression. Exp Neurol 219, 2-13.

Pallanti, S., Bernardi, S., Di Rollo, A., Antonini, S., and Quercioli, L. (2010). Unilateral low frequency versus sequential bilateral repetitive transcranial magnetic stimulation: is simpler better for treatment of resistant depression? Neuroscience 167, 323-328.

Parker, G. J., and Alexander, D. C. (2005). Probabilistic anatomical connectivity derived from the microscopic persistent angular structure of cerebral tissue. Philos Trans R Soc Lond B Biol Sci 360, 893-902.

Parker, G. J., Haroon, H. A., and Wheeler-Kingshott, C. A. (2003). A framework for a streamline-based probabilistic index of connectivity (PICo) using a structural interpretation of MRI diffusion measurements. J Magn Reson Imaging 18, 242-254.

Pascual-Leone, A., and Walsh, V. (2001). Fast backprojections from the motion to the primary visual area necessary for visual awareness. Science 292, 510-512.

Pascual-Leone, A., Cohen, L. G., Brasil-Neto, J. P., Valls-Sole, J., and Hallett, M. (1994). Differentiation of sensorimotor neuronal structures responsible for induction of motor evoked potentials, attenuation in detection of somatosensory stimuli, and induction of

sensation of movement by mapping of optimal current directions. Electroencephalogr Clin Neurophysiol 93, 230-236.

Pascual-Leone, A., Rubio, B., Pallardo, F., and Catala, M. D. (1996). Rapid-rate transcranial magnetic stimulation of left dorsolateral prefrontal cortex in drug-resistant depression. Lancet 348, 233-237.

Pascual-Leone, A., Rubio, B., Pallardo, F., and Catala, M. D. (1996). Rapid-rate transcranial magnetic stimulation of left dorsolateral prefrontal cortex in drug-resistant depression. Lancet 348, 233-237.

Passingham, R. E., Stephan, K. E., and Kotter, R. (2002). The anatomical basis of functional localization in the cortex. Nat Rev Neurosci 3, 606-616.

Pauling, L. (1977). Magnetic properties and structure of oxyhemoglobin. Proc Natl Acad Sci U S A 74, 2612-2613.

Pena-Gomez, C., Sala-Lonch, R., Junque, C., Clemente, I. C., Vidal, D., Bargallo, N., Falcon, C., Valls-Sole, J., Pascual-Leone, A., and Bartres-Faz, D. (2011). Modulation of large-scale brain networks by transcranial direct current stimulation evidenced by resting-state functional MRI. Brain Stimul 5, 252-263.

Perri R, Serra L, Carlesimo GA, Caltagirone C (2007) Preclinical dementia: an Italian multicentre study on amnestic mild cognitive impairment. Dement Geriatr Cogn Disord 23:289-300.

Petersen, R. C. (2000). Mild cognitive impairment: transition between aging and Alzheimer's disease. Neurologia 15, 93-101.

Petersen, R. C. (2004). Mild cognitive impairment as a diagnostic entity. J Intern Med 256, 183-194.

Petrella, J. R., and Doraiswamy, P. M. (2013). From the bridges of Konigsberg to the fields of Alzheimer: connecting the dots. Neurology 80, 1360-1362.

Pierpaoli, C., and Basser, P. J. (1996). Toward a quantitative assessment of diffusion anisotropy. Magn Reson Med 36, 893-906.

Pierpaoli, C., Jezzard, P., Basser, P. J., Barnett, A., and Di Chiro, G. (1996). Diffusion tensor MR imaging of the human brain. Radiology 201, 637-648.

Pleger, B., Blankenburg, F., Bestmann, S., Ruff, C. C., Wiech, K., Stephan, K. E., Friston, K. J., and Dolan, R. J. (2006). Repetitive transcranial magnetic stimulation-induced changes in sensorimotor coupling parallel improvements of somatosensation in humans. J Neurosci 26, 1945-1952.

Polania, R., Paulus, W., and Nitsche, M. A. (2011). Modulating cortico-striatal and thalamo-cortical functional connectivity with transcranial direct current stimulation. Hum Brain Mapp 33, 2499-2508.

Pooley, R. A. (2005). AAPM/RSNA physics tutorial for residents: fundamental physics of MR imaging. Radiographics 25, 1087-1099.

Price, G., Cercignani, M., Parker, G. J., Altmann, D. R., Barnes, T. R., Barker, G. J., Joyce, E. M., and Ron, M. A. (2008). White matter tracts in first-episode psychosis: a DTI tractography study of the uncinate fasciculus. Neuroimage 39, 949-955.

Price, J. L., and Morris, J. C. (1999). Tangles and plaques in nondemented aging and "preclinical" Alzheimer's disease. Ann Neurol 45, 358-368.

Rajkowska, G., and Goldman-Rakic, P. S. (1995). Cytoarchitectonic definition of prefrontal areas in the normal human cortex: II. Variability in locations of areas 9 and 46 and relationship to the Talairach Coordinate System. Cereb Cortex 5, 323-337.

Ridding, M. C., and Rothwell, J. C. (2007). Is there a future for therapeutic use of transcranial magnetic stimulation? Nat Rev Neurosci 8, 559-567.

Rosazza, C., and Minati, L. (2011). Resting-state brain networks: literature review and clinical applications. Neurol Sci 32, 773-785.

Rosazza, C., Minati, L., Ghielmetti, F., Mandelli, M. L., and Bruzzone, M. G. (2012). Functional connectivity during resting-state functional MR imaging: study of the correspondence between independent

component analysis and region-of-interest-based methods. AJNR Am J Neuroradiol 33, 180-187.

Rossini, D., Lucca, A., Magri, L., Malaguti, A., Smeraldi, E., Colombo, C., and Zanardi, R. (2010). A symptom-specific analysis of the effect of high-frequency left or low-frequency right transcranial magnetic stimulation over the dorsolateral prefrontal cortex in major depression. Neuropsychobiology 62, 91-97.

Rothwell, J. C. (1997). Techniques and mechanisms of action of transcranial stimulation of the human motor cortex. J Neurosci Methods 74, 113-122.

Rubinov, M., and Sporns, O. (2010). Complex network measures of brain connectivity: uses and interpretations. Neuroimage 52, 1059-1069.

Ruff, C. C., Driver, J., and Bestmann, S. (2009). Combining TMS and fMRI: from 'virtual lesions' to functional-network accounts of cognition. Cortex 45, 1043-1049.

Schutter, D. J. (2010). Quantitative review of the efficacy of slow-frequency magnetic brain stimulation in major depressive disorder. Psychol Med 40, 1789-1795.

Shehzad, Z., Kelly, A. M., Reiss, P. T., Gee, D. G., Gotimer, K., Uddin, L. Q., Lee, S. H., Margulies, D. S., Roy, A. K., Biswal, B. B., et al. (2009). The resting brain: unconstrained yet reliable. Cereb Cortex 19, 2209-2229.

Siebner, H. R., Bergmann, T. O., Bestmann, S., Massimini, M., Johansen-Berg, H., Mochizuki, H., Bohning, D. E., Boorman, E. D., Groppa, S., Miniussi, C., et al. (2009). Consensus paper: combining transcranial stimulation with neuroimaging. Brain Stimul 2, 58-80.

Smith, S. M., and Nichols, T. E. (2009). Threshold-free cluster enhancement: addressing problems of smoothing, threshold dependence and localisation in cluster inference. Neuroimage 44, 83-98.

Smith, S. M., Fox, P. T., Miller, K. L., Glahn, D. C., Fox, P. M., Mackay, C. E., Filippini, N., Watkins, K. E., Toro, R., Laird, A. R., and Beckmann, C. F. (2009). Correspondence of the brain's functional architecture during activation and rest. Proc Natl Acad Sci U S A 106, 13040-13045.

Smith, S. M., Fox, P. T., Miller, K. L., Glahn, D. C., Fox, P. M., Mackay, C. E., Filippini, N., Watkins, K. E., Toro, R., Laird, A. R., and Beckmann, C. F. (2009). Correspondence of the brain's functional architecture during activation and rest. Proc Natl Acad Sci U S A 106, 13040-13045.

Smith, S. M., Jenkinson, M., Johansen-Berg, H., Rueckert, D., Nichols, T. E., Mackay, C. E., Watkins, K. E., Ciccarelli, O., Cader, M. Z., Matthews, P. M., and Behrens, T. E. (2006). Tract-based spatial statistics: voxelwise analysis of multi-subject diffusion data. Neuroimage 31, 1487-1505.

Song, S. K., Sun, S. W., Ju, W. K., Lin, S. J., Cross, A. H., and Neufeld, A. H. (2003). Diffusion tensor imaging detects and differentiates axon and myelin degeneration in mouse optic nerve after retinal ischemia. Neuroimage 20, 1714-1722.

Song, S. K., Sun, S. W., Ramsbottom, M. J., Chang, C., Russell, J., and Cross, A. H. (2002). Dysmyelination revealed through MRI as increased radial (but unchanged axial) diffusion of water. Neuroimage 17, 1429-1436.

Sporns, O., Honey, C. J., and Kotter, R. (2007). Identification and classification of hubs in brain networks. PLoS One 2, e1049.

Sporns, O., Tononi, G., and Kotter, R. (2005). The human connectome: A structural description of the human brain. PLoS Comput Biol 1, e42.

Thomason, M. E., Race, E., Burrows, B., Whitfield-Gabrieli, S., Glover, G. H., and Gabrieli, J. D. (2009). Development of spatial and verbal working memory capacity in the human brain. J Cogn Neurosci 21, 316-332.

Tijms, B. M., Wink, A. M., de Haan, W., van der Flier, W. M., Stam, C. J., Scheltens, P., and Barkhof, F. (2013). Alzheimer's disease: connecting findings from graph theoretical studies of brain networks. Neurobiol Aging 34, 2023-2036.

Tomassini, V., Jbabdi, S., Klein, J. C., Behrens, T. E., Pozzilli, C., Matthews, P. M., Rushworth, M. F., and Johansen-Berg, H.

(2007). Diffusion-weighted imaging tractography-based parcellation of the human lateral premotor cortex identifies dorsal and ventral subregions with anatomical and functional specializations. J Neurosci 27, 10259-10269.

Tuch, D. S., Reese, T. G., Wiegell, M. R., and Wedeen, V. J. (2003). Diffusion MRI of complex neural architecture. Neuron 40, 885-895.

Vallar, G., Bottini, G., and Paulesu, E. (2003). Neglect syndromes: the role of the parietal cortex. Adv Neurol 93, 293-319.

van Asselen, M., Kessels, R. P., Neggers, S. F., Kappelle, L. J., Frijns, C. J., and Postma, A. (2006). Brain areas involved in spatial working memory. Neuropsychologia 44, 1185-1194.

van den Heuvel, M. P., and Hulshoff Pol, H. E. (2010). Exploring the brain network: a review on resting-state fMRI functional connectivity. Eur Neuropsychopharmacol 20, 519-534.

van den Heuvel, M. P., Mandl, R. C., Kahn, R. S., and Hulshoff Pol, H. E. (2009). Functionally linked resting-state networks reflect the underlying structural connectivity architecture of the human brain. Hum Brain Mapp 30, 3127-3141.

van den Heuvel, M., Mandl, R., Luigjes, J., and Hulshoff Pol, H. (2008). Microstructural organization of the cingulum tract and the level of default mode functional connectivity. J Neurosci 28, 10844-10851.

van der Werf, Y. D., Sanz-Arigita, E. J., Menning, S., and van den Heuvel, O. A. (2010). Modulating spontaneous brain activity using repetitive transcranial magnetic stimulation. BMC Neurosci 11, 145.

Van Essen, D. C., Smith, S. M., Barch, D. M., Behrens, T. E., Yacoub, E., and Ugurbil, K. (2013). The WU-Minn Human Connectome Project: an overview. Neuroimage 80, 62-79.

Vannini, P., Almkvist, O., Dierks, T., Lehmann, C., and Wahlund, L. O. (2007). Reduced neuronal efficacy in progressive mild cognitive impairment: a prospective fMRI study on visuospatial processing. Psychiatry Res 156, 43-57.

Vargas, M. E., and Barres, B. A. (2007). Why is Wallerian degeneration in the CNS so slow? Annu Rev Neurosci 30, 153-179.

Vercammen, A., Knegtering, H., Liemburg, E. J., den Boer, J. A., and Aleman, A. (2010b). Functional connectivity of the temporo-parietal region in schizophrenia: effects of rTMS treatment of auditory hallucinations. J Psychiatr Res 44, 725-731.

Voineskos, A. N., Farzan, F., Barr, M. S., Lobaugh, N. J., Mulsant, B. H., Chen, R., Fitzgerald, P. B., and Daskalakis, Z. J. (2010). The role of the corpus callosum in transcranial magnetic stimulation induced interhemispheric signal propagation. Biol Psychiatry 68, 825-831.

Wager, T. D., and Smith, E. E. (2003). Neuroimaging studies of working memory: a meta-analysis. Cogn Affect Behav Neurosci 3, 255-274.

Wahl, M., Lauterbach-Soon, B., Hattingen, E., Jung, P., Singer, O., Volz, S., Klein, J. C., Steinmetz, H., and Ziemann, U. (2007). Human motor corpus callosum: topography, somatotopy, and link between microstructure and function. J Neurosci 27, 12132-12138.

Wang, J., Zuo, X., Dai, Z., Xia, M., Zhao, Z., Zhao, X., Jia, J., Han, Y., and He, Y. (2013). Disrupted functional brain connectome in individuals at risk for Alzheimer's disease. Biol Psychiatry 73, 472-481.

Wheeler-Kingshott, C. A., and Cercignani, M. (2009). About "axial" and "radial" diffusivities. Magn Reson Med 61, 1255-1260.

Wiegell, M. R., Tuch, D. S., Larsson, H. B., and Wedeen, V. J. (2003). Automatic segmentation of thalamic nuclei from diffusion tensor magnetic resonance imaging. Neuroimage 19, 391-401.

Wilson, B., Cockburn, J., and Halligan, P. (1987). Development of a behavioral test of visuospatial neglect. Arch Phys Med Rehabil 68, 98-102.

Yeterian, E. H., and Pandya, D. N. (1985). Corticothalamic connections of the posterior parietal cortex in the rhesus monkey. J Comp Neurol 237, 408-426.

Yeterian, E. H., and Pandya, D. N. (1988). Corticothalamic connections of paralimbic regions in the rhesus monkey. J Comp Neurol 269, 130-146.

Yeterian, E. H., and Pandya, D. N. (1989). Thalamic connections of the cortex of the superior temporal sulcus in the rhesus monkey. J Comp Neurol 282, 80-97.

Yeterian, E. H., and Pandya, D. N. (1991). Corticothalamic connections of the superior temporal sulcus in rhesus monkeys. Exp Brain Res 83, 268-284.

Yeterian, E. H., and Pandya, D. N. (1997). Corticothalamic connections of extrastriate visual areas in rhesus monkeys. J Comp Neurol 378, 562-585.

Yogarajah, M., Powell, H. W., Parker, G. J., Alexander, D. C., Thompson, P. J., Symms, M. R., Boulby, P., Wheeler-Kingshott, C. A., Barker, G. J., Koepp, M. J., and Duncan, J. S. (2008). Tractography of the parahippocampal gyrus and material specific memory impairment in unilateral temporal lobe epilepsy. Neuroimage 40, 1755-1764.

Zaehle, T., Sandmann, P., Thorne, J. D., Jancke, L., and Herrmann, C. S. (2011). Transcranial direct current stimulation of the prefrontal cortex modulates working memory performance: combined behavioural and electrophysiological evidence. BMC Neurosci 12, 2.

Zalesky, A., Fornito, A., and Bullmore, E. T. (2010). Network-based statistic: identifying differences in brain networks. Neuroimage 53, 1197-1207.

Zanto, T. P., Rubens, M. T., Thangavel, A., and Gazzaley, A. (2011). Causal role of the prefrontal cortex in top-down modulation of visual processing and working memory. Nat Neurosci 14, 656-661.

Zhang, D., Snyder, A. Z., Fox, M. D., Sansbury, M. W., Shimony, J. S., and Raichle, M. E. (2008). Intrinsic functional relations between human cerebral cortex and thalamus. J Neurophysiol 100, 1740-1748.

Zhang, D., Snyder, A. Z., Shimony, J. S., Fox, M. D., and Raichle, M. E. (2010). Noninvasive functional and structural connectivity mapping of the human thalamocortical system. Cereb Cortex 20, 1187-1194

ACKNOWLEDGMENTS

Desidero ringraziare il Prof. Pier Paolo Battaglini, per i suoi preziosi consigli e per l'appoggio che mi ha sempre dimostrato.

Il Dott. Marco Bozzali e Dott. Giacomo Koch, per avermi consentito di crescere come ricercatrice e per la fiducia che mi hanno dato durante questi tre anni.

Ringrazio Barbara S, Barbara B, Elena, Elisa, Giovanni, Giusy, Laura, Mario, Sonia, Steve, Valentina e Viviana per come sono diventati amici, non più solo colleghi.

Un particolare grazie alla Prof.ssa Mara Cercignani, per tutto quello che mi ha insegnato ma soprattutto per il suo entusiasmo contagioso.

LIST OF PUBBLICATIONS

M. Bozzali, **C. Matropasqua**, M. Cercignani, G. Giulietti, S. Bonni, C. Caltagirone, G. Koch.Microstructural Damage of the Posterior Corpus Callosum Contributes to the Clinical Severity of Neglect. PLOS ONE. (2012).

Brusa L, Ponzo V, **Mastropasqua C**, Picazio S, Bonnì S, Di Lorenzo F, Iani C, Stefani A, Stanzione P, Caltagirone C, Bozzali M, Koch G. Theta Burst Stimulation Modulates Cerebellar-Cortical Connectivity in Patients with Progressive Supranuclear Palsy. Brain Stimul. (2013).

Bonnì S, **Mastropasqua C**, Bozzali M, Caltagirone C, Koch G.Theta burst stimulation improves visuo-spatial attention in a patient with traumatic brain injury. Neurol Sci. (2013).

L. Minati, D. Chan, **C. Mastropasqua**, L. Serra, B.Spanò , C. Marra , C. Caltagirone, M. Cercignani, M. Bozzali. Widespread alterations in functional brain network architecture in amnestic mild cognitive impairment. J Alzheimers Dis. (2014).

L. Serra, G. Silvestri, A. Petrucci, B. Basile, M. Masciullo, E Makovac, M Torso, B. Spanò, **C. Mastropasqua**, N.Harrison, M. Bianchi, M. Giacanelli, C. Caltagirone, M. Cercignani, M. Bozzali. Personality traits in Myotonic Dystrophy type 1 are explained by abnormal functional brain connectivity. JAMA Neurology. (2014). (in press).

C. Matropasqua, M. Bozzali, , G. Koch, M. Cercignani. Functional anatomy of the thalamus as a model of integrated structural and functional connectivity of the human brain in vivo. (under review)

C. Mastropasqua, M. Bozzali, C. Caltagirone, M. Cercignani, V. Ponzo, G. Koch. cTBS induces changes in functional connectivity during rest. (under review).

Sonia Bonnì, Domenica Veniero, **C.Mastropasqua**, M. Bozzali, C.Caltagirone, G. Koch. TMS evidence for a selective role of the precuneus in source memory retrieval (submitted).

L.Serra, M. Musicco, M.Cercignani, M. Torsoa, B.Spanò, **C. Mastropasqua**, R.Perri, L. Fadda, D. Castelli, C. Marra, G. Bruno, C.Caltagirone, M. Bozzali. The potential protective effect of different levels of cognitive reserve on risk to develop Alzheimer's disease. A longitudinal study (in preparation).